Journal Pre-proof

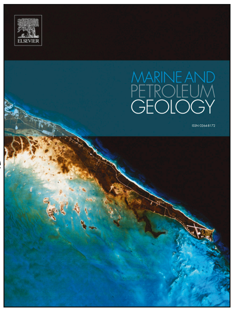

Tectono-stratigraphy of the Shushan Basin, Western Desert, Egypt: A window into the evolution of the SE Mediterranean province

Ahmed I. Albrkawy, Tiago M. Alves, Thomas Blenkinsop

PII: S0264-8172(25)00104-7

DOI: https://doi.org/10.1016/j.marpetgeo.2025.107387

Reference: JMPG 107387

To appear in: *Marine and Petroleum Geology*

Received Date: 15 July 2024

Revised Date: 19 December 2024

Accepted Date: 14 March 2025

Tectono-stratigraphy of the Shushan Basin, Western Desert, Egypt: A window into the evolution of the SE Mediterranean province

Ahmed I. Albrkawy[1,2], Tiago M. Alves[1], Thomas Blenkinsop[1]

[1]3D Seismic Lab, School of Earth and Environmental Sciences, Cardiff University, Main Building, Park Place, Cardiff, CF10 3AT, United Kingdom.

[2]Geology Department, Faculty of Science, Suez Canal University, Egypt.

Abstract

The SE Mediterranean is a key region documenting the geological history of the Mesozoic Tethys Ocean while comprising one of the most promising provinces in the world in terms of energy resources. Using 2D seismic reflection data tied to exploration wells, this work analyses the Shushan Basin of northern Egypt within a context dominated by continental rifting, ocean propagation, and closure of the Tethys Ocean. Nine (9) seismic megasequences and four (4) major structural trends are identified in the Shushan Basin. In the centre of the basin, the interpreted megasequences document four (4) major tectonic episodes: i) a Palaeozoic early-rift stage, ii) a syn-rift stage lasting from the Early Jurassic to Early Cretaceous, iii) an Aptian-Cenomanian post-rift stage, and iv) a syn-compressional phase that started in the Late Cretaceous and ended in the Miocene. Importantly, the data in this work suggest the presence of up to 1.6 km of Upper Palaeozoic-Triassic strata below the Lower Jurassic Ras Qattara Formation. Widespread extension occurred from the Late Triassic to

Early Cretaceous, a period of time in which graben and half-graben basins were formed and delimited by E-W and NW-SE striking faults. Later in the basin's evolution, mild tectonic reactivation predominated and was accompanied by a (post-rift) thermal episode in Northern Egypt. As a corollary, we show that the tectonic episodes interpreted in this work reflect the position of the Shushan Basin near the junction between the southern margin of the Tethys Ocean, the Syrian Arc system, and the Red Sea continental rift. Consequently, regional faults interpreted in this work are grouped into four distinct families with distinct trends: i) Red Sea, ii) Tethyan, iii) Syrian Arc, and iv) Aqaba.

Keywords: Tethys Ocean; Northwest Desert; Seismic megasequences; Red Sea rifting; Syrian Arc system; basin analysis.

1. Introduction

The SE Mediterranean province is a remnant of the Tethys Ocean, a broad Mesozoic seaway that separated Africa and Eurasia during Mesozoic continental rifting (Stampfli et al., 2001; Garfunkel, 2004; Bosworth et al., 2008, Bakheit et al., 2014; Granot, 2016; Segev et al., 2018). Plate tectonic reconstructions place North Africa as part of a Mesozoic WNW-striking rift axis that developed between Africa, Adria and the Rhodope/Turkish plates (Dewey, 1973; Dercourt et al. 1986; Savostin et al., 1986; Jolivet, 2023). Against this backdrop, continental collision and resulting Variscan orogenesis dominated the Late Palaeozoic evolution of NW Africa, Iberia and NW Europe, and were followed by North Atlantic spreading in the Mesozoic. Alpine-related tectonics has predominated on was the western portion of the Tethys Ocean since the Late Cretaceous (Kley and Voigt, 2008; Skogseid et al., 2000; Granot and Dyment, 2015; Fernandez, 2019; Martín-Chivelet, et al., 2019; Simancas, 2019). In comparison, the Levant region near what are now Syria, Lebanon, Israel and Northern Egypt recorded continental rifting and ocean spreading throughout the Palaeozoic and Mesozoic, before continental collision ensued (Jolivet et al., 2021). The northern and eastern parts of the Tethys Ocean recorded successive episodes of Late Cretaceous-Early Cenozoic compression at first, changing into back-arc extension in a second stage. This led to the fragmentation and subsidence of older mountain belts in Eurasia, particularly near what are now the Aegean Sea, Southern Italy and Southern Turkey (Van Hinsbergen et al., 2020). However, these sa,e episodes affected the North African margin of the Tethys Ocean in diverse ways, with tectonic reactivation and compression being comparatively diffuse (Jolivet et al., 2021; Moustafa, and El-Barkooky, 2024).

Northern Egypt was part of the so-called Mesogean Ocean during the Mesozoic, a putative southern branch of the Tethys Ocean that was split from its northern branch by the relatively large Greater Apulian (or Adria) tectonic plate (Şengör and Yilmaz, 1981; Stampfli and Borel, 2002; Barrier and Vrielynck, 2008; van Hinsbergen et al., 2020). The old Adria tectonic plate is now part of the metamorphic basement units that compose the bulk of Greece (Hellenides) and Turkey (Taurides), and has been more recently subjected to extension, slab roll-back, and orogenic collapse in the Aegean and Libyan seas (Sachpazi et al., 2015; Roche at al., 2019). South of the Libyan Sea, the continental margin of Egypt was less impacted by tectonics and maintained its Mesozoic rift-related structural fabric (Keeley, 1994). All these aspects suggest the establishment of a complex tectonic setting, making it difficult to correlate the evolution of the northern and southern margins of the paleo-Tethys Ocean in tectono-stratigraphic terms. This poses significant limitations to ongoing efforts to find new hydrocarbon and geoenergy resources in the broader, modern SE Mediterranean region.

The Shushan Basin evolved on the passive continental margin of Northern Africa (Mansour et al., 2020; Yousef et al., 2023). It is part of a continuum of basins that spans from the western Alpine Tethys margin of Northwest Africa to the Levant Basin, near Lebanon (Fig. 1). This paper aims to define the main seismic-stratigraphic megasequences of the Shushan Basin as part of this continuum, integrating them within the broader development of the Tethys Ocean, Syrian Arc system and the Red Sea. In summary, this work addresses four main research questions:

a) What are the key seismic-stratigraphic megasequences of the Shushan Basin and their seismic internal characters?
b) Which predominant structural trends controlled the evolution of the Shushan Basin?
c) How do these structural trends relate to the broader geological evolution of the SE Mediterranean province?
d) What specific geological events controlled the thermal and burial histories of the Shushan Basin?

2. Data and Methods

The study area covers 450 km² of Northern Egypt, over the Amoun and Shams oil fields. It is located approximately 150 km to the south of the city of Marsa Matruh (Fig. 1). The seismic data interpreted in this work were shot at a ground altitude varying between 207 m (680 ft) and 230 m (780 ft) above mean sea level (Fig. 2). The acquired seismic signal was sampled with a 4 s interval, 1501 samples per trace, and has a recording window of 6.0 s twtt.

Seismic data were tied in this work to five (5) exploration wells crossing Meso-Cenozoic strata down to the top of the Ras Qattara Formation, a Lower Jurassic syn-rift unit found at a depth varying from 2595 m (8,513 ft) in well Amoun-NE-02, to 4219 m (13,845 ft) in well Amoun-03 (Fig. 2). In addition, a synthetic seismogram was computed to optimize our seismic-well ties; we used density and calibrated sonic-log data to generate a series of reflection coefficients (RCs). These RCs generated the synthetic seismogram in Fig. 3, which was tied to the available seismic data.

The seismic data were tied to borehole stratigraphic markers that span the top of the Ras Qattara Formation (Early Jurassic) to the top of the Khoman Formation (Top Cretaceous). Check-shot velocity data were obtained from wells Amoun-NE-1X and Shams-15 (Fig. 2). Calibrating sonic logs with check-shot velocity data aided our seismic-to-well ties by providing further stratigraphic control to our seismic picks (Fig. 3). Wireline data were also employed to define the internal character of seismic megasequences (Fig. 5). Wireline logs used for such a purpose include gamma-ray (GR), deep resistivity (LLD), shallow resistivity (LLS), density (RHOB), neutron (NPHI), and calliper (CALI) curves.

In the last stage of our analysis, we built a 3D structural model for the study area. This model was interpreted taking into account the known evolutions of the modern-day Eastern Mediterranean region and the Mesozoic Tethys Ocean. It was used to discern the main structural trends in the Shushan Basin, relating them with those recognised in other Northern Egyptian basins (Fig. 4). Structural and isochron maps were also generated to characterise the main tectono-stratigraphic episodes that controlled the Shushan Basin's geological history.

3. Geological setting

3.1 Regional tectonic zones

The Shushan Basin lies in the Western Desert of Egypt along what is the Meso-Cenozoic continental margin of the Afro-Arabian shield (Fig. 1). The Western Desert occupies two-thirds of Egypt, stretching from the Mediterranean Sea's shoreline in the north to the

Sudanese border in the south (Fig. 1). It is approximately 1,000 km long in a N-S direction, and 600 km wide in an E-W direction.

The study area is part of the Egyptian Platform, a geological term referring to the old Mesozoic continental margin that bordered the Afro-Arabian shield into the Levant region (Fig. 1). The Egyptian Platform dips to the north and shows an increase in sediment thickness in the same direction. According to Schlumberger (1984) and Youssef (2003), the Egyptian Platform is divided into five structural zones (Fig. 1):

I) The Craton or Nubian-Arabian Shield of southern Egypt, where exhumed Precambrian rocks predominate. High-grade metamorphic rocks such as gneisses and migmatites are found in this zone along the western bank of the Nile River (Schandelmeier et al., 1987; Azzaz et al., 1994; Stern et al.,1994).

II) The Stable Zone, or Shelf, is characterised by its relatively thin Mesozoic cover, which only partly blankets a Precambrian to Palaeozoic basement (Zaher et al., 2023). Mesozoic strata in this zone reach a maximum thickness of 396 m (1,300 ft) and consist of fluvial clastics. These strata gradually thicken to the north, reaching 792 m (2,600 ft) near the Unstable Zone, which is described below (Schlumberger, 1984; Said, 2017).

III) The Unstable Zone, or Shelf, comprises strata with a maximum thickness of 6,300 m (20,600 ft) near its northern boundary. The study area is located in this zone (Fig. 1). Drilled strata are Upper Palaeozoic to Cenozoic in age and relate to important crustal extension, recording a marked increase in sediment thickness towards the Hinge Zone (Schlumberger, 1984; Keeley, 1989; Abdelazeem et al., 2021).

IV) The Hinge Zone is located between the Unstable Zone and the Nile Delta Cone (Fig. 1). Here, depositional facies and sediment stacking patterns were significantly controlled by a combination of tectonic subsidence and eustasy (Tassy et al., 2015). The Hinge Zone extends along Egypt's modern coastline from North Sinai to East Libya (Fig. 1).

V) The Nile Delta Cone is formed by thick Pliocene-Quaternary strata and reveals two orthogonal NW and NE structural trends (Fig. 1). It is located seawards from a faulted hinge formed below the Nile River mouth and the modern coastline. North of this hinge, faulting created the sediment accommodation space necessary for the development of vast slope-channel systems (Keeley, 1994; Dolson et al., 2005).

3.2 Tectono-stratigraphy of the Western Desert

The Western Desert of Egypt per se is subdivided into two main regions. The first region comprises the Northwestern Desert, which spans the Unstable and Hinge Zones with their thick Meso-Cenozoic strata. The study area is located in one of the principal depocentres of the Northwestern Desert and was affected by multiple phases of tectonic deformation (Mohamed et al., 2016). It reveals distinct structural trends, tilt blocks, and gentle folds, all reflecting a setting dominated by multiple phases of extension and tectonic compression (Krenkel, 1924; Keeley, 1989; Moustafa 2008; Eyal, 2011). The other tectonic region is the Southwestern Desert, where the Stable Zone and Nubian-Arabian Shield are located (Fig. 1). It is characterised by its minor structural complexity and relatively thin Meso-Cenozoic strata. While the Northwestern Desert comprises alternations of marine and continental strata, the Southwestern Desert is dominated by continental units (Schlumberger, 1984).

Three (3) tectonic episodes controlled the evolution of the Shushan Basin and the larger SE Mediterranean province: i) continental rifting in the Permian and subsequent Mesozoic spreading of the Tethys Ocean, ii) tectonic inversion in the Late Cretaceous-Early Eocene associated with closure of the Tethys Ocean and subsequent development of the Syrian Arc system, and iii) rifting of the Red Sea, occurring since the Eocene between the African and

Arabian Plates (Stampfli et al. 2001; Garfunkel 2004; Schlumberger, 1984; Bosworth et al. 2015; Shahar, 1994; Ring, 2003). All in all, the lithostratigraphy of the Northwestern Desert basins can be divided into three main stratigraphic intervals: i) a Cambrian to Cenomanian lower clastic unit, ii) a middle unit composed of Turonian to Eocene carbonates and fine clastics, iii) an upper clastic unit developed from the upper Eocene to the Pleistocene (Fig. 5). In the Northwestern Desert, WEC (1984) and Cheng (2020) have identified important regressive intervals in the Early Triassic (Regressive Systems Tract 1, or RST 1), Early Jurassic (RST 2), Early Cretaceous (RST 3), Early Oligocene (RST 4), and Miocene (RST 5) (Fig. 5). Conversely, marine transgressions are by Late Jurassic (Transgressive Systems Tract 1, or TST 1), Early Cretaceous (TST 2), Late Cretaceous (TST 3), Middle Miocene (TST 4) and Pliocene (TST 5) strata (Fig. 5).

4. Seismic megasequence interpretation

Previous magnetic and gravimetric data from the Shushan Basin have indicated Top Basement at a depth of more than 5000 m, or 16,500 ft (Mohamed et al., 2016; Saada, 2016). This depths is just below some of the wells interpreted in this work; these can be more than 4,000 m long though only reaching the top of Lower Jurassic strata (Fig. 5).

The data interpreted in this paper reveal nine (9) new seismic megasequences and 16 seismic units (SUs) in the Shuchan Basin (Fig. 6). Changes in environmental conditions are tied in this section to the alternating transgressive and regressive systems tracts mentioned in Section 3.2. This allowed us to interpret distinct seismic magesequences bounded by basinwide unconformities and equivalent to stratigraphic Groups (Mitchum et al., 1979; Hubbard et al., 1985). Within these seismic megasequences occur distinct seismic units (SUs) that are correlated, in this work, with particular stratigraphic formations drilled by exploration boreholes. Key seismic horizons interpreted in seismic data are summarised in Fig. 6 and Table 1.

4.1 Megasequence 1: Cambrian(?) to Carboniferous

Megasequence 1 is roughly 0.75 s or 1,600 m (5250 ft) thick and comprises chaotic to moderate-amplitude reflections near its base (Fig. 6). Such a character suggests the presence of siliciclastic deposits in its interior, which were likely eroded from an immature basement relief. Hence, strata in Megasequence 1 reflect relatively short sediment transporting distances (Keeley, 1994; Hamimi et al., 2020). Megasequence 1 comprises the Siwa/Faghour groups (SU1) and the Desouqy Formation (SU2), both composed of alternating shales and sands (Mahmoud et al., 2023). In the study area, the base of SU1 is poorly imaged and the Top Basement horizon was not reached by exploration wells. However, there is still evidence in seismic data for the presence of continuous, moderate-amplitude reflections, offset by younger syn-rift faults, below the Ras Qattara Formation (Figs. 7-10). The base of SU1 is thus interpreted to be the top of the basement in the study area.

The sub-parallel, medium-amplitude strata observed near the top of Megasequence 1 likely correlate with a Late Carboniferous transgression (Fig. 6). Seismic Unit 2 is 1.0 s or 714 m (2,340 ft) thick and contains fluvial-deltaic sediments intercalated with relatively scarce limestones (Schlumberger, 1984) (Figs. 6-9).

4.2 Megasequence 2: Permian to Triassic

Megasequence 2 correlates with the Eghi Group (SU3) of the Sushan Basin (Fig. 6). High- to moderate-amplitude sub-parallel reflections with a moderate frequency predominate in this unit (Fig. 6). Hence, SU3 is roughly 0.20 s or 426 m (1,400 ft) thick and likely comprises fine to coarse-grained clastics deposited after Carboniferous tectonic uplift (Figs. 7-10). It marks a change in depositional environments when compared to SU2; it is a shallowing-upwards sequence in which continental strata predominate (Schlumberger, 1984; Keeley, 1994). The upper part of SU3 reveals a seismic package that is approximately 0.05 s twtt, or 100 m (320 ft) thick, with its parallel high-amplitude reflections suggesting the presence of fine-grained marine strata (Fig. 6).

4.3 Megasequence 3: Jurassic

Megasequence 3 is up to 0.65 s twtt or 1,300 m (4,250 ft) thick and comprises three distinct seismic units correlated with the Ras Qattara (SU4), Khatatba (SU5) and Masajid (SU6) formations (Fig. 6). Megasequence 3 is here recognised as a promising unconventional shale gas target in the Shushan Basin. The Lower Jurassic Ras-Qattara Formation (SU4) is imaged as an irregular, low-amplitude, and low-frequency interval (Fig. 7). It records the accumulation of coarse-grained clastic sediments during the Early Jurassic (Shalaby et al., 2011). The Middle Jurassic Khatatba Formation (SU5) shows high-amplitude, continuous internal reflections and a maximum thickness of 0.25 s, or 537 m (1765 ft) (Fig. 6). This unit is composed of shales and sands throughout the Northwestern Desert (Gentzis et al., 2018).

The Masajid Formation (SU6) is uppermost Jurassic in age and can be found throughout the study area (Figs. 6 and 7). It is defined by its moderate to low-amplitude, sub-parallel internal reflections (Fig. 7-10). Low-frequency reflections, roughly 0.50 s or 104 m (342 ft) thick, are associated with cyclic changes in depositional environment. They relate to the presence of alternating marine carbonates (oolitic, reefal and dolomitic limestone) and shales in SU6 (MA, 1982; Schlumberger, 1984; Dolson et al., 2001; Bakr, 2009; Abdelazeem et al., 2021).

The top of SU6 coincides with an erosional unconformity of regional expression associated with a phase of renewed normal faulting (Fig. 6). Marking the Jurassic-Cretaceous boundary, this same unconformity is recorded from Lebanon to Libya, i.e. along the whole of the SE Mediterranean province, and also in southern Europe and Turkey (Schlumberger, 1984; Bosellini and Morsilli, 1997; Tlig, 2015; Vincent et al., 2018; Maksoud et al., 2020; Yousef et al., 2023).

4.4 Megasequence 4: Berriasian to Lower Aptian

Megasequence 4 comprises one single seismic unit (SU7), the Alam El-Bueib Formation, also named *Shushan Formation* in the Northwestern Desert (Figs. 7-10). This SU7 is composed of regular and parallel, high-frequency, moderate-amplitude reflections (Fig. 6). It is 0.40 s, or 900 m (2,960 ft) thick, correlating with the presence of shale, argillaceous sandstone and limestone in its interior (Ramadan et al., 2016; Makled and Shazly, 2023).

Multiple half-graben and graben basins were formed in the Early Cretaceous, and imposed a general E-W structural trend to the whole of the Northwestern Desert, including the Shushan Basin (Bosworth et al., 2008; Moustafa, 2008; Shehata et al., 2018). Consequently, the Alam El-Bueib Formation (SU7) is a good hydrocarbon source interval in the Western Desert (Alsharhan and Abd El-Gawad 2008).

4.5 Megasequence 5: Aptian to Cenomanian

Megasequence 5 is divided into three seismic units, the Alamein (SU8), Dahab-Kharita (SU10), and Bahariya (SU10) formations (Fig. 6). The Alamein Formation (SU8) is a key reservoir interval in the Western Desert due to its high secondary porosity and permeability (Elsheikh et al., 2021). It is capped by shales in the Dahab and Kharita Formations (SU9).

Seismic Unit 8 (SU8) is identified in the lower part of Megasequence 5 and comprises 0.10 s or 125 m (411 ft) of dolomites. It is an important interval as it forms a prominent seismic marker throughout the Northwestern Desert. Seismic Unit 8 (SU8) is characterised by its high-amplitude, low-frequency continuous reflections (Fig. 6).

The Bahariya Formation (SU10) is identified towards the top of Megasequence 4 and shows regular internal seismic reflections with high amplitude and high frequency (Fig. 6). It contains thin beds of limestone, fine sand, and shale (Catuneanu et al., 2006; Mansour et al., 2020). This interval is up to 0.50 s or 776 m (2,550 ft) thick and marks a Cenomanian transgression maximum. Both the Kharita (SU9) and Bahariya (SU10) formations are good reservoir intervals in the Western Desert (Mansour et al., 2020).

4.6 Megasequence 6: Turonian to Maastrichtian

Megasequence 6 includes the Abu-Roash Group (Turonian) and the Khoman Formation (Maastrichtian) in its interior (Fig. 6). The Abu-Roash Group (SU11) has a maximum thickness of 0.50 s or 648 m (197 ft), revealing sub-parallel, moderate to low-amplitude, low-frequency internal reflections (Fig. 6). SU11 is composed of alternating carbonates and fine sands (Abdelhady and Mohamed, 2017; Shehata et al., 2023). It exceeds 1000 m or 3,280 ft in the Abu Gharadiq Basin where is sub-divided into its typical seven rock members (A-G) (Khalek et al., 1989) (Fig. 1). However, exploration wells only found the Abu-Roash C-G members in the study area.

Uppermost Cretaceous strata in Megasequence 6 belong to the Khoman Formation (SU12), a carbonate interval reaching a thickness of 0.30 s or 613 m (2,014 ft) (Figs. 6-9). This SU12 shows internal reflections with low continuity, frequency and amplitude (Fig. 6). Uppermost Cretaceous strata relate to a transitional phase between Jurassic continental rifting and the episodes of tectonic compression that formed the Syrian Arc system (EGPC, 1992; Sarhan and Basal, 2020; Elhossainy et al., 2022).

4.7 Megasequence 7: Paleocene-Oligocene

A regional unconformity separates Megasequence 7 from Upper Cretaceous strata below (Figs. 7-10). Megasequence 7 comprises a single seismic unit (SU13) with low continuity and amplitude (Fig. 6). A maximum 0.10 s or 142 m (465 ft) of strata are recognised in the study area despite the fact that no cores have been retrieved from SU13 (Figs. 7-10). In other parts of the Northwest Desert, this same units is relatively thick and correlates with the Esna (Paleocene), Thebes (Lower to middle Eocene) and Mokattam (Middle Eocene) formations (Figs. 7-10). These formations comprise white chalky, cherty limestone and dolomite deposited in tidal-flat to open shelf-slope environments (Sheikh Faris, 1985; Shahin et al., 2023).

Early to Middle Eocene carbonates are overlain by fine- to coarse-grained continental deposits marking an Early Oligocene regressive episode. These regressive strata are included in the Ghoroud (or Dabaa) Formation (Schlumberger, 1984; Farouk and Khalifa, 2010), and are recognised as part of SU13 in this work. Tectonic compression and uplift led to the erosion of a significant portion of this unit, as documented by the prominent erosional unconformity at its top (Figs. 7-10).

4.8 Megasequence 8: Miocene

Megasequence 8 correlates with the Marmarica Formation (SU14), a dolomitic interval overlying the clastic Mohgra Formation in the Qattara Depression (Albritton et al., 1990; Anan et al., 2022). The unit is around 0.25 s or 355 m (1,146ft) thick and characterised by its amplitude contrast with SU13. Internal reflections in SU14 are continuous and bright. This unit documents a phase of tectonic uplift in the Shushan Basin, occurred from Late Eocene to the Late Miocene, that accompanied a gradual sea-level drop (Georgalis et al., 2020, Anan et al., 2022) (Figs. 7-10).

4.9 Megasequence 9: Pliocene-Quaternary

Pliocene-Quaternary strata only occur near the northern limit of the Northwestern Desert, where the El-Hammam Formation (SU 15) is composed of sandstone, sandy fossiliferous limestone and detrital limestone accumulated in nearshore environments (Schlumberger, 1984). In seismic data, SU15 comprises sub-parallel internal reflections with poor continuity (Fig. 6). It reaches a thickness of 0.30 s or 426 m (1,400 ft) in the Shushan Basin (Figs. 6-9). Its offshore equivalent is the Kurkar Formation, composed of marls and shales filling deep-water basins on the modern continental slope (Reda et al., 2022).

5. 3D structural model

Tectonic faults in the Shushan Basin were interpreted and subsequently used to build a 3D structural model on Petrel®. In addition, we mapped the boundaries of the nine (9) interpreted megasequences, and Marmarica (Miocene) formations, and exported them to the 3D structural model (Figs. 11-14). Time-structural maps for these seismic horizons reveal distinct fault strikes and a generalised deepening-upwards trend in the Mesozoic due to continental rifting. In contrast, uplift and gentle folding is recognised between the Late Cretaceous and Early Eocene in the NE of the study area (Fig. 13). Through these tectonic phases, the southeastern part of the study area was always located at the southern shoulder of the Shushan Basin.

Isochron maps for the Ras-Qattara (Jurassic), Alam El-Buieb (Lower Cretaceous), and Khoman (Upper Cretaceous) formations, reveal important thickness variations near faults (Figs. 15 and 16). In contrast, the Masajid (Upper Jurassic), Alamein (Upper Aptian), Upper Baharia (Lower Cenomanian), and Abu-Roash (Turonian) formations show minor changes in thickness, and essentially mark periods of tectonic quiescence (Figs. 17 and 18).

Isochron data for the Ghoroud (Oligocene), and Marmarica (Miocene) formations clearly document the end of Early Cretaceous continental rifting. Minor changes in stratal thickness are observed on the isochron maps in Fig. 19. This lack of growth strata in relates to the start of uplift and tectonic compression in the study area, following widespread tectonic inversion in the Levant region.

The Jurassic Megasequence 3 was chosen to exemplify the structural framework of the Shushan Basin (Fig. 20). Faults show variable lengths, from minor faults with a few hundred meters to major faults that are 10 km long (Fig. 20). Fault frequency was measured for each main fault strike and projected in relation to the geographic north (Fig. 21). In addition, fault length was measured and expressed as a percentage to reveal the total length of faults in each direction vs. the total length of faults in all directions. All in all, length frequencies reveal the predominant strikes, with the largest number and longest faults, in a study area. Faults' length frequency, as measured in this work, can be expressed as:

$$\text{Length frequency} = \frac{\text{total length of faults in each direction}}{\text{total length of faults in all directions}}$$

In terms of their frequency, the study area shows a high number of faults that strike to the W and NW (10 faults in total). In comparison, six (6) faults strike to the NNE, and four (4) faults to the NE (Fig. 21a). Most of the faults show a NNE strike (35%), while NE-striking faults have the lowest ratio (7%) (Fig. 21b). In conclusion, E-W faults are the most common and the longest in the Shushan Basin.

6. Well stratigraphic correlations

In this section we use the seismic unit (SU) nomenclature adopted in Section 4 so to relate seismic and borehole units in a direct, straightforward way.

Megasequence 3 comprises three distinct units, the Ras Qattara (SU4), Khatatba (SU5) and Masajid (SU6) formations. The Lower Jurassic Ras Qattara Formation (SU4) documents thickness changes during the early stages of Mesozoic continental rifting (Figs. 22 and 23d). However, the top of the Ras Qattara Formation was only drilled in well Amoun-1, where it shows high gamma-ray values. Density and neutron-log are relatively low (Fig. 23d). Above SU4, the Khatatba Formation (SU5) records a moderate to high gamma-ray and moderate density, correlating with the presence of shales and sands in its interior (Fig. 23).

The top of Khatatba Formation (SU5) is marked by an increase in calliper readings where consolidated strata with low permeability are found. In contrast, the Masajid Formation (SU6) records low gamma-ray values but a high density, a character correlating with the presence of limestone and dolomite in its interior (Fig. 23).

Well Amoun-NE-03 documents a sharp increase in the thickness of Megasequence 4 (Fig. 23c). Gamma-ray curves show abrupt variations, which are typically observed in interbedded shales and sands. In comparison, the density and neutron logs vary moderately across the megasequence. Calliper logs reveal a sharp increase at the top of the unit (Fig. 23c).

Megasequence 5 is marked by its relatively high resistivity readings, particularly at the base of the Alamein (SU8) and Bahariya (SU10) formations (Fig. 23b). These two intervals comprise conventional oil reservoirs in the study area. The Alamein Formation (SU8) shows a characteristic signature of dolomitic reservoirs: high density values against low gamma-ray, neutron, and calliper readings (Fig. 23b). This same Alamein Formation is then sealed by a thin shaley interval with relatively high gamma-ray values, the Dahab Formation (lower SU9) (Fig. 23b). In contrast, the gamma-ray curves reveal alternating high and low values in the overlying Kharita Formation (upper SU9), suggesting the presence of interbedded shale and sand in this unit. Seismic Unit 10 (Bahariya Formation) shows moderate to high gamma-ray values and a moderate resistivity, reflecting the presence of medium- to fine-grained clastics (Fig. 23b). Finally, calliper logs reveal that the upper boundary of Megasequence 5 (SU10) correlates with a sharp increase in borehole diameter. This SU10 also reveals low gamma-ray values in the carbonate-rich parts of the Bahayria Formation (Fig. 23b).

Megasequence 6 documents minor changes in thickness, thus confirming that tectonic quiescence predominated in the Sushan Basin for a time before the onset of Syrian Arc compression in the Late Cretaceous (Fig. 23a). Megasequence 6 consists of the Abu-Roash Group (SU11) and the Khoman Formation (SU12). The Abu-Roash Group reveals moderate to high gamma-ray values and the calliper curves divides it into five of its characteristic members, C to G (Fig. 23a). The Khoman Formation (SU12) coincides with the upper part of Megasequence 6 and records low to moderate gamma-ray values, low resistivity, and relatively high calliper readings. These readings are associated with the presence of carbonate intervals in SU12.

7. Thermal and burial history models

Burial and thermal models were computed for well Amoun-NE-3 using PetroMod® (Fig. 24 and Supplementary File 1). This well was found to be the most complete in terms of the stratigraphic and wireline information it provides. It targeted a broad footwall block occurring to the NW of faults D1 to D5 (Figs. 11-14) and drilled as far as the top of the Ras Qattara Formation (Lower Jurassic).

Well Amoun-NE-3 reveals a period of enhanced subsidence at the start of Early Jurassic continental rifting, with discrete pulses predominating in the region until the Early Cretaceous (Fig. 24). In the Late Cretaceous and Paleogene, tectonic compression related to the Syrian Arc resulted in minor exhumation of the Shushan Basin. This uplift event was followed by a younger stage of tectonic subsidence, which was accompanied by a regional thermal pulse occurring from the end of the Oligocene until the present day (Fig. 24). Thermal models thus reveal that Jurassic and older strata reached the oil and gas windows in the Early Cretaceous, with the oil-prone Khatatba Formation (SU5) first entering the oil window in the Late Cretaceous, and for a second time in the Miocene (Fig. 24). Thermal conductivity was secured at a regional scale by the porous, siliciclastic Upper Palaeozoic succession (Fig. 24). At present, the top of the Ras Qattara Formation records bottom-hole temperatures near 135ºC, while Upper Palaeozoic and older units are modelled as reaching temperatures of around 180ºC (Fig. 24).

8. Fault families in the Shushan Basin

Four major fault families (A-D) are identified in the study area, as shown in Fig. 25. These faults follow the main structural trends of the Unstable Zone of northern Egypt (Fig. 26). Hence, fault families were labelled using a nomenclature that stresses their orientations relative to principal geological features, or regions, rather than referring their chronological order.

8.1. Fault family A (Red Sea trend)

Fault Family A strikes to the NW and follows what is known as the Gulf of Suez or Red Sea trend (Figs. 25 and 26). A total of 10 faults with a length frequency of 28% compose this family in the study area. Hence, Fault Family A is not the most frequent. The Red Sea trend relates to a basement structural fabric developed during Precambrian subduction. This fabric was reactivated during the rifting of the Red Sea, particularly so in eastern Egypt (Mart and Hall, 1984; El Gaby et al., 1987; Meshref, 1990; Bakheit et al, 2014).

8.2 Fault family B (Tethyan trend)

This second family of faults is E-W striking and parallel to the so-called Mediterranean or Tethyan trend (Figs. 25 and 26). It is the dominant family in the Shushan Basin and comprises faults striking N70 to N110. It is known to be one of the principal and oldest tectonic trends in northern Egypt (El-Shazly, 1966, 1977; Bakheit et al, 2014, Said, 2017). Fault Family B relates to the Early Jurassic reactivation of Late Precambrian structures (Meshref and El-Sheikh, 1973; Meshref, 1982; Youssef et al., 1998). In the study area, it is formed by 10 faults with a length frequency of 30%.

8.3. Fault family C (Syrian Arc trend)

Fault Family C relates to the so-called Syrian Arc System, also known as the North Sinai fold trend (Figs. 25 and 26). This family strikes N45 to N60, comprises four (4) faults, and reveals a length frequency of 7%. Fault Family C documents a phase of tectonic compression that started in the Late Cretaceous, itself responsible for folding and thrusting throughout northern Egypt (Moustafa and El-Barkooki, 2024). This broad zone of compression extends towards eastern Libya and the Sinai Peninsula (El-Shazly et al., 1966 1977; Halsey, and Gardener, 1975; Kuss et al., 2000; Moustafa, 2013; Ibraheem et al., 2018; Gaber, 2022).

8.4. Fault family D (Aqaba trend)

Fault Family D correlates with the Aqaba trend, which comprises structures that strike N05 to N20 (Figs. 25 and 26). In the study area, fault Family D comprises six (6) faults for a length frequency of 35%. The Aqaba trend is associated with the left-lateral tectonic movements thataffected East Egypt before the onset of Oligocene rifting of the Red Sea and

Gulf of Suez (Youssef, 1968; Halsey, and Gardener, 1975; Lyberis, 1988; Bakheit et al, 2014; Ibraheem et al., 2018).

9. Discussion

9.1 Main tectonic stages controlling the evolution of the Shushan Basin

The tectonic evolution of the study area is summarised in Fig. 27, where regional-scale changes in stress directions are summarised from the Palaeozoic to the Quaternary.

9.1.1 Early syn-rift stage (Late Palaeozoic)

The Shushan Basin was influenced by the NW-striking faults during the Palaeozoic and, consequently, deposition was controlled by Fault Family A, a Late Precambrian basement trend (Keeley, 1989; Elkhodary and Youssef, 2013; Bakheit et al, 2014; Granot, 2016) (Fig. 27a). Megasequence 1 was deposited over an unconformable surface that marks the top of the Precambrian basement, but Fault Family A does not show significant changes in thickness across any of the mapped faults. Nevertheless, the depth to basement was re-interpreted here to reveal the presence of thick Upper Palaeozoic and Triassic strata in the Sushan Basin, as also identified in other parts of the Northwestern Desert (Keeley, 1994).

Strata in Megasequence 1, including the Siwa/Faghour Groups (SU1) and the Desouqy Formation (SU2), were likely accumulated during an early phase of subsidence characterised by the broad, regional sagging of the Northwestern Desert. The end of this stage is marked by an erosional surface topping the Carboniferous Desouqy Formation (SU2) (Fig. 6).

9.1.2 Syn-rift I (Triassic – Jurassic)

The Early Mesozoic Megasequences 2 and 3 reflect N-S directed extension that resulted in the generation of E-W faults (Figs. 27b and 28a). Late Triassic-Early Jurassic strata mark the start of the extensional tectonics commonly associated with the first stage of Gondwana rifting, and is herein called Syn-rift I (Stampfli et al. 2001; Garfunkel 2004; Bosworth et al. 2008, Bakheit et al, 2014). At this time, Megasequences 2 and 3 formed under the influence of transgressive and regressive cycles in sea level, which deposited alternating clastic and carbonate strata. Isochron data for the Ras Qattara Formation (Lower Jurassic) denote changes in thickness around active faults, i.e. important syn-rift tectonic subsidence (Fig. 15). In contrast, the Masajid Formation (SU6) reveals minor changes in thickness near the same faults, suggesting that Syn-Rift 1 ended in the Late Jurassic (Tlig, 2015; Maksoud et al., 2020; Yousef et al., 2023) (Fig. 17). The end of Syn-rift I is documented by an erosional unconformity spanning the whole of the Northwestern Desert (Fig. 6).

9.1.3 Syn-rift II (Early Cretaceous)

The Early Cretaceous documents a rotation in the direction of crustal extension throughout NE Africa, resulting in renewed tectonic subsidence (Fig. 27c). This second phase of rifting, Syn-rift II, generated E-W faults not only in the study area (Fault Family B), but also in the Abu Gharadig and Ginidi basins (El-Shazly, 1966 1977; Bosworth et al., 2008; Moustafa, 2008; Elkhodary and Youssef, 2013; Bakheit et al, 2014, Said, 2017) (Fig. 1). Once again, crustal extension generated a series of half-grabens filled by syn-rift wedges ('growth strata') (Figs. 7-10). Isochron and well data for the Early Cretaceous Alam El-Buieb Formation (SU7) record significant strata growth around active normal faults (Fig. 14).

9.1.4 Post-rift stage (Aptian to Cenomanian)

The Late Aptian-Cenomanian marks the end of tectonic extension in the SE Mediterranean. As a result, Megasequence 5 records only slight changes in thickness in the Late Aptian Alamein (SU8) and Cenomanian Bahariya (SU10) formations (Figs. 17-18). Still in Megasequence 5, a carbonate interval in SU10 records a Cenomanian transgression maximum in the Northwestern Desert (Catuneanu et al., 2006; Cheng, 2019) (Fig. 17b). Overall, Megasequence 5 materialises a post-rift phase and is characterised by its good reservoir and trap potential in units such as the Alamein Formation, one of the main hydrocarbon reservoirs in the Northwestern Desert (Elsheikh, et al, 2021).

9.1.5 Compressional phase I (Late Cretaceous- Early Eocene)

The Shushan Basin was affected by compressional episodes from the Late Cretaceous to the Early Tertiary that were related to tectonic convergence between Africa, the Arabian Plate, and Eurasia (Shahar, 1994; Eyal, 2011). Tectonic movements formed what is known as Syrian Arc System and resulted in the reactivation (and mild inversion in some areas) of syn-rift faults, particularly those in Fault Family C (Figs. 27d and 28b). Tectonic compression formed local folds in Megasequence 6 and an erosional unconformity at the top of the Baharyia Formation (Cenomanian). Isochron and well data from the Turonian Abu-Roash Formation (SU11) reveal minor changes in thickness and the end of normal fault propagation (Fig. 18b). In addition, the absence of Abu-Roach members A and B in the study area confirmed the importance of Late Cretaceous tectonics in the Shushan Basin. Similarly to other regions of the Eastern Mediterranean, local tectonic exhumation at the end of the

Cretaceous led to the erosion of parts of the Abu-Roach Group, and the effective loss of members A and B in the study area.

9.1.6 Compressional phase II (Late Eocene-Miocene)

The last episode of compression recorded in the Shushan Basin relates to the opening of the Gulf of Suez and Red Sea, when the Arabian Plate started to separate from the African Plate in the Oligocene-Early Miocene (Fig. 29a). Some authors have also suggested a second phase of Syrian Arc compression affecting Northern Egypt during the Miocene (Shahar, 1994; Ring, 2003; Moustafa and El-Barkooky, 2024). At this time, the Shushan Basin experienced gentle folding in the northeastern part of the study area, with tectonic uplift affecting Megasequences 1 to 8 (Fig. 8). In particular, the top of Megasequence 8 (Marmarica Formation) shows enhanced erosion on existing structural highs (Figs. 7-10), a character also recorded in other parts of the Northwestern Desert (Abdelazeem et al., 2021).

Compressional Phase II also relates to the presence of a series of intrusive and extrusive basalts in the Unstable Zone near some of the inverted structures associated with the Red Sea and Gulf of Suez opening (Schlumberger, 1984; Robertson et al., 2009; Bosworth et al. 2015). This magmatic event provided a renewed, additional heat source for North Egypt's basins, leading to further kerogen maturation (Fig. 24).

9.2. Tectono-stratigraphic markers of a common geological evolution in the Tethys Ocean realm

The tectono-stratigraphic analysis in the previous section reveals important details about the history of the SE Mediterranean province. It confirms that the Shushan Basin is one of the oldest basins in the region. It also shows its similarities with the tectono-stratigraphic evolution of other Mediterranean and North Atlantic basins.

The published tectono-stratigraphic models for the Matruh Basin, Northwestern Desert, consider four major tectonic stages affecting this latter region a) a syn-rift Jurassic-Barremian syn-rift stage, b) an Aptian-Coniacian post-rift stage, c) Santonian-Middle Eocene basin inversion and d) Eocene basin inversion (Yousef et al., 2023). Tectono-stratigraphic models for the Shushan and Matruh basins confirm that the onset of Mesozoic continental rifting coincides with the events that led to the opening of the Tethys Ocean. However, the data in this work also suggest that the Shushan Basin started its development in the Late Palaeozoic, and that syn-rift tectonics continued towards the early Mesozoic. This agrees with data in Jagger et al. (2020), who addressed the evolution of syn-rift basins in Northeast Libya. In similarity with the data in this work, the Northeast Libyan basins document a Late-Palaeozoic rift onset, important Mesozoic extension, and mild basin inversion starting in the Late Cretaceous. As in Northern Egypt, Syrian Arc compression resulted in gentle folding and local exhumation along the northern margin of Cyrenaica (East Libya).

The early syn-rift stage records two main regional unconformities in the study area: a) a first unconformity at the top of Carboniferous strata, and b) a second coinciding with the top of Upper Permian-Triassic strata. Both unconformities can be correlated with collisional stages of the Late Palaeozoic Variscan belt (Matte, 2001; Simancas, 2019). In parallel, southern Europe was also affected by extensional tectonics from the end of the Triassic to Early Cretaceous times, in a tectonic phase extending into the Arctic-North Atlantic and the Tethys Ocean margins. Extensional tectonics is recorded at this time around the Iberian microplate and induced salt tectonics in some basins (Ziegler, 1987; Alves et al., 2002;

Fernandez, 2019; Martín-Chivelet, et al., 2019). Late Triassic to Late Jurassic rifting can be correlated to a principal phase of continental rifting in Northern Africa, itself associated with rifting and subsequent continental break-up of the Ionian, Herodotus and Levant pull-apart basins (Channell et al., 2022).

The second syn-rift stage in the Shushan Basin coincides with the onset of seafloor spreading during the Early Cretaceous, which finally opened an ocean at the Atlantic margin of NW Europe and a series of minor seas in what is now the Alpine region of central Europe (Knott et al., 1993; Skogseid et al., 2000; Granot and Dyment, 2015; Channell et al., 2022). In the Late Cretaceous and Tertiary, Alpine orogeny resulted in fault reactivation and mild inversion of the Mesozoic grabens, with fold-and-thrust systems formed at that time in Central and Southern Europe. This phase may be partly correlated to Fault Family A in the study area (Ziegler, 1987; Neubauer et al., 2003; Kley and Voigt, 2008). Based on a velocity model from NE Algerian margin, Arab et al. (2016) suggested that basin inversion occurred before basin rifting in the Late Oligocene, generating NW striking faults with lateral (strike-slip) during the Lesser Kabylia mountains rise in the North Algeria. Similar fault trends were recently identified in parts of Northern Egypt by Moustafa and El-Barkooky (2024) in structures that match Fault Family A (Red Sea trend) in the Shushan Basin. Tectonic inversion was recognised by Moustafa and El-Barkooky (2024) as having started at the end of the Cretaceous, but the data in this work confirms Fault Family A was also reactivated in Oligocene-Miocene times during the opening of the Gulf of Suez and Red Sea. Additionally, Miocene volcanism in Northern Algeria and Levant Basin can also be partly synchronous with the magmatic intrusions recorded across Northern Egypt. Generally, convergence between Africa and Eurasia reactivated pre-existing faults and caused local thrusts and uplift near Africa’s Mediterranean margins, thus documenting the closure of the Tethys Ocean and the birth of the Mediterranean Sea as an endorheic basin.

At a regional scale, the Shushan Basin is thus interpreted in this work as recording a Late Palaeozoic pre-rift stage, which developed into the fully-fledged Syn-rift I during the Triassic and Early Jurassic. A second rifting stage (Syn-rift II) started in the Early Cretaceous and coincides with the opening of the Levant Basin. While the pre-rift and Syn-rift I phases can be associated with rifting and later opening of the Herodotus basin (part of the southern Tethys Ocean) in the Palaeozoic and early Mesozoic, Syn-Rift II is likely associated with the opening of the Levant Basin in the Cretaceous (see Brew et al.; 2001; Gvirtzman et al., 2011; Granot, 2016; Segev et al. 2018). The extensional tectonics associated with the formation of the Herodotus basin resulted in an increase in accommodation space along the old shoreline of the Tethys Ocean, near the study area. For the older megasequence in this work (Megasequence 1), we suggest the presence of coarse siliciclastic deposits eroded from an immature basement relief. In contrast, the opening of the Levant Basin is recorded, in the study area, by a deepening-upwards marine setting that preceded tectonic reactivation and local uplift at the start of Syrian Arc tectonics (Late Cretaceous).

10. Conclusions

The Shushan Basin was influenced by multiple syn-rift episodes, which were followed by fault reactivation and uplift associated with Syrian Arc compression. This work proves that the stratigraphy of the Shushan Basin can be divided into nine (9) seismic-stratigraphic megasequences spanning the previously defined lower clastic, middle carbonate, and upper clastic units. These megasequences correlate with the main tectonic events that controlled the evolution of the Shushan Basin and are bounded by regional unconformities present throughout the Western Desert of Egypt. Main conclusions of this work are as follows:

a) Seismic data suggest the presence of thick Palaeozoic strata below the Mesozoic rift depocentres mapped in this work. This observation is important as it opens new petroleum and geothermal energy plays in the Western Desert of Egypt.

b) The Shushan Basin evolved as a series of half-graben and graben depocentres from Early Jurassic to the Early Cretaceous. These depocentres were deeper towards the north and formed in response to continental rifting of Gondwana and subsequent Tethys Ocean opening. Graben and half-graben depocentres were, at this time, E-W striking.

c) A first phase of fault reactivation is recorded in the Late Cretaceous. Compressional episodes related to the closure of the Tethys Ocean near the Levant, and subsequent evolution of the Syrian Arc System, were responsible for fault reactivation and tectonic uplift in North Egypt and East Libya. In the study area, the gentle (forced) folding and reactivation of syn-rift structures generated efficient hydrocarbon traps.

d) The Oligocene-Miocene boundary coincided with the last episode of tectonic reactivation in the Shushan Basin. Tectonic reactivation at this time relates to continental rifting, and later opening of the Red Sea and Gulf of Suez, and occurred in response to left-lateral strike-slip movements between the Arabic Plate and Africa.

e) Cenozoic tectonics is associated with basaltic intrusions near source intervals in the Northwestern Desert. These magma intrusions are key to the maturation history of source rocks in the Jurassic Khatatba Formation (SU5). They also enhance thus-far untapped geothermal prospects in the Shushan Basin.

As in a great part of the Levant region, the Late-Cretaceous-Cenozoic compressional episodes that affected the Shushan Basin were able to generate new structural traps and, eventually, new migration paths for hydrocarbon generated from Mesozoic and putatively Palaeozoic source rocks. Basin inversion was therefore responsible for: 1) the mild reactivation of rift-related normal faults and (2) very moderate forced folding of the Meso-

Cenozoic overburden against structural buttresses such as the footwalls adjacent to normal faults. If one assumes the presence of a Palaeozoic energy play in the Shushan Basin, particularly one that is similar to East Libya's, some of the deeper structures observed in seismic broaden the range of potential traps for hydrocarbons and geothermal heat. All in all, the absence of significant exhumation in the Shushan basin, and the younger Late Cenozoic thermal pulse recorded by thermal models in the region, favoured source rock maturation and reservoir rock preservation. Consequently, untapped Lower Jurassic and Late Palaeozoic strata - blanketed by relatively thick strata - show great potential for natural gas and geothermal-heat generation.

Acknowledgements

The Egyptian Mission Sector is acknowledged for its support to A. Albrkawy's PhD project. We sincerely thank the Egyptian General Petroleum Corporation (EGPC) and the Khalda Petroleum Company for their data provision of Amoun and Shams oil fields. We thank Schlumberger for software support to the 3D Seismic Lab, Cardiff University. Editor M. Fetter, O. Fernandez and two anonymous reviews are acknowledged for their constructive comments, which significantly improved early drafts of this work.

References

Aal, A.A., El Barkooky, A., Gerrits, M., Meyer, H., Schwander, M., Zaki, H. (2000). Tectonic evolution of the Eastern Mediterranean Basin and its significance for hydrocarbon prospectivity in the ultradeepwater of the Nile Delta. The Leading Edge, 19(10), 1086-1102. https://doi.org/10.1190/1.1438485

Abdelazeem, M., Fathy, M.S., Gobashy, M. (2021). Magnetometric identification of sub-basins for hydrocarbon potentialities in Qattara Ridge, North Western Desert, Egypt. Pure and Applied Geophysics, 178(3), 995-1020. https://doi.org/10.1007/s00024-021-02678-2

Abdelhady, A.A., Mohamed, R.S. (2017). Paucispecific macroinvertebrate communities in the Upper Cretaceous of El Hassana Dome (Abu Roash, Egypt): environmental controls vs adaptive strategies. Cretaceous Research, 74, 120-136. https://doi.org/10.1016/j.cretres.2017.02.014

Albritton Jr, C.C., Brooks, J.E., Issawi, B., Swedan, A. (1990). Origin of the Qattara depression, Egypt. Geological Society of America Bulletin, 102(7), 952-960. https://digitalcommons.usf.edu/kip_articles/4111

Alsharhan, A.S., Abd El-Gawad, E.A. (2008). Geochemical characterization of potential Jurassic/Cretaceous source rocks in the Shushan Basin, northern Western Desert, Egypt. Journal of Petroleum Geology, 31(2), 191-212. https://doi.org/10.1111/j.1747-5457.2008.00416.x

Alves, T.M., Gawthorpe, R.L., Hunt, D.W., Monteiro, J.H. (2002). Jurassic tectono-sedimentary evolution of the Northern Lusitanian Basin (offshore Portugal). Marine and Petroleum Geology, 19(6), 727-754. https://doi.org/10.1016/S0264-8172(02)00036-3

Anan, T., Reda, A., El Belasy, A., El-Shahat, A. (2022). Facies analysis and sequence stratigraphy of the Middle Miocene Marmarica Formation at Siwa area, north Western Desert, Egypt. Geological Journal, 57(7), 2749-2769. https://doi.org/10.1002/gj.4437

Arab, M., Rabineau, M., Déverchère, J., Bracene, R., Belhai, D., Roure, F., Marok, A., Bouyahiaoui, B., Granjeon, D., Andriessen, P., Sage, F. (2016). Tectonostratigraphic evolution of the eastern Algerian margin and basin from seismic data and onshore-offshore correlation. Marine and Petroleum Geology, 77, 1355-1375. https://doi.org/10.1016/j.marpetgeo.2016.08.021

Azzaz, S.A., Soliman, M.M., Sabet, A.H., El-Tokhy, M., Elbaroudy, A.F. (1994). Pan African basement of Bir Safsaf Area East Sahara African craton. Qatar University Science Journal, 14 (1), 172-183. https://qspace.qu.edu.qa/handle/10576/9861

Bakheit, A.A., Abdel Aal, G.Z., El-Haddad, A.E., Ibrahim, M.A. (2014). Subsurface tectonic pattern and basement topography as interpreted from aeromagnetic data to the south of El-Dakhla Oasis, western desert, Egypt. Arabian Journal of Geosciences, 7, 2165-2178. https://doi.org/10.1007/s12517-013-0896-3

Bakr, M.M. (2009). Molecular organic geochemistry of crude oil from Shushan and Abu Gharadig basins, Western Desert, Egypt. Earth Sciences, 20(2). http://dx.doi.org/10.4197/Ear.20-2.6

Barrier, E., Vrielynck, B., Bergerat, F., Brunet, M.F., Mosar, J., Poisson, A., Sosson, M. (2008). Palaeotectonic maps of the Middle East: Tectono-sedimentary-palinspastic maps from Late Norian to Pliocene. Middle East Basins Evolution Programme, CGMW, Atlas, 2008, Maps, pp. 1-14.

Bosellini, A., Morsilli, M. (1997). A Lower Cretaceous drowning unconformity on the eastern flank of the Apulia Platform (Gargano Promontory, southern Italy). Cretaceous Research, 18(1), 51-61. https://doi.org/10.1006/cres.1996.0049

Bosworth, W., El-Hawat, A. S., Helgeson, D. E., Burke, K. (2008). Cyrenaican “shock absorber” and associated inversion strain shadow in the collision zone of northeast Africa. Geology, 36(9), 695-698. https://doi.org/10.1130/G24909A.1

Bosworth, W., Stockli, D.F., Helgeson, D.E. (2015). Integrated outcrop, 3D seismic, and geochronologic interpretation of Red Sea dike-related deformation in the Western Desert, Egypt–the role of the 23 Ma Cairo “mini-plume”. Journal of African Earth Sciences, 109, 107-119. https://doi.org/10.1016/j.jafrearsci.2015.05.005

Brew, G., Barazangi, M., Al-Maleh, A. K., Sawaf, T. (2001). Tectonic and geologic evolution of Syria. GeoArabia, 6(4), 573-616. https://doi.org/10.2113/geoarabia0604573a

Brune, S., Autin, J. (2013). The rift to break-up evolution of the Gulf of Aden: Insights from 3D numerical lithospheric-scale modelling. Tectonophysics, 607, 65-79. https://doi.org/10.1016/j.tecto.2013.06.029

Catuneanu, O., Khalifa, M.A., Wanas, H.A. (2006). Sequence stratigraphy of the lower Cenomanian Bahariya Formation, Bahariya Oasis, Western Desert, Egypt. Sedimentary Geology, 190(1-4), 121-137. https://doi.org/10.1016/j.sedgeo.2006.05.010

Channell, J.E.T., Muttoni, G., Kent, D.V. (2022). Adria in Mediterranean paleogeography, the origin of the Ionian Sea, and Permo-Triassic configurations of Pangea. Earth-Science Reviews, 230, 104045. https://doi.org/10.1016/j.earscirev.2022.104045

Cheng, J.E. (2019). Basin Classification of Shoushan Basin, Western Desert, Egypt. Earth Sciences Malaysia (ESMY), 1, 35-38. Doi: 10.26480/esmy.01.2019.35.38

Cheng, J.E. (2020). Petroleum System of Shoushan Basin, Western Desert, Egypt. Acta Scientifica Malaysia (ASM), 4(1), 01-08. Doi: https://doi.org/10.26480/gbr.01.2020.01.08

Dercourt, J., Zonenshain, L.P., Ricou, L.-E., Kazmin, V.G., Le Pichon, X., Knipper, A.L., Grandjacket, C., Sbortshikov, I.M., Geyssant, J., Lepvrier, C., Pechersky, D.H., Boulin, J., Sibuet, J.-C., Savostin, L.A., Sorokhtin, O., Westphal, M., Bazhenov, M.L., Lauer, J.P., Biju-Duval, B. (1986). Geological evolution of the Tethys belt from the Atlantic to the Pamirs since the Lias. Tectonophysics, 123(1-4), 241-315. https://doi.org/10.1016/0040-1951(86)90199-X

Dewey, J.F., Pitman III, W.C., Ryan, W.B., Bonnin, J. (1973). Plate tectonics and the evolution of the Alpine system. Geological society of America bulletin, 84(10), 3137-3180. https://doi.org/10.1130/0016-7606(1973)84<3137:PTATEO>2.0.CO;2

Dolson, J. C., Boucher, P.J., Siok, J., Heppard, P.D. (2005). Key challenges to realizing full potential in an emerging giant gas province: Nile Delta/Mediterranean offshore, deep water, Egypt. In: Petroleum Geology Conference Series. Geological Society, London, Vol. 6 (1). pp. 607-624. https://doi.org/10.1144/0060607

Dolson, J.C., Shann, M.V., Matbouly, S.I., Hammouda, H., Rashed, R. M. (2001). Egypt in the twenty-first century: petroleum potential in offshore trends. GeoArabia, 6(2), 211-230. https://doi.org/10.2113/geoarabia0602211

Elhossainy, M.M., El-Shafeiy, M., Al-Areeq, N.M., Hamdy, D. (2022). Petroleum generation modelling of the Middle-Late Cretaceous sediments in the Abu Gharadig Field, Northwestern Desert, Egypt. Geological Journal, 57(9), 3851-3880. https://doi.org/10.1002/gj.4519

Elkhodary, S.T., Youssef, M.A.S. (2013). Integrated potential field study on the subsurface structural characterization of the area North Bahariya Oasis, Western Desert, Egypt. Arabian Journal of Geosciences, 6, 3185-3200. https://doi.org/10.1007/s12517-012-0590-x

El-Shazly, E.M. (1966). Structural development of Egypt. In U.A.R. Geological Society Egypt, Fourth Annual Meeting, Program Abstracts, pp. 31-38.

El Shazly, E.M. (1977). The geology of the Egyptian region. In: Nairn, A.E.M., Kanes, W.H., Stehli, F.G. (eds) The Ocean Basins and Margins. Springer, Boston, MA., pp. 379-444. https://doi.org/10.1007/978-1-4684-3036-3_10

Elsheikh, A., Setto, I., Abdelhady, A. A. (2021). Reservoir characterization and 3D modeling of the Aptian Alamein Formation in North Razzak area (North Western Desert, Egypt). Journal of African Earth Sciences, 173, 104039. https://doi.org/10.1016/j.jafrearsci.2020.104039

Eyal, Y. (2011). The Syrian Arc Fold System: age and rate of folding. In Geophysical Research Abstracts, vol. 13, EGU2011-7401.

Farouk, S., Khalifa, M.A. (2010). Facies tracts and sequence development of the Middle Eocene–Middle Miocene successions of the southwestern Qattara Depression, northern Western Desert, Egypt. Palaontologie, Stratigraphie, Fazies, 18(C536), 195-215.

Fernandez, O. (2019). The Jurassic evolution of the Africa-Iberia conjugate margin and its implications on the evolution of the Atlantic-Tethys triple junction. Tectonophysics, 750, 379-393. https://doi.org/10.1016/j.tecto.2018.12.006

Gaber, G. M. (2022). Evaluation of Sedimentary Basins for Hydrocarbon Exploration Using Aeromagnetic Data, Northwestern Sinai Peninsula, Egypt. https://doi.org/10.21203/rs.3.rs-1910620/v1

Garfunkel, Z. (2004). Origin of the Eastern Mediterranean basin: a reevaluation. Tectonophysics, 391(1-4), 11-34. https://doi.org/10.1016/j.tecto.2004.07.006

Gentzis, T., Carvajal-Ortiz, H., Deaf, A., Tahoun, S.S. (2018). Multi-proxy approach to screen the hydrocarbon potential of the Jurassic succession in the Matruh Basin, North Western Desert, Egypt. International Journal of Coal Geology, 190, 29-41. https://doi.org/10.1016/j.coal.2017.12.001

Georgalis, G. L., Gawad, M. K. A., Hassan, S. M., El-Barkooky, A. N., Hamdan, M. A. (2020). Oldest co-occurrence of Varanus and Python from Africa—first record of squamates from the early Miocene of Moghra Formation, Western Desert, Egypt. PeerJ, 8, e9092. https://doi.org/10.7717/peerj.9092

Granath, J.W., Dickson, W. (2017). Organization of African Intra-Plate Tectonics. Search and Discovery Article #30555

Granot, R. (2016). Palaeozoic oceanic crust preserved beneath the eastern Mediterranean. Nature Geoscience, 9(9), 701-705. https://doi.org/10.1038/ngeo2784

Granot, R., Dyment, J. (2015). The cretaceous opening of the South Atlantic Ocean. Earth and Planetary Science Letters, 414, 156-163. https://doi.org/10.1016/j.epsl.2015.01.015

Gvirtzman, Z., Steinberg, J., Bar, O., Buchbinder, B., Zilberman, E., Siman-Tov, R., Calvo, R., Grossowicz, L., Almogi-Labin, A., Rosensaft, M. (2011). Retreating Late Tertiary shorelines in Israel: Implications for the exposure of north Arabia and Levant during Neotethys closure. Lithosphere, 3(2), 95-109. https://doi.org/10.1130/L124.1

Halsey, J. H., Gardner, W. C. (1975). Tectonic analysis of Egypt using Earth Satellite data. Lecture given to Egyptian Petrol Geol Cairo GPC.

Hamimi, Z., El-Barkooky, A., Frías, J. M., Fritz, H., Abd El-Rahman, Y. (Eds.). (2020). The geology of Egypt (p. 711). Cham: Springer.

Ibraheem, I. M., Elawadi, E. A., El-Qady, G. M. (2018). Structural interpretation of aeromagnetic data for the Wadi El Natrun area, northwestern desert, Egypt. Journal of African Earth Sciences, 139, 14-25. https://doi.org/10.1016/j.jafrearsci.2017.11.036

Jagger, L.J., Bevan, T.G., McClay, K.R. (2020). Tectono-stratigraphic evolution of the SE Mediterranean passive margin, offshore Egypt and Libya. Geological Society, London, Special Publications, 476(1), 365-401. https://doi.org/10.1144/SP476.10

Jolivet, L. (2023). Tethys and Apulia (Adria), 100 years of reconstructions. Comptes Rendus. Géoscience, 355(S2), 1-20. Doi: 10.5802/crgeos.198

Jolivet, L., Baudin, T., Calassou, S., Chevrot, S., Ford, M., Issautier, B., Lasseur, E., Masini, E., Manatschal, G., Mouthereau, F., Thinon, I., Vidal, O. (2021). Geodynamic evolution of a wide plate boundary in the Western Mediterranean, near-field versus far-field interactions. BSGF-Earth Sciences Bulletin, 192(1), 48. https://doi.org/10.1051/bsgf/2021043

Keeley, M.L. (1989). The Palaeozoic history of the western desert of Egypt. Basin Research, 2(1), 35-48. https://doi.org/10.1111/j.1365-2117.1989.tb00025.x

Keeley, M.L. (1994). Phanerozoic evolution of the basins of Northern Egypt and adjacent areas. Geologische Rundschau, 83(4), 728-742. https://doi.org/10.1007/BF00251071

Khalek, M.A., El Sharkawi, M.A., Darwish, M., Hagras, M., Sehim, A. (1989). Structural history of Abu Roash district, Western Desert, Egypt. Journal of African Earth Sciences (and the Middle East), 9(3-4), 435-443. https://doi.org/10.1016/0899-5362(89)90027-4

Kley, J., Voigt, T. (2008). Late Cretaceous intraplate thrusting in central Europe: Effect of Africa-Iberia-Europe convergence, not Alpine collision. Geology, 36(11), 839-842. https://doi.org/10.1130/G24930A.1

Knott, S.D., Burchell, M.T., Jolley, E.J., Fraser, A. J. (1993). Mesozoic to Cenozoic plate reconstructions of the North Atlantic and hydrocarbon plays of the Atlantic margins. In: Petroleum Geology Conference Series, Geological Society, London, Vol. 4 (10), pp. 953-974. https://doi.org/10.1144/004095

Krenkel, E. (1924). Gregory, J.W. (1925). The Syrian Arc. Nature, 115, 514. https://doi.org/10.1038/115514a0

Kuss, J., Scheibner, C., Gietl, R. (2000). Carbonate platform to basin transition along an upper Cretaceous to lower Tertiary Syrian arc uplift, Galala Plateaus, Eastern Desert of Egypt. GeoArabia, 5(3), 405-424. https://doi.org/10.2113/geoarabia0503405

Lyberis, N. (1988). Tectonic evolution of the Gulf of Suez and the Gulf of Aqaba. Tectonophysics, 153(1-4), 209-220. https://doi.org/10.1016/0040-1951(88)90016-9

Mahmoud, A.I., Metwally, A.M., Mabrouk, W.M., Leila, M. (2023). Controls on hydrocarbon accumulation in the pre-rift Paleozoic and late syn-rift Cretaceous sandstones in PTAH oil field, north Western Desert, Egypt: Insights from seismic stratigraphy, petrophysical rock-typing and organic geochemistry. Marine and Petroleum Geology, 155, 106398. https://doi.org/10.1016/j.marpetgeo.2023.106398

Makky, A.F., El Sayed, M.I., El-Ata, A.S.A., Abd El-Gaied, I.M., Abdel-Fattah, M.I., Abd-Allah, Z.M. (2014). Source rock evaluation of some upper and lower Cretaceous sequences, West Beni Suef concession, Western Desert, Egypt. Egyptian Journal of Petroleum, 23(1), 135-149. https://doi.org/10.1016/j.ejpe.2014.02.016

Makled, W.A., Shazly, T.F. (2023). Inter-basinal cyclostratigraphic correlation of Neocomian–Barremian Alam El Buieb Formation in the northern part of the Western Desert, Egypt. Egyptian Journal of Geology, 67(1), 111-121. Doi: 10.21608/egjg.2023.206691.1045

Maksoud, S., Granier, B., Gèze, R., Alméras, Y., Toland, C., Azar, D. (2020). The Jurassic/Cretaceous boundary in Lebanon. Revision of the Salima Formation. Cretaceous Research, 107, 104268. https://doi.org/10.1016/j.cretres.2019.104268

Mansour, A., Gentzis, T., El Nady, M.M., Mostafa, F., Tahoun, S.S. (2020). Hydrocarbon potential of the Albian-early Cenomanian formations (Kharita-Bahariya) in the North Western Desert, Egypt: a review. Journal of Petroleum Science and Engineering, 193, 107440. https://doi.org/10.1016/j.petrol.2020.107440

Mart, Y., Hall, J.K. (1984). Structural trends in the northern Red Sea. Journal of Geophysical Research: Solid Earth, 89(B13), 11352-11364. https://doi.org/10.1029/JB089iB13p11352

Martín-Chivelet, J., López-Gómez, J., Aguado, R., Arias, C., Arribas, J., Arribas, M. E., Aurell, M., Bádenas, B., Benito, M.I., Bober-Arnal, T., Casas-Sainz, A., Castro. J.M., Coruña, F., de Gea, G.A., Fornós. J.J., Fregenal-Martinez, M., García-Senz, J., Garófano, D., Gelabert, J., Giménez, J., González-Acebrón, L., Gumerà, J., Liesa, C.L., Mas, R.…Vilas, L. (2019). In: Quesada, C., Oliveira, J. (eds) The Geology of Iberia: A Geodynamic Approach. Regional Geology Reviews. Springer, Cham. https://doi.org/10.1007/978-3-030-11295-0_5

Matte, P. (2001). The Variscan collage and orogeny (480–290 Ma) and the tectonic definition of the Armorica microplate: a review. Terra nova, 13(2), 122-128. https://doi.org/10.1046/j.1365-3121.2001.00327.x

Meshref, W.M. (1982, January). Regional structural setting of northern Egypt. In: Proceedings of the 6th Egyptian general petroleum corporation exploration seminar, Cairo, pp. 17-34.

Meshref, W.M. (1990). Tectonic Framework of Egypt: In: Said, R., Ed., Geology of Egypt, Balkema/Rotterdam/Bookfield, Netherlands, 113-156.

Meshref, W.M., El Sheikh, M.M. (1973). Magnetic tectonic trend analysis in northern Egypt. Egyptian Journal of Geology, 17, 179-184.

Mohamed, H.S., Senosy, M.M., Zaher, M.A. (2016). Interactive interpretation of airborne gravity, magnetic, and drill-hole data within the crustal framework of the northern Western Desert, Egypt. Journal of Applied Geophysics, 134, 291-302. https://doi.org/10.1016/j.jappgeo.2016.09.002

Moustafa, A.R. (2008). Mesozoic-Cenozoic basin evolution in the northern Western Desert of Egypt. In: 3rd symposium on the sedimentary Basins of Libya, The Geology of East Libya, Vol. 3, pp. 29-46.

Moustafa, A.R. (2013). Fold-related faults in the Syrian Arc belt of northern Egypt. Marine and Petroleum Geology, 48, 441-454. https://doi.org/10.1016/j.marpetgeo.2013.08.007

Moustafa, A.R. and El-Barkooky, A. (2024). Spatial and temporal variation of Syrian Arc structures in the onshore and offshore Eastern Mediterranean region. The Leading Edge, 43(9), 578-587. https://doi.org/10.1190/tle43090578.1

Neubauer, F., Heinrich, C.A., and Geode ABCD Working Group (2003). Late Cretaceous and Tertiary geodynamics and ore deposit evolution of the Alpine–Balkan–Carpathian–Dinaride orogen. Mineral exploration and Sustainable development. Millpress, Rotterdam, 1133-1136.

Ramadan, F.S., El Nady, M.M., Eysa, E. A., Mahdy, S.A. (2016). Isopach, lithofacies changes, and source rocks chracteristics of Khatatba and Alam El Bueib formations of some wells in North East Western Desert, Egypt. Petroleum Science and Technology, 34(23), 1920-1928. https://doi.org/10.1080/10916466.2016.1238931

Reda, M., Fathy, M., Gawad, E.A. (2022). Comprehensive 3D reservoir modelling and basin analysis: An insight into petroleum geology to re-evaluate the hydrocarbon possibilities in the Siwa Basin, North-Western Desert, Egypt. Geological Journal, 57(4), 1600-1616. https://doi.org/10.1002/gj.4362

Ring, U.W.E., Johnson, C., Hetzel, R., Gessner, K. (2003). Tectonic denudation of a Late Cretaceous–Tertiary collisional belt: regionally symmetric cooling patterns and their relation to extensional faults in the Anatolide belt of western Turkey. Geological Magazine, 140(4), 421-441. https://doi.org/10.1017/S0016756803007878

Robertson, A.H.F., Parlak, O., Koller, F. (2009). Tethyan tectonics of the Mediterranean region: Some recent advances. Tectonophysics, 473(1), 1-3. Doi: 10.1016/j.tecto.2008.10.036

Roche, V., Jolivet, L., Papanikolaou, D., Bozkurt, E., Menant, A., Rimmelé, G. (2019). Slab fragmentation beneath the Aegean/Anatolia transition zone: Insights from the tectonic and metamorphic evolution of the Eastern Aegean region. Tectonophysics, 754, 101-129. https://doi.org/10.1016/j.tecto.2019.01.016

Saada, S.A. (2016). Curie point depth and heat flow from spectral analysis of aeromagnetic data over the northern part of Western Desert, Egypt. Journal of Applied Geophysics, 134, 100-111. https://doi.org/10.1016/j.jappgeo.2016.09.003

Sachpazi, M., Laigle, M., Charalampakis, M., Diaz, J., Kissling, E., Gesret, A., Becel, A., Flueh, E., Miles, P., Hirn, A. (2016). Segmented Hellenic slab rollback driving Aegean deformation and seismicity. Geophysical Research Letters, 43(2), 651-658. https://doi.org/10.1002/2015GL066818

Said, R. (Ed.). (2017). The geology of Egypt. Routledge, pp. 744. ISBN 9789061918561

Sarhan, M. A., Basal, A. M. K. (2020). Total organic carbon content deduced from resistivity-porosity logs overlay: a case study of Abu Roash formation, Southwest Qarun field, Gindi Basin, Egypt. NRIAG Journal of Astronomy and Geophysics, 9(1), 190-205. https://doi.org/10.1080/20909977.2020.1736761

Savostin, L. A., Sibuet, J.C., Zonenshain, L.P., Le Pichon, X., Roulet, M. J. (1986). Kinematic evolution of the Tethys belt from the Atlantic Ocean to the Pamirs since the Triassic. Tectonophysics, 123(1-4), 1-35. https://doi.org/10.1016/0040-1951(86)90192-7

Schandelmeier, H., Richter, A., Harms, U. (1987). Proterozoic deformation of the East Saharan Craton in southeast Libya, south Egypt and north Sudan. Tectonophysics, 140(2-4), 233-246. https://doi.org/10.1016/0040-1951(87)90231-9

Schlumberger, S. (1984). Well evaluation conference (WEC), Egypt. Schlumberger Middle East, 201.

Segev, A., Sass, E., Schattner, U. (2018). Age and structure of the Levant basin, Eastern Mediterranean. Earth-Science Reviews, 182, 233-250. https://doi.org/10.1016/j.earscirev.2018.05.011

Şengör, A. C., Yilmaz, Y. (1981). Tethyan evolution of Turkey: a plate tectonic approach. Tectonophysics, 75(3-4), 181-241. https://doi.org/10.1016/0040-1951(81)90275-4

Seton, M., Müller, R. D., Zahirovic, S., Gaina, C., Torsvik, T., Shephard, G., Talsma, A., Gurnis, M., Turner, M., Maus, S., Chandler, M. (2012). Global continental and ocean basin reconstructions since 200 Ma. Earth-Science Reviews, 113(3-4), 212-270. https://doi.org/10.1016/j.earscirev.2012.03.002

Shahar, J. (1994). The Syrian arc system: an overview. Palaeogeography, Palaeoclimatology, Palaeoecology, 112(1-2), 125-142. https://doi.org/10.1016/0031-0182(94)90137-6

Shahin, A., El Khawagah, S., Shahin, B. (2023). Middle Eocene–early Miocene planktonic foraminiferal biostratigraphy, chronostratigraphy, sea-level reconstruction and sequence biostratigraphy at N. El Faras-1X well, Qattara Depression, Western Desert, Egypt. Geological Journal, 58(4), 1587-1606. https://doi.org/10.1002/gj.4679

Shalaby, M.R., Hakimi, M.H., Abdullah, W.H. (2011). Geochemical characteristics and hydrocarbon generation modeling of the Jurassic source rocks in the Shoushan Basin, north Western Desert, Egypt. Marine and Petroleum Geology, 28(9), 1611-1624. https://doi.org/10.1016/j.marpetgeo.2011.07.003

Shehata, A.A., El Fawal, F.M., Ito, M., Abdel Aal, M.H., Sarhan, M.A. (2018). Sequence stratigraphic evolution of the syn-rift Early Cretaceous sediments, West Beni Suef Basin, the Western Desert of Egypt with remarks on its hydrocarbon accumulations. Arabian Journal of Geosciences, 11, 1-18. https://doi.org/10.1007/s12517-018-3688-y

Shehata, A.A., Sarhan, M.A., Abdel-Fattah, M.I., Mansour, S. (2023). Geophysical Assessment for the Oil Potentiality of the Abu Roash "G" Reservoir in West Beni Suef Basin, Western Desert, Egypt. Journal of African Earth Sciences, 199, 104845. https://doi.org/10.1016/j.jafrearsci.2023.104845

Sheikh, H.A., Faris, M. (1985). The Eocene-Oligocene boundary in some wells of the Western Desert, Egypt. Neues Jahrbuch für Geologie und Paläontologie Monatshefte, 1, 23-28. Doi: 10.1127/njgpm/1985/1985/23

Simancas, J.F. (2019). Variscan cycle. In: Quesada, C., Oliveira, J. (eds) The Geology of Iberia: A Geodynamic Approach: Volume 2: The Variscan Cycle, Regional Geology Reviews. Springer, Cham. 1-25. https://doi.org/10.1007/978-3-030-10519-8_1

Skogseid, J., Planke, S., Faleide, J.I., Pedersen, T., Eldholm, O., Neverdal, F. (2000). NE Atlantic continental rifting and volcanic margin formation. Geological Society, London, Special Publications, 167(1), 295-326. https://doi.org/10.1144/GSL.SP.2000.167.01.1

Stampfli, G. M., Borel, G. D., Marchant, R., Mosar, J. (2002). Western Alps geological constraints on western Tethyan reconstructions. Journal of the Virtual Explorer, 8, 77-106. Doi: 10.3809/jvirtex.2002.00057

Stampfli, G.M., Mosar, J., Favre, P., Pillevuit, A., Vannay, J.C. (2001). Permo-Mesozoic evolution of the western Tethys realm: the Neo-Tethys East Mediterranean basin connection. *In:* Ziegler, P.A. Cavalza, W., Robertson, A.H.F. & Crasquin-Soleau (eds.), Peri-Tethys Memoir 6: Peri-Tethyan Rift, Wrench Basins and Passive Margins. Mémoires du Muséum National d'Histoire Naturelle, 186, 51-108.

Stern, R.J., Kröner, A., Bender, R., Reischmann, T., Dawoud, A.S. (1994). Precambrian basement around Wadi Halfa, Sudan: a new perspective on the evolution of the East Saharan Craton. Geologische Rundschau, 83, 564-577. https://doi.org/10.1007/BF01083228

Tari, G., Hussein, H., Novotny, B., Hannke, K., Kohazy, R. (2012). Play types of the deep-water Matruh and Herodotus basins, NW Egypt. Petroleum Geoscience, 18(4), 443-455. https://doi.org/10.1144/petgeo2012-01

Tassy, A., Crouzy, E., Gorini, C., Rubino, J.L., Bouroullec, J.L., Sapin, F. (2015). Egyptian Tethyan margin in the Mesozoic: Evolution of a mixed carbonate-siliciclastic shelf edge (from Western Desert to Sinai). Marine and Petroleum Geology, 68, 565-581. https://doi.org/10.1016/j.marpetgeo.2015.10.011

Tlig, S. (2015). The Upper Jurassic and Lower Cretaceous series of southern Tunisia and northwestern Libya revisited. Journal of African Earth Sciences, 110, 100-115. https://doi.org/10.1016/j.jafrearsci.2015.06.014

Van Hinsbergen, D.J., Torsvik, T.H., Schmid, S.M., Maţenco, L.C., Maffione, M., Vissers, R.L., Spakman, W. (2020). Orogenic architecture of the Mediterranean region and kinematic reconstruction of its tectonic evolution since the Triassic. Gondwana Research, 81, 79-229. https://doi.org/10.1016/j.gr.2019.07.009

Vincent, S.J., Guo, L., Flecker, R., BouDagher-Fadel, M.K., Ellam, R. M., Kandemir, R. (2018). Age constraints on intra-formational unconformities in Upper Jurassic-Lower Cretaceous carbonates in northeast Turkey; geodynamic and hydrocarbon implications. Marine and Petroleum Geology, 91, 639-657. https://doi.org/10.1016/j.marpetgeo.2018.01.011

Yousef, M., Moustafa, A.R., Bosworth, W. (2023). Structural and tectonostratigraphic evolution of Matruh Basin, northern Western Desert, Egypt: An example of an inverted rift basin. Journal of African Earth Sciences, 203, 104958. https://doi.org/10.1016/j.jafrearsci.2023.104958

Youssef, M.I. (1968). Structural pattern of Egypt and its interpretation. AAPG Bulletin, 52(4), 601-614. https://doi.org/10.1306/5D25C44D-16C1-11D7-8645000102C1865D

Youssef, M.M. (2003). Structural setting of central and south Egypt: an overview. Micropaleontology, 49(Suppl_1), 1-13. https://doi.org/10.2113/49.Suppl_1.1

Youssef, M.M., Ibrahim, H.A., Bakheit, A. A., Senosy, M.M. (1998). Tectonic patterns developed within the Sohag region, middle Egypt. Journal of African Earth Sciences, 26(2), 327-339. https://doi.org/10.1016/S0899-5362(98)00015-3

Zaher, M.A., El-Hadidy, M., El-Qady, G., Rabeh, T., Atya, M., El-hady, S., Tantawy, A.A., El-Hemaly, I., Deep, M.A., Awad, A., Salama, H., Khalifa, M.M., Leila, M. (2023). Origin of mysterious geothermal gas emissions in the middle of the Western Desert, stable shelf area, Dakhla Oasis, Egypt. Scientific Reports, 13, 16466. https://doi.org/10.1038/s41598-023-43492-1

Captions

Fig. 1. Location of the study area and main structural zones as projected on a regional map of Egypt. The Western Desert is divided into five distinct structural zones: I) the Craton, or Nubian Shield, II) the Stable Zone, III) the Unstable Zone, IV) the Hinge Zone, and V) the Nile Delta Cone. The study area is mostly in the northern part of the Unstable Zone near its boundary with the Hinge Zone. This map is modified from WEC (1984), Meshref and EGPC (1995), Aal et al. (2000) and Tari et al. (2012).

Fig. 2. Base map showing the seismic and borehole data available for this study over the Shams and Amoun oil fields, Shushan Basin. The data set consists of 24 N-S and E-W seismic profiles, complemented by six arbitrary profiles. All the seismic data were processed in the time domain. The five wells in the study area were drilled to the top of the Lower Jurassic Ras Qattara Formation (Fig. 5).

Fig. 3. Interval velocity log, and synthetic seismogram for well Amoun-01, correlated with arbitrary seismic profile 01 (see Fig. 2 for location of the seismic profile). The correlation panel reveals a good tie between seismic horizons (A-E) on the seismic profile and the computed seismogram. Such a valid correlation is confirmed by significant changes in interval velocity against the formation tops identified at borehole. Well tops were gathered from (and confirmed) by well completion data and reports.

Fig. 4. Workflow proposed in this work for the tectono-stratigraphic analysis of the Shushan Basin and palaeogeographic mapping of SE Mediterranean megabasin.

Fig. 5. General stratigraphy of the Unstable Zone of the Northwestern Desert, Egypt, revealing alternating cycles of transgression and regression. Panel is modified from WEC (1984).

Fig. 6. Seismic-stratigraphic panel revealing main megasequences and constituting seismic units interpreted in this work. The panel relates the nine (9) interpreted megasequences to five (5) major tectonic phases and 16 different seismic units (SUs).

Fig. 7. (a) Uninterpreted seismic profile 14779, and (b) corresponding interpretation highlighting the nine (9) megasequences interpreted in this work. Faults B1, B3, and B8 show normal offsets, are E-W striking, and delimit a series of horst and grabens at this location. In this seismic profile, older strata in Megasequences 1 to 3 dip towards the north. In contrast, younger strata (Megasequences 7 and 8) dip gently towards the south due to moderate tectonic uplift associated with the Syrian Arc system and opening of the Red Sea.

Fig. 8. (a) Uninterpreted seismic profile 15042, and (b) corresponding interpretation revealing the presence of two of the main fault families interpreted in the study area. Fault family B strikes E-W, while fault family D follows a NNE-SSW strike. Fault B7 shows evidence for reactivation and local forced folding, both of which were controlled by the gentle Cenozoic uplift of the NE part of the study area. Evidence for tectonic reactivation includes the presence of strata gently dipping towards the south within Megasequences 7 and 8, and the mild forced folding developed between faults D6 and B7.

Fig. 9. (a) Uninterpreted seismic profile 7347, and (b) corresponding interpretation imaging two families of normal faults (A and D). These fault families form a horst in the centre of the

seismic profile. Also imaged are local forced folds in a zone of intense deformation developed between faults D1 and D6. These forced folds are best imaged in Megasequences 1 to 4.

Fig. 10. (a) Uninterpreted seismic profile 7505, and (b) corresponding interpretation highlighting the gentle deformation (folding) that affects Megasequences 1 to 6 near fault families A, B and D. The immediate hanging-wall of Fault D3 shows gentle uplift. This constitutes further evidence for fault reactivation and gentle folding in the study area.

Fig. 11. TWTT structural maps for the: (a) top basement horizon (base SU1), and (b) top Desouqy Formation (Carboniferous – top SU2). These maps reveal the strikes of structures crossing Palaeozoic strata in the Shushan Basin. The four fault families impose a general northward deepening to the basin.

Fig. 12. TWTT structural maps for the: (a) top Ras Qattara Formation (Lower Jurassic – top SU4), and (b) top Masajid Formation (Upper Jurassic – top SU6). These maps reveal the multiple strikes of structures developed during early Mesozoic rifting of the Shushan Basin (Syn-Rift I stage).

Fig. 13. TWTT structural maps for the: (a) top Bahariya Formation (Cenomanian – top SU10), and (b) top Khoman Formation (Campanian-Maastrichtian – top SU12). Starting from the Cretaceous up to Miocene times, the structural maps reveal the formation of structures that reflect a second stage of continental rifting (Syn-Rift II).

Fig. 14. TWTT structural maps for the: (a) top Ghoroud Formation (Oligocene – top SU13), and (b) top Marmarica Formation (Miocene – top SU14). The structural maps reveal gentle uplift in the NE, reflecting the effect of compressional movements initiated in the Late Cretaceous.

Fig. 15. Isochron maps for the: (a) the Ras Qattara Formation (Lower Jurassic – SU4), and (b) Alam El Buieb Formation (Lower Cretaceous – SU7). These maps reveal important changes in strata thickness near faults, confirming the impact of syn-rift extension in the study area.

Fig. 16. Isochron maps for the: (a) Masajid Formation (Upper Jurassic – SU6), and (b) Alamein Formation (Upper Aptian – SU8). These maps reveal minor changes in strata thickness near faults, documenting periods of quiescence between continental-rifting episodes.

Fig. 17. Isochron map for the Khoman Formation (Campanian-Maastrichtian – SU12) revealing significant changes in strata thickness near faults, representing a last stage of faulting in the Late Cretaceous. This episode of growth faulting accompanied the onset of tectonic inversion and uplift in the Levant region, near Lebanon and Syria.

Fig. 18. Isochron maps for the: (a) Baharia Formation (Cenomanian – SU10), and (b) Abu-Roash Formation (Turonian – SU11). These maps reveal very minor changes in strata thickness near faults, effectively showing that tectonic extension ended in the Late Cretaceous in the Shushan Basin.

Fig. 19. Isochron map for the: (a) Ghoroud Formation (Oligocene –SU13) and (b) Marmarica Formation (Miocene – SU14). The maps reveal minor changes in strata thickness near faults, confirming the establishment of a post-rift phase in the study area.

Fig. 20. 3D structural model and corresponding cross-sections depicting the main structures crossing Jurassic strata in a N-S (a) and E-W (b) direction. The A-B profile highlights that a series of normal faults and half-graben basins impose a general northward tilt to the Shushan Basin. The C-D profile shows a series of normal faults recording gentle reactivation and local uplift, a character linked to the effect of Late Cretaceous-Cenozoic tectonic compression.

Fig. 21. Rose diagrams depicting: (a) the frequency of faults measured for each strike direction within 15° around the geographic north; (b) Faults' length expressed as a percentage of total length vs. the total number of faults. The diagrams reveal that E-W striking faults have a high length frequency.

Fig. 22. Integrated tectono-stratigraphic panel for the Shushan Basin based on the megasequence interpretation proposed in this work.

Fig. 23. Correlation panels highlight key variations in petrophysical properties across the four (4) Mezosoic megasequences drilled in the study area, starting from Megasequence 3 (Jurassic) to the Megasequence 6 (Upper Cretaceous).

Fig. 24. (a) Subsidence and (b) thermal models for Amoun-NE-3 well located in the depocenter of the Shushan Basin. The subsidence and thermal models show evidence for multiple phases of maturation in the Jurassic Khatatba Formation and older strata near the

basement. Amoun-NE-3 well shows an increase in temperature and subsidence starting from the Early Cretaceous during different tectonic events.

Fig. 25. Fault surfaces interpreted on Petrel® and categorised into four fault families: A, B, C, and D. Interpreted faults reveal multiple strikes that are related to the several tectonic episodes affecting the Shushan Basin from the Late Paleozoic to the Miocene.

Fig. 26. Diagram representing predominant structural trends interpreted in the SE Mediterranean region. The study area is influenced by four structural trends: i) Red Sea, ii) Tethyan, iii) Syrian Arc, and iv) Aqaba trends. The Tethyan Trend is the predominant trend in NE Africa and was developed during Mesozoic continental rifting and subsequent expansion of the Tethys Ocean.

Fig. 27. Geological models illustrating the evolution of the Shushan Basin. Main structures in the study area reflect six main tectonic episodes: a) Early syn-rift, b) Syn-rift I, c) Syn-rift II, d) Compressional phase I, e) Compressional phase II, and f) post-compressional phase predominating at present. Continental rift ended in the Early Cretaceous, preceding a phase of compression and mild fault reactivation in the Late Cretaceous, which continued into the Miocene. In this model, strike and dip directions are given by the right-hand rule.

Fig. 28. Paleogeographic maps summarising the evolution of NE Africa sub-plate in the: a) Triassic-Jurassic, and b) Early Cretaceous. NE Africa records the development of an early-stage, prograding continental margin during the Palaeozoic. From the Late Triassic to the Cenomanian, the study area recorded the deposition of a deepening-upwards sequence with a maximum transgression occurring in the early Aptian. This transgressive event accompanied

a major change in the direction of regional stress, and immediately preceded the onset of tectonic compression in the Levant region. Regional tectonic information on the map is based on based on Savostin et al. (1986). Seton et al. (2012), Brune and Autin (2013), Granath and Dickson (2017), Fairhead (2023) and Jolivet (2023).

Fig. 29. NE evolution of Africa in the: a) Late Eocene-Miocene, and b) Pliocene-Quaternary. The Oligocene records the last development stage of the Tethys Ocean, near what would later be the Central Mediterranean Sea. Tectonic convergence between Eurasia and Africa was established in the Levant region and Northern Egypt by this time. However, left lateral movement started between the Arabic Peninsula and North Africa in the Mid to Late Cenozoic, rifting the Red Sea and Gulf of Suez and inducing strike-slip tectonics along the Gulf of Aqaba. Regional tectonic information on the map is based on based on Savostin et al. (1986). Seton et al. (2012), Brune and Autin (2013), Granath and Dickson (2017), Fairhead (2023) and Jolivet (2023).

Table 1. Seismic megasequences defined in the Shushan Basin, Northwestern Desert, Egypt.

Seismic megasequences	Age of base	Average TWT thickness (s)	Internal characters	Lithology	Stratigraphic units
Meg. 9	Pliocene-Quaternary	0.25	Irregular seismic reflections with moderate frequency.	Sands, and detrital limestone bars	El-Hammam Fm.
Meg. 8	Miocene	0.25	Moderate continuity, amplitude seismic reflections.	Dolomites and fine clastics	Marmarica Fm.
Meg. 7	Paleocene to Oligocene	0.10	Subparallel, low amplitude seismic reflections.	Chalky limestones and dolomites	Ghoroud Fm. Mokattam Fm.
Meg. 6	Turonian to Maastrichtian	0.50	Moderate amplitude irregular seismic reflection to subparallel, low frequency, moderate amplitude seismic reflection.	Alternating carbonates, shales and sands	Khoman Fm. Abu Roash Gr.
Meg. 5	Aptian to Cenomanian	0.50	Regular, high amplitude and frequency seismic reflection to low amplitude and continuity seismic reflections	Dolomites, shales and sands	Bahariya Fm. Kharita Fm. Dahab Fm. Alamein Fm.
Meg. 4	Berriasian to Lower Aptian	0.50	Regular, high frequency, moderate amplitude seismic reflections	Shales, sands and carbonates	Alam El-Bueib Fm.
Meg. 3	Jurassic	0.75	Moderate to low amplitude, low frequency seismic reflections to high amplitude, high frequency continuous seismic reflections	Limestone, shales, sands and dolomitic limestone	Masajid Fm. Khatatba Fm. Ras Qattara Fm.

Meg. 2	Permian to Triassic	0.15	High to medium amplitude subparallel seismic reflections	Coarse-grained clastics	Eghi Gr.
Meg. 1	Cambrian to Carboniferous	0.75	Medium amplitude, subparallel seismic reflections to chaotic to medium amplitude seismic reflections	Coarse siliciclastics and shales	Desouqy Fm. Faghour Gr.

FIGURES

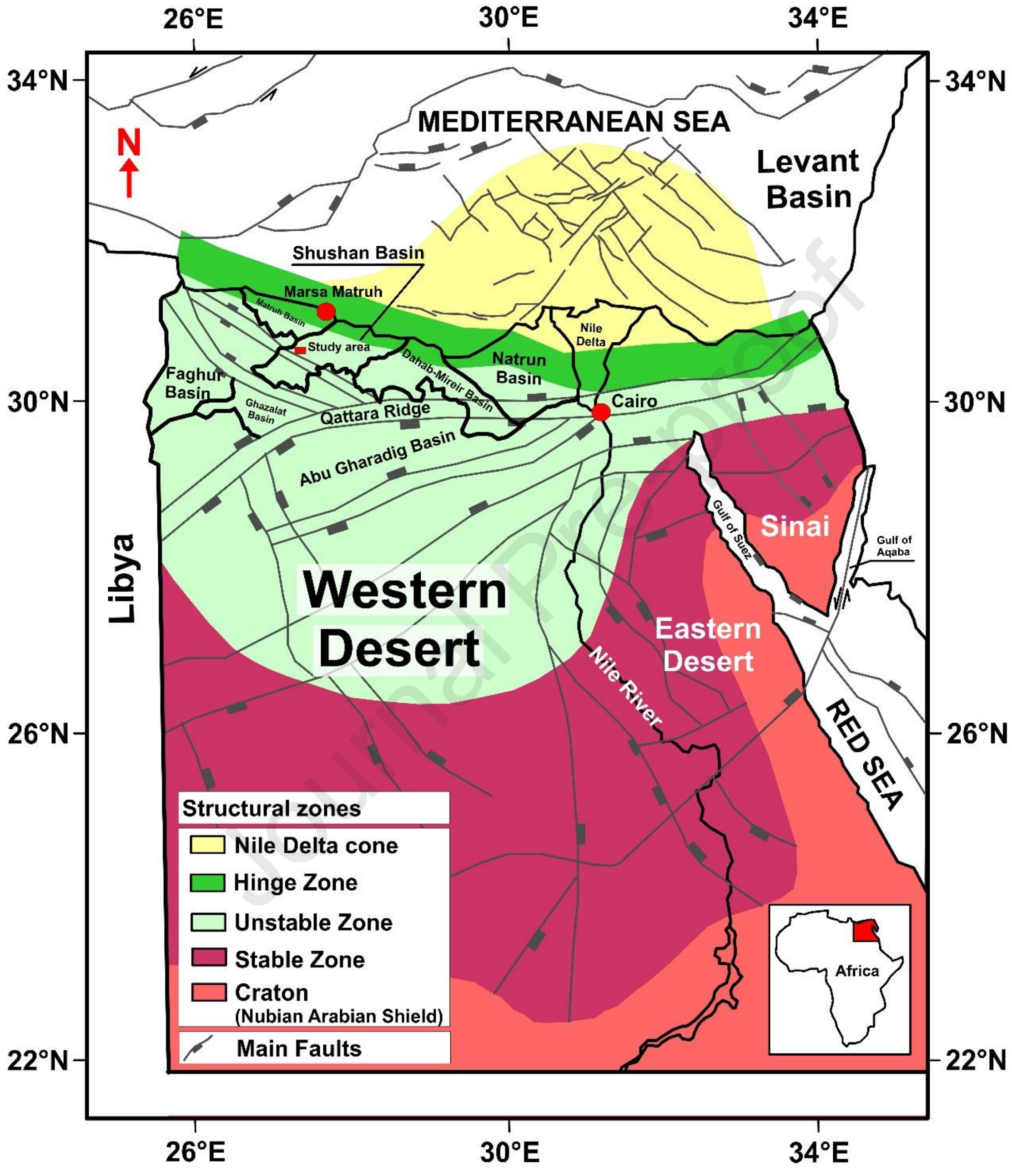

Fig. 1.

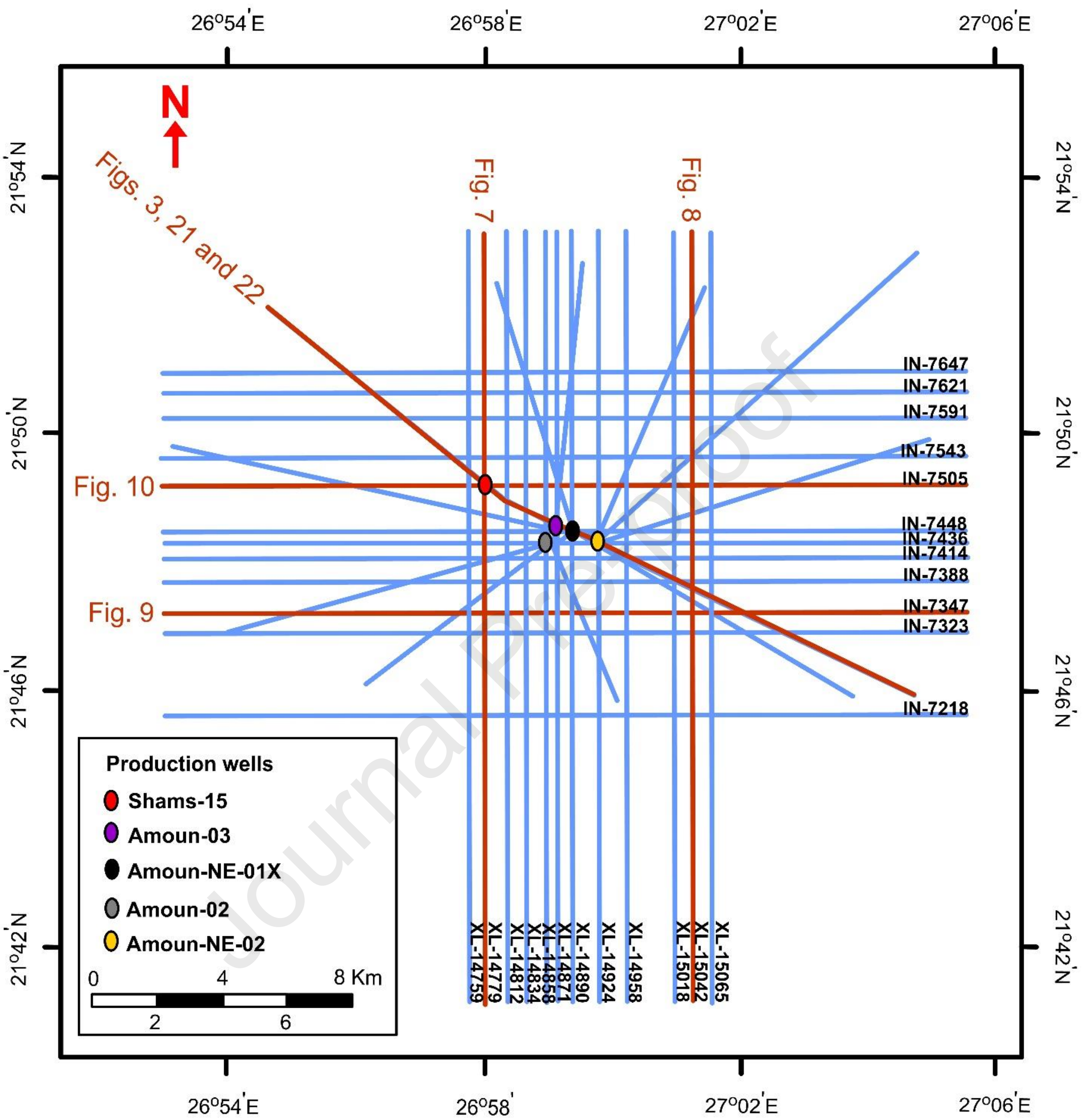
26°54'E
26°58'E
27°02'E
27°06'E
21°54'N
21°50'N
21°46'N
21°42'N
N
Figs. 3, 21 and 22
Fig. 7
Fig. 8
Fig. 10
Fig. 9
IN-7647
IN-7621
IN-7591
IN-7543
IN-7505
IN-7448
IN-7436
IN-7414
IN-7388
IN-7347
IN-7323
IN-7218
XL-14759
XL-14779
XL-14812
XL-14834
XL-14858
XL-14871
XL-14890
XL-14924
XL-14958
XL-15018
XL-15042
XL-15065
Production wells
Shams-15
Amoun-03
Amoun-NE-01X
Amoun-02
Amoun-NE-02
0
4
8 Km
2
6
26°58'

Fig. 2.

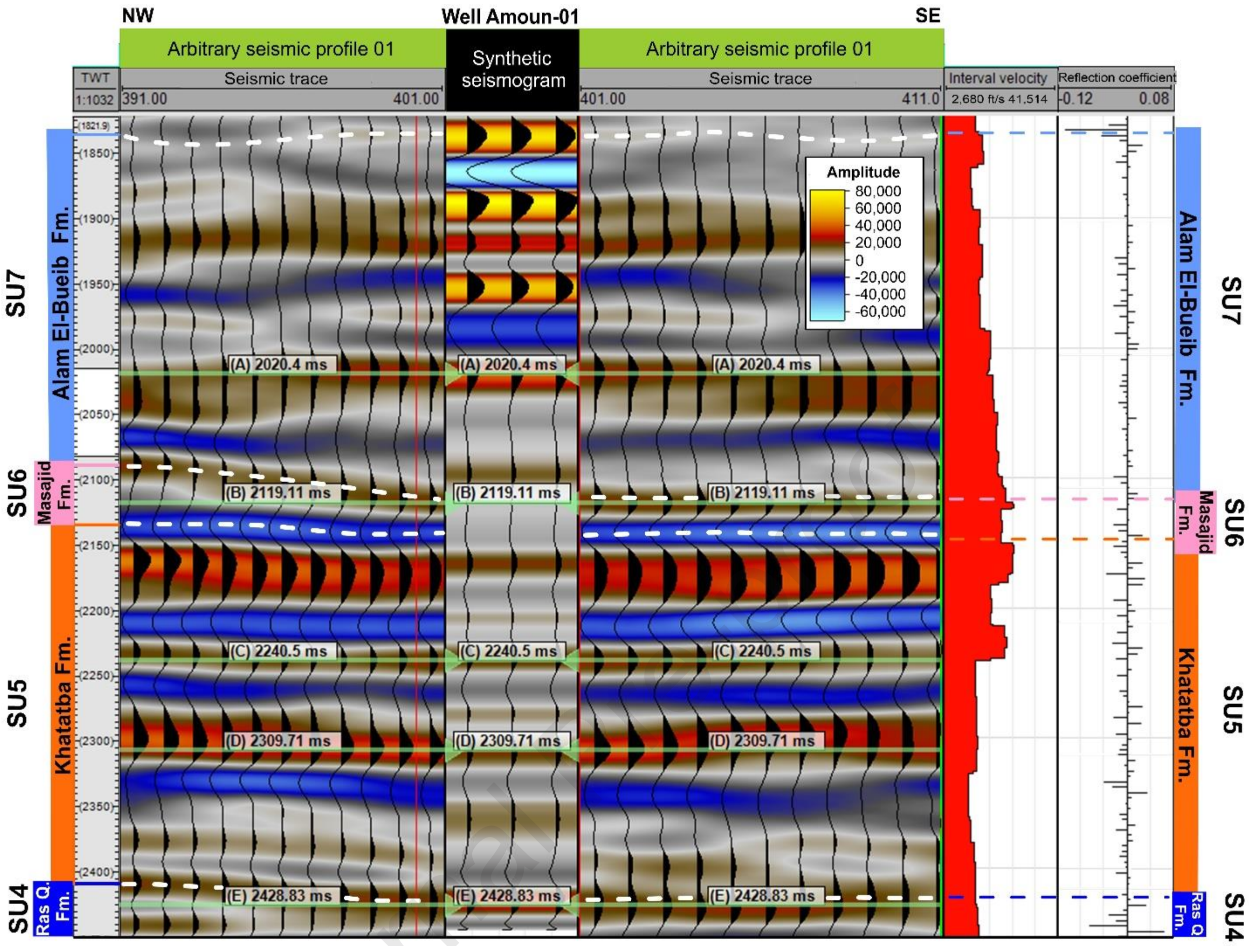
NW
Well Amoun-01
SE
Arbitrary seismic profile 01
Synthetic seismogram
Arbitrary seismic profile 01
TWT
1:1032
Seismic trace
391.00
401.00
401.00
411.0
Interval velocity
2,680 ft/s 41,514
Reflection coefficient
-0.12
0.08
Amplitude
80,000
60,000
40,000
20,000
0
-20,000
-40,000
-60,000
(A) 2020.4 ms
(B) 2119.11 ms
(C) 2240.5 ms
(D) 2309.71 ms
(E) 2428.83 ms
SU7
SU6
SU5
SU4
Alam El-Bueib Fm.
Masajid Fm.
Khatatba Fm.
Ras Q. Fm.

Fig. 3.

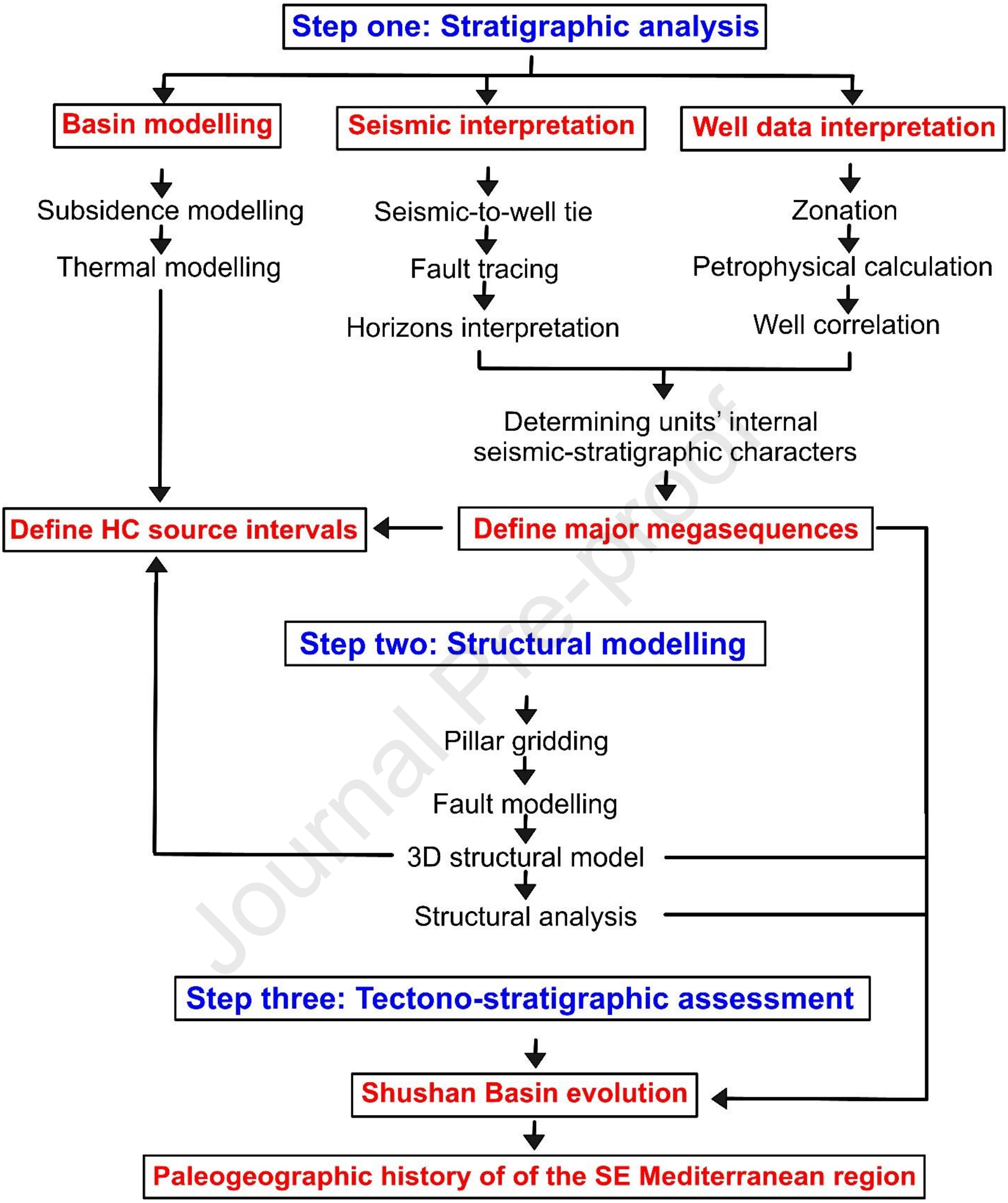
Step one: Stratigraphic analysis
Basin modelling
Seismic interpretation
Well data interpretation
Subsidence modelling
Thermal modelling
Seismic-to-well tie
Fault tracing
Horizons interpretation
Zonation
Petrophysical calculation
Well correlation
Determining units' internal seismic-stratigraphic characters
Define HC source intervals
Define major megasequences
Step two: Structural modelling
Pillar gridding
Fault modelling
3D structural model
Structural analysis
Step three: Tectono-stratigraphic assessment
Shushan Basin evolution
Paleogeographic history of of the SE Mediterranean region

Fig. 4.

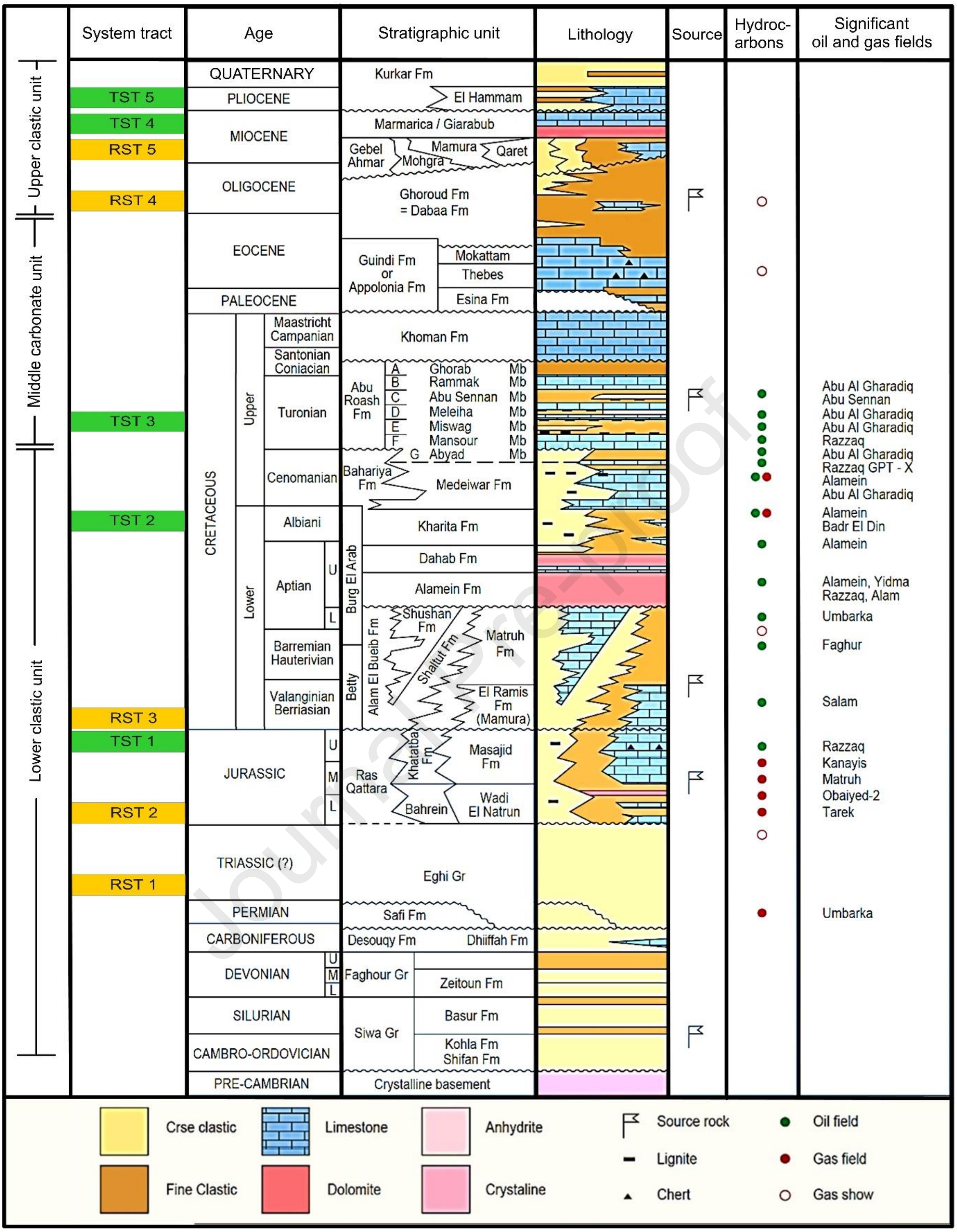
System tract
Age
Stratigraphic unit
Lithology
Source
Hydrocarbons
Significant oil and gas fields
Upper clastic unit
Middle carbonate unit
Lower clastic unit
TST 5
TST 4
RST 5
RST 4
TST 3
TST 2
RST 3
TST 1
RST 2
RST 1
QUATERNARY
PLIOCENE
MIOCENE
OLIGOCENE
EOCENE
PALEOCENE
CRETACEOUS
Upper
Lower
Maastricht Campanian
Santonian Coniacian
Turonian
Cenomanian
Albiani
Aptian
Barremian Hauterivian
Valanginian Berriasian
JURASSIC
TRIASSIC (?)
PERMIAN
CARBONIFEROUS
DEVONIAN
SILURIAN
CAMBRO-ORDOVICIAN
PRE-CAMBRIAN
Kurkar Fm
El Hammam
Marmarica / Giarabub
Gebel Ahmar
Mamura
Mohgra
Qaret
Ghoroud Fm = Dabaa Fm
Guindi Fm or Appolonia Fm
Mokattam
Thebes
Esina Fm
Khoman Fm
Abu Roash Fm
A Ghorab Mb
B Rammak Mb
C Abu Sennan Mb
D Meleiha Mb
E Miswag Mb
F Mansour Mb
G Abyad Mb
Bahariya Fm
Medeiwar Fm
Kharita Fm
Dahab Fm
Alamein Fm
Burg El Arab
Alam El Bueib Fm
Betty
Shushan Fm
Shaltut Fm
Matruh Fm
El Ramis Fm (Mamura)
Khatatba Fm
Masajid Fm
Ras Qattara
Bahrein
Wadi El Natrun
Eghi Gr
Safi Fm
Desouqy Fm
Dhiiffah Fm
Faghour Gr
Zeitoun Fm
Siwa Gr
Basur Fm
Kohla Fm
Shifan Fm
Crystalline basement
Abu Al Gharadiq
Abu Sennan
Abu Al Gharadiq
Abu Al Gharadiq
Razzaq
Abu Al Gharadiq
Razzaq GPT - X
Alamein
Abu Al Gharadiq
Alamein
Badr El Din
Alamein
Alamein, Yidma
Razzaq, Alam
Umbarka
Faghur
Salam
Razzaq
Kanayis
Matruh
Obaiyed-2
Tarek
Umbarka
Crse clastic
Fine Clastic
Limestone
Dolomite
Anhydrite
Crystaline
Source rock
Lignite
Chert
Oil field
Gas field
Gas show

Fig. 5.

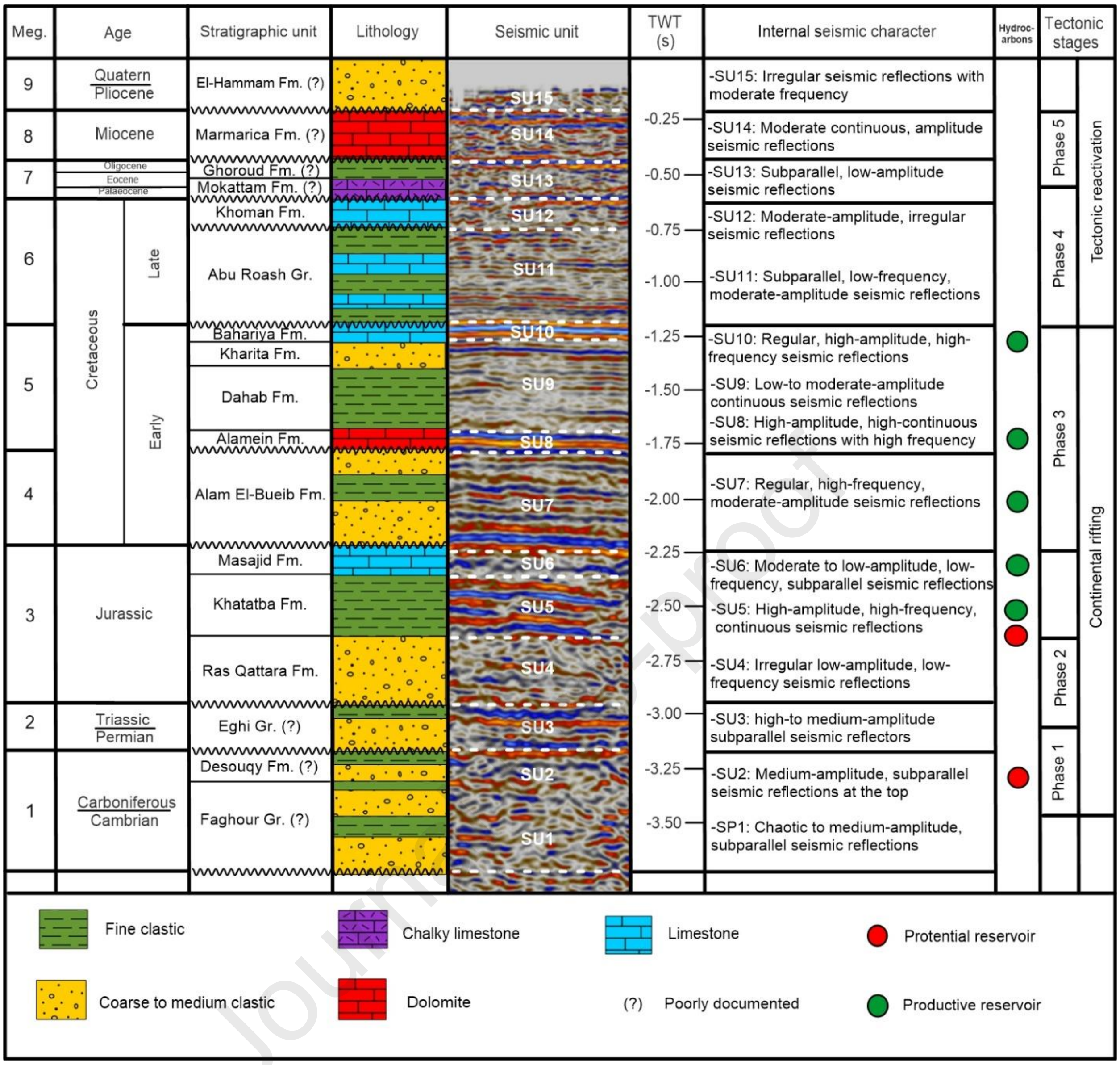

Meg.
Age
Stratigraphic unit
Lithology
Seismic unit
TWT (s)
Internal seismic character
Hydroc-arbons
Tectonic stages
Quatern
Pliocene
Miocene
Oligocene
Eocene
Palaeocene
Cretaceous
Late
Early
Jurassic
Triassic
Permian
Carboniferous
Cambrian
El-Hammam Fm. (?)
Marmarica Fm. (?)
Ghoroud Fm. (?)
Mokattam Fm. (?)
Khoman Fm.
Abu Roash Gr.
Bahariya Fm.
Kharita Fm.
Dahab Fm.
Alamein Fm.
Alam El-Bueib Fm.
Masajid Fm.
Khatatba Fm.
Ras Qattara Fm.
Eghi Gr. (?)
Desouqy Fm. (?)
Faghour Gr. (?)
-SU15: Irregular seismic reflections with moderate frequency
-SU14: Moderate continuous, amplitude seismic reflections
-SU13: Subparallel, low-amplitude seismic reflections
-SU12: Moderate-amplitude, irregular seismic reflections
-SU11: Subparallel, low-frequency, moderate-amplitude seismic reflections
-SU10: Regular, high-amplitude, high-frequency seismic reflections
-SU9: Low-to moderate-amplitude continuous seismic reflections
-SU8: High-amplitude, high-continuous seismic reflections with high frequency
-SU7: Regular, high-frequency, moderate-amplitude seismic reflections
-SU6: Moderate to low-amplitude, low-frequency, subparallel seismic reflections
-SU5: High-amplitude, high-frequency, continuous seismic reflections
-SU4: Irregular low-amplitude, low-frequency seismic reflections
-SU3: high-to medium-amplitude subparallel seismic reflectors
-SU2: Medium-amplitude, subparallel seismic reflections at the top
-SP1: Chaotic to medium-amplitude, subparallel seismic reflections
Phase 5
Phase 4
Phase 3
Phase 2
Phase 1
Tectonic reactivation
Continental rifting
Fine clastic
Chalky limestone
Limestone
Protential reservoir
Coarse to medium clastic
Dolomite
(?) Poorly documented
Productive reservoir

Fig. 6.

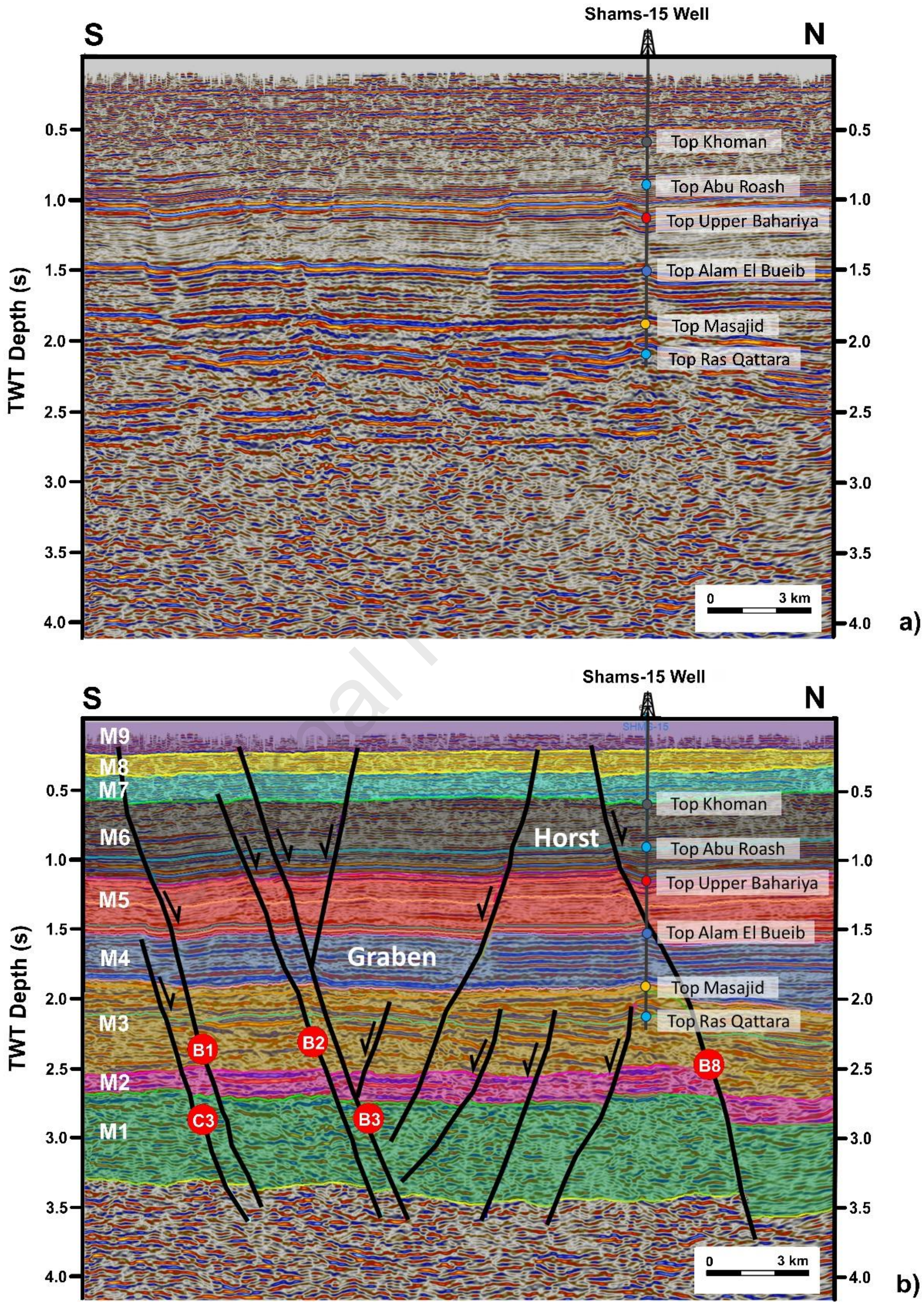

Shams-15 Well
S
N
0.5
1.0
1.5
2.0
2.5
3.0
3.5
4.0
TWT Depth (s)
Top Khoman
Top Abu Roash
Top Upper Bahariya
Top Alam El Bueib
Top Masajid
Top Ras Qattara
0
3 km
a)
M9
M8
M7
M6
M5
M4
M3
M2
M1
Horst
Graben
B1
B2
B3
C3
B8
b)

Fig. 7.

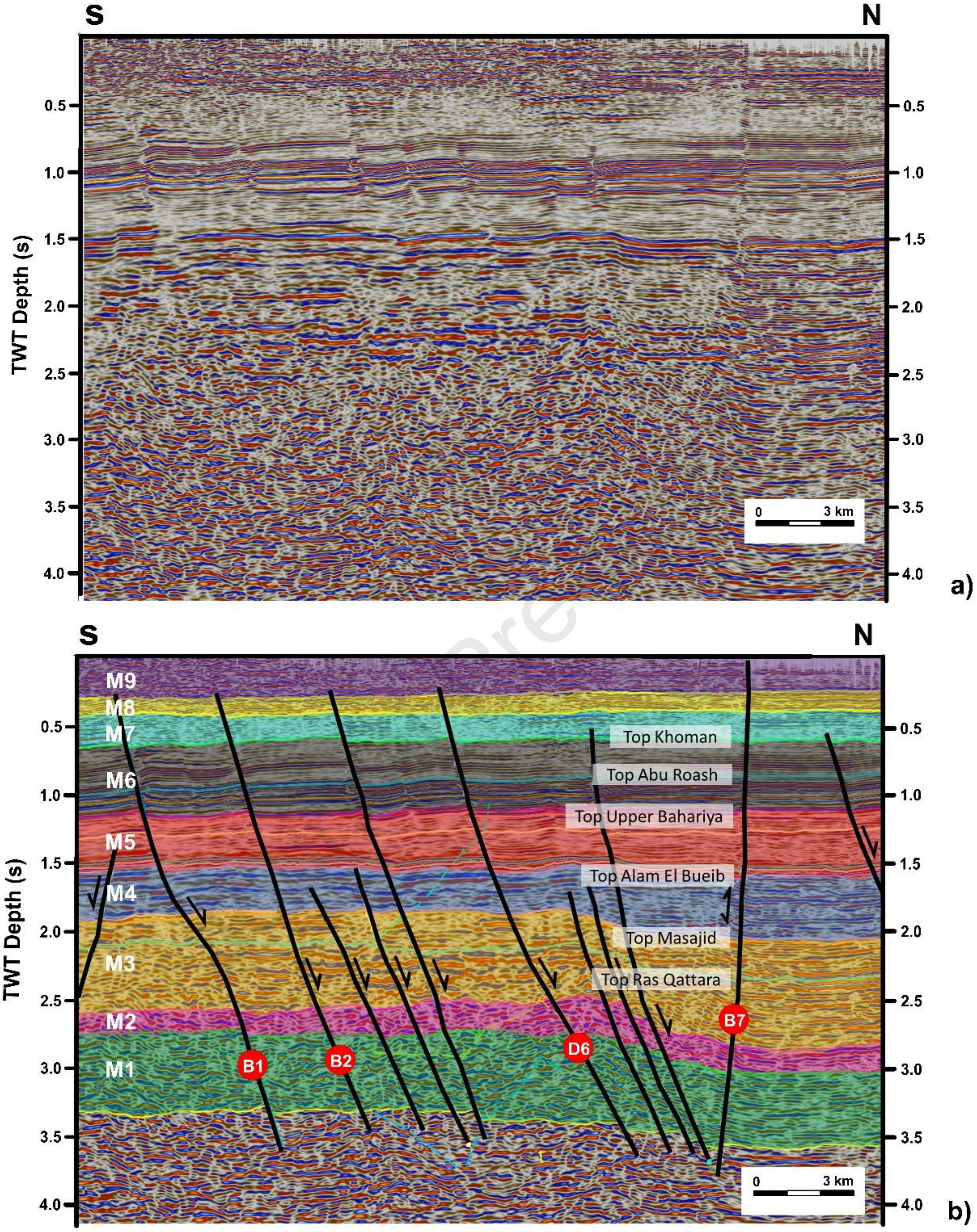
S
N
TWT Depth (s)
0.5
1.0
1.5
2.0
2.5
3.0
3.5
4.0
0
3 km
a)
M9
M8
M7
M6
M5
M4
M3
M2
M1
Top Khoman
Top Abu Roash
Top Upper Bahariya
Top Alam El Bueib
Top Masajid
Top Ras Qattara
B1
B2
D6
B7
b)

Fig. 8.

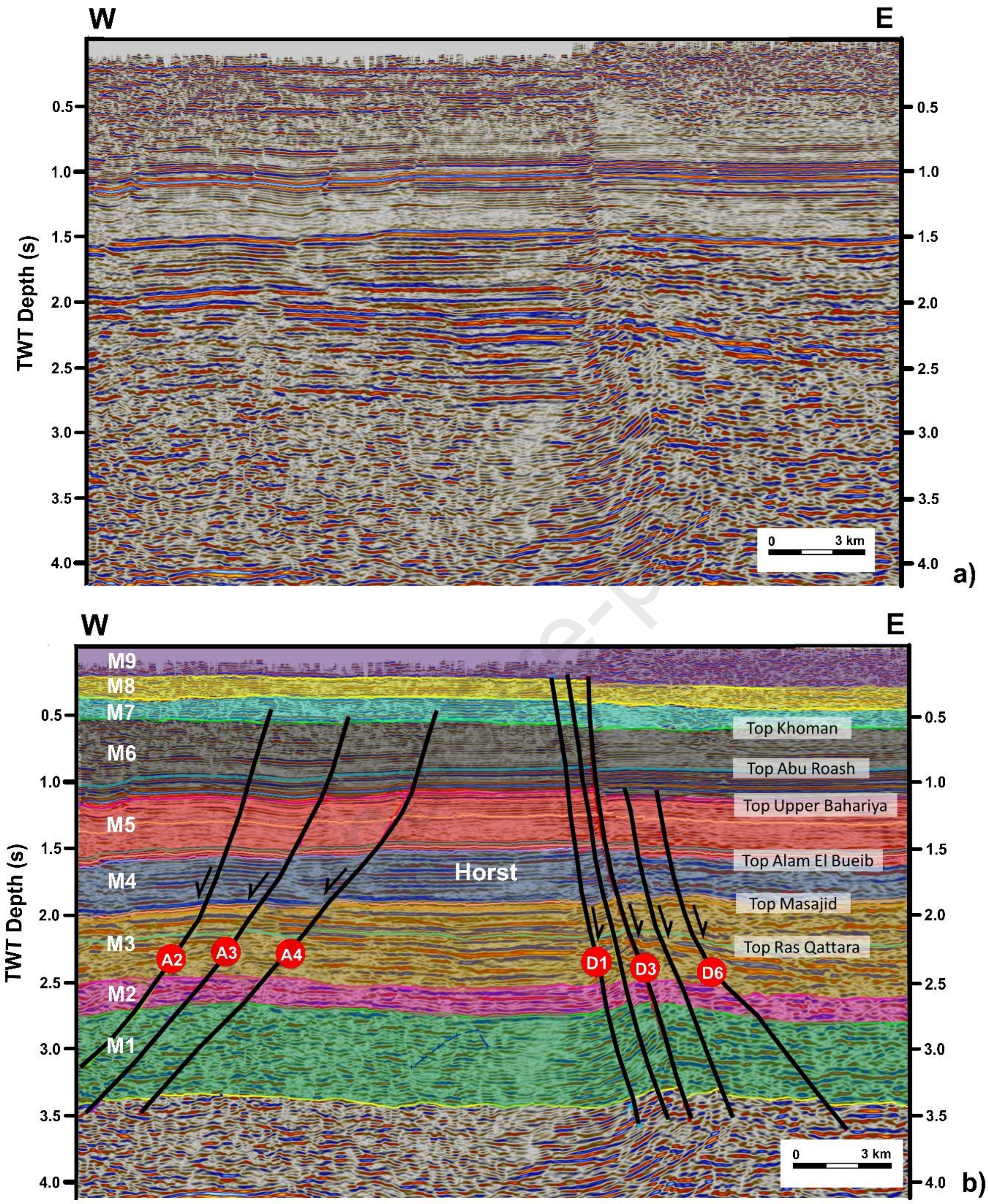
W
E
TWT Depth (s)
0.5
1.0
1.5
2.0
2.5
3.0
3.5
4.0
0
3 km
a)
W
E
M9
M8
M7
M6
M5
M4
M3
M2
M1
Horst
A2
A3
A4
D1
D3
D6
Top Khoman
Top Abu Roash
Top Upper Bahariya
Top Alam El Bueib
Top Masajid
Top Ras Qattara
TWT Depth (s)
0.5
1.0
1.5
2.0
2.5
3.0
3.5
4.0
0
3 km
b)

Fig. 9.

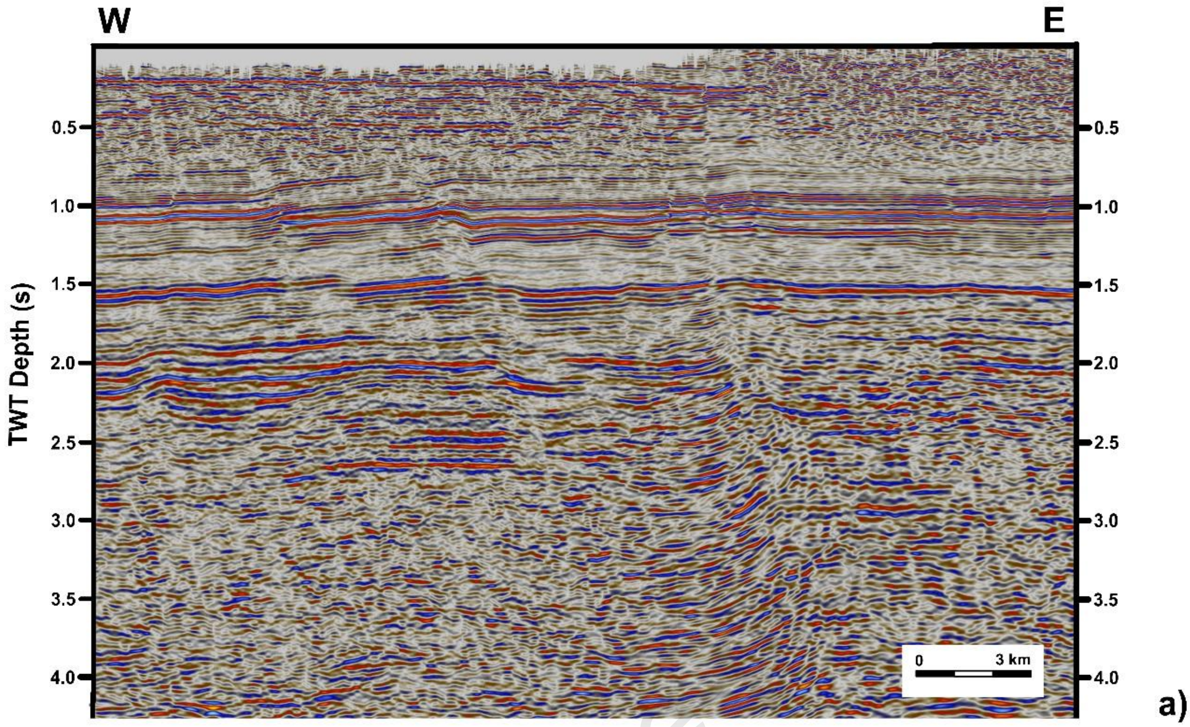
W
E
TWT Depth (s)
0.5
1.0
1.5
2.0
2.5
3.0
3.5
4.0
0
3 km
a)

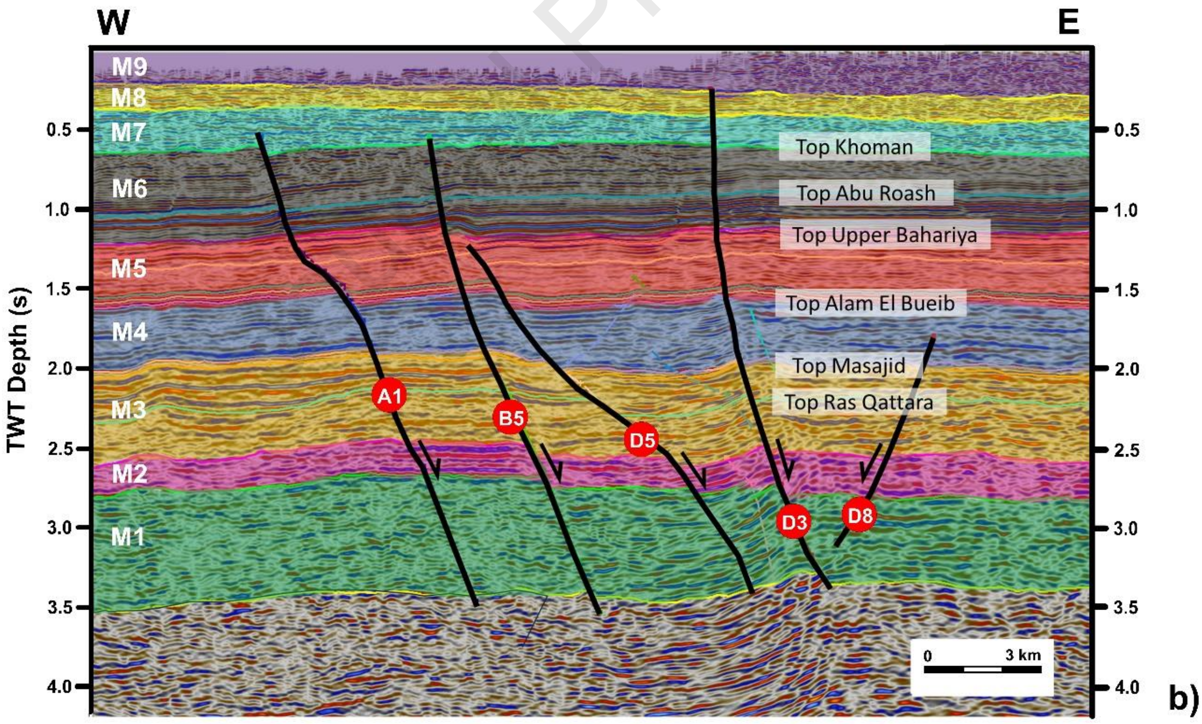
W
E
TWT Depth (s)
M9
M8
M7
M6
M5
M4
M3
M2
M1
Top Khoman
Top Abu Roash
Top Upper Bahariya
Top Alam El Bueib
Top Masajid
Top Ras Qattara
A1
B5
D5
D3
D8
0.5
1.0
1.5
2.0
2.5
3.0
3.5
4.0
0
3 km
b)

Fig. 10.

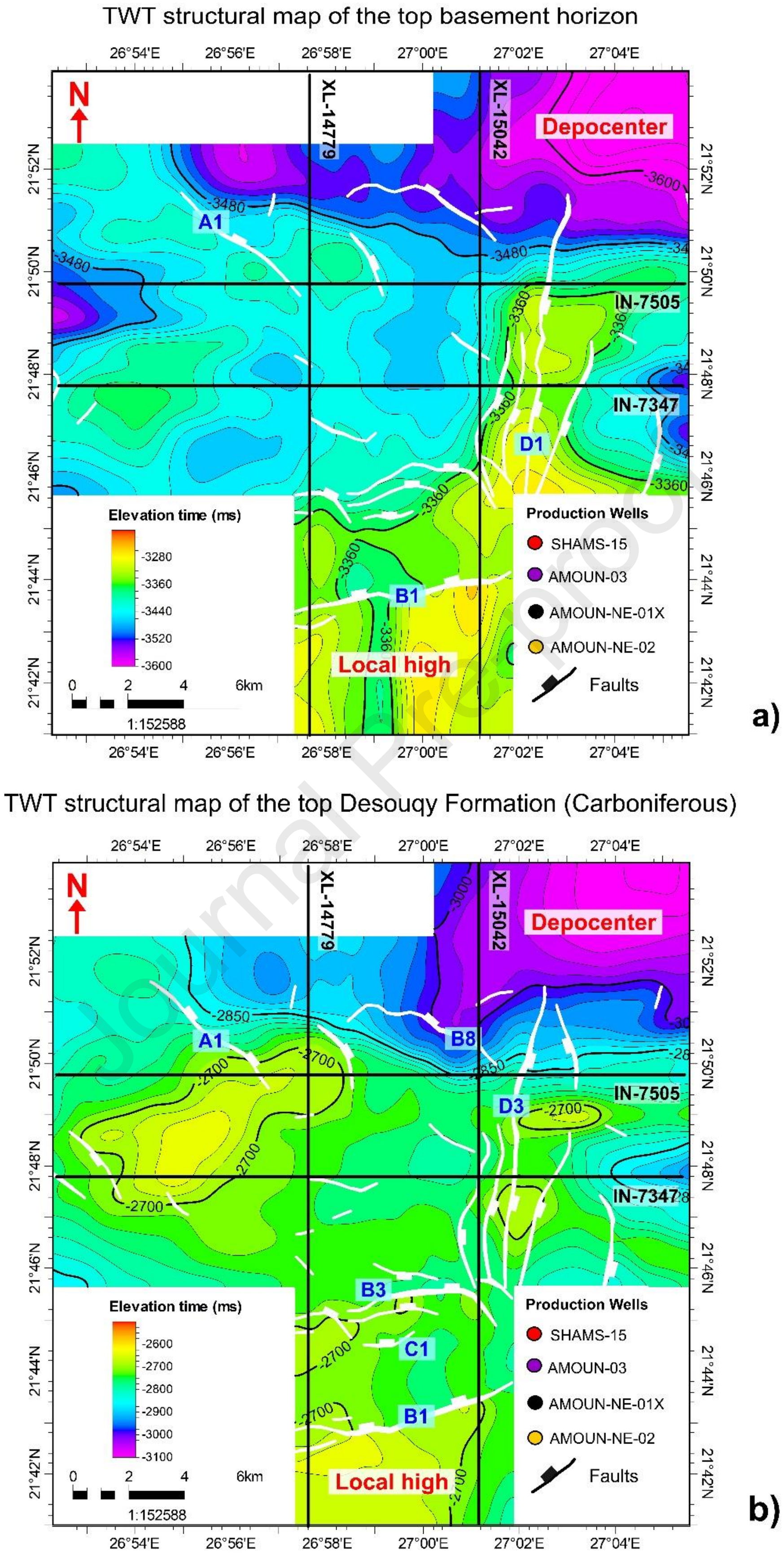
TWT structural map of the top basement horizon
26°54'E
26°56'E
26°58'E
27°00'E
27°02'E
27°04'E
21°52'N
21°50'N
21°48'N
21°46'N
21°44'N
21°42'N
N
XL-14779
XL-15042
Depocenter
A1
IN-7505
IN-7347
D1
B1
Local high
-3480
-3600
-3360
Elevation time (ms)
-3280
-3360
-3440
-3520
-3600
0
2
4
6km
1:152588
Production Wells
SHAMS-15
AMOUN-03
AMOUN-NE-01X
AMOUN-NE-02
Faults
a)
TWT structural map of the top Desouqy Formation (Carboniferous)
26°54'E
26°56'E
26°58'E
27°00'E
27°02'E
27°04'E
21°52'N
21°50'N
21°48'N
21°46'N
21°44'N
21°42'N
N
XL-14779
XL-15042
Depocenter
A1
B8
IN-7505
D3
IN-7347
B3
C1
B1
Local high
-3000
-2850
-2700
Elevation time (ms)
-2600
-2700
-2800
-2900
-3000
-3100
0
2
4
6km
1:152588
Production Wells
SHAMS-15
AMOUN-03
AMOUN-NE-01X
AMOUN-NE-02
Faults
b)

Fig. 11.

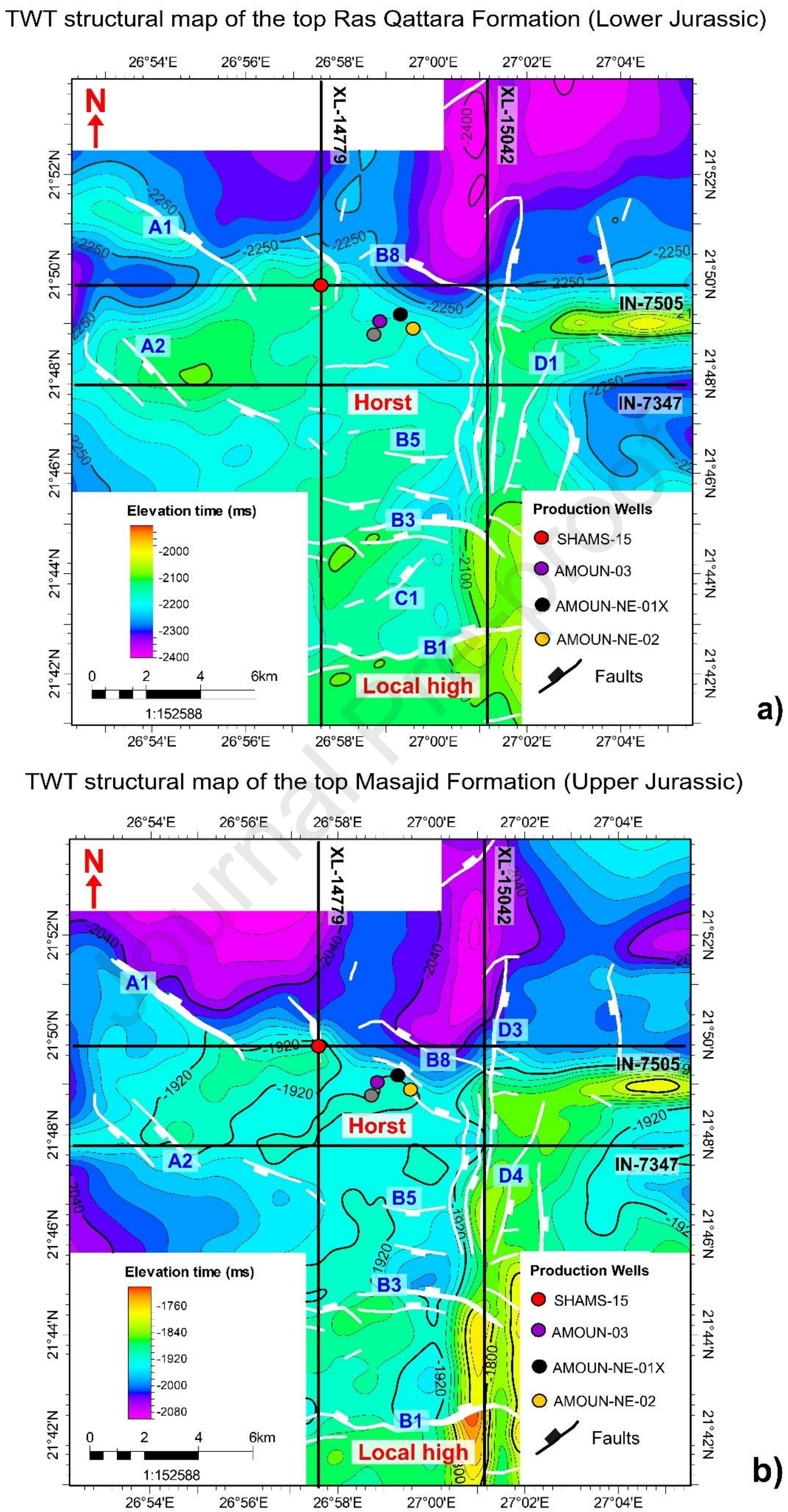
TWT structural map of the top Ras Qattara Formation (Lower Jurassic)
26°54'E
26°56'E
26°58'E
27°00'E
27°02'E
27°04'E
21°52'N
21°50'N
21°48'N
21°46'N
21°44'N
21°42'N
N
XL-14779
XL-15042
IN-7505
IN-7347
-2250
-2400
-2100
A1
A2
B8
D1
Horst
B5
B3
C1
B1
Local high
Elevation time (ms)
-2000
-2100
-2200
-2300
-2400
0
2
4
6km
1:152588
Production Wells
SHAMS-15
AMOUN-03
AMOUN-NE-01X
AMOUN-NE-02
Faults
a)
TWT structural map of the top Masajid Formation (Upper Jurassic)
-2040
-1920
-1800
A1
A2
B8
D3
D4
Horst
B5
B3
B1
Local high
Elevation time (ms)
-1760
-1840
-1920
-2000
-2080
b)

Fig. 12.

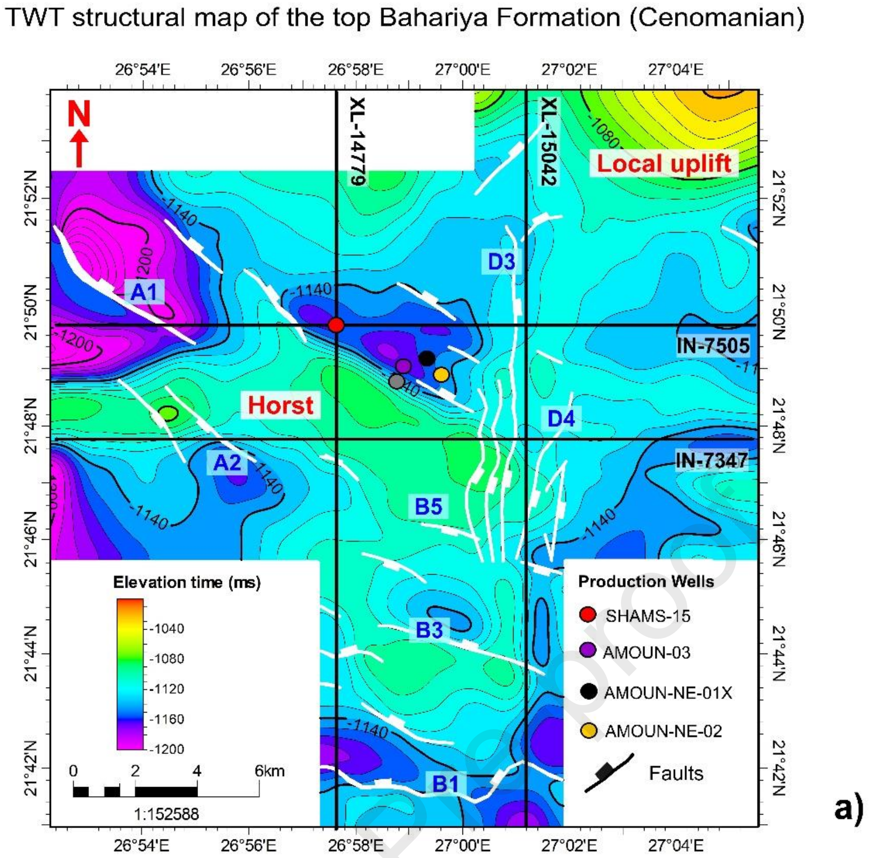
TWT structural map of the top Bahariya Formation (Cenomanian)
XL-14779
XL-15042
Local uplift
A1
D3
IN-7505
Horst
D4
A2
IN-7347
B5
B3
B1
Elevation time (ms)
Production Wells
SHAMS-15
AMOUN-03
AMOUN-NE-01X
AMOUN-NE-02
Faults
1:152588
a)

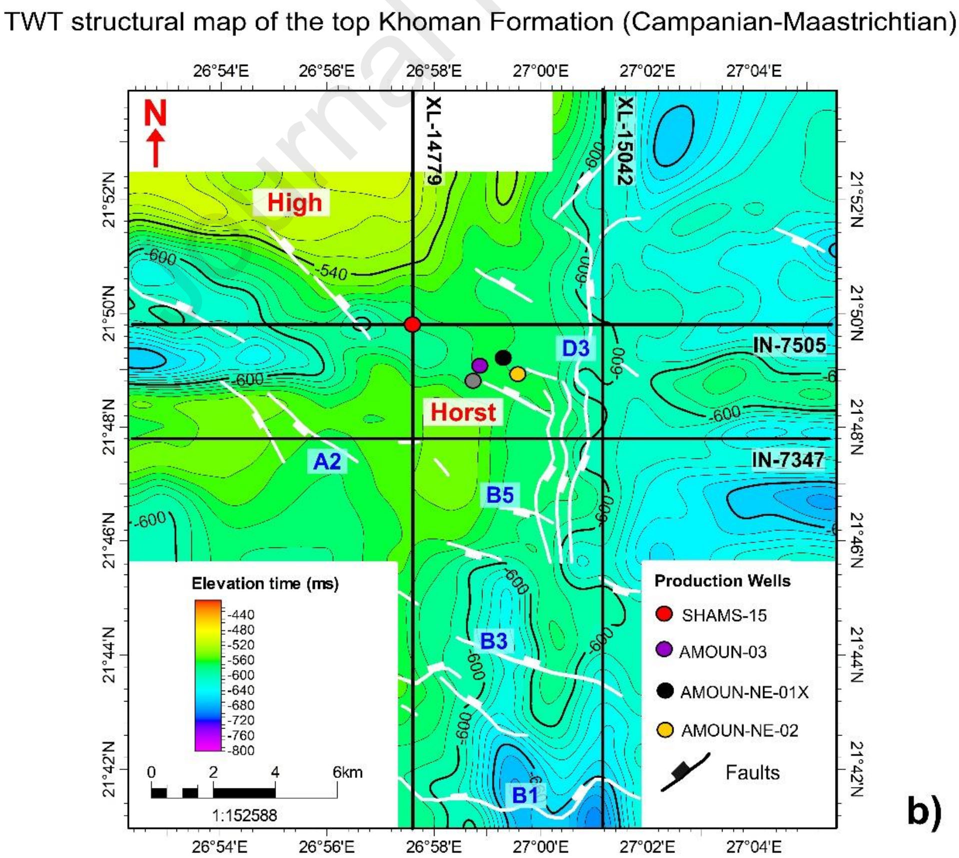
TWT structural map of the top Khoman Formation (Campanian-Maastrichtian)
XL-14779
XL-15042
High
D3
IN-7505
Horst
A2
IN-7347
B5
B3
B1
Elevation time (ms)
Production Wells
SHAMS-15
AMOUN-03
AMOUN-NE-01X
AMOUN-NE-02
Faults
1:152588
b)

Fig. 13.

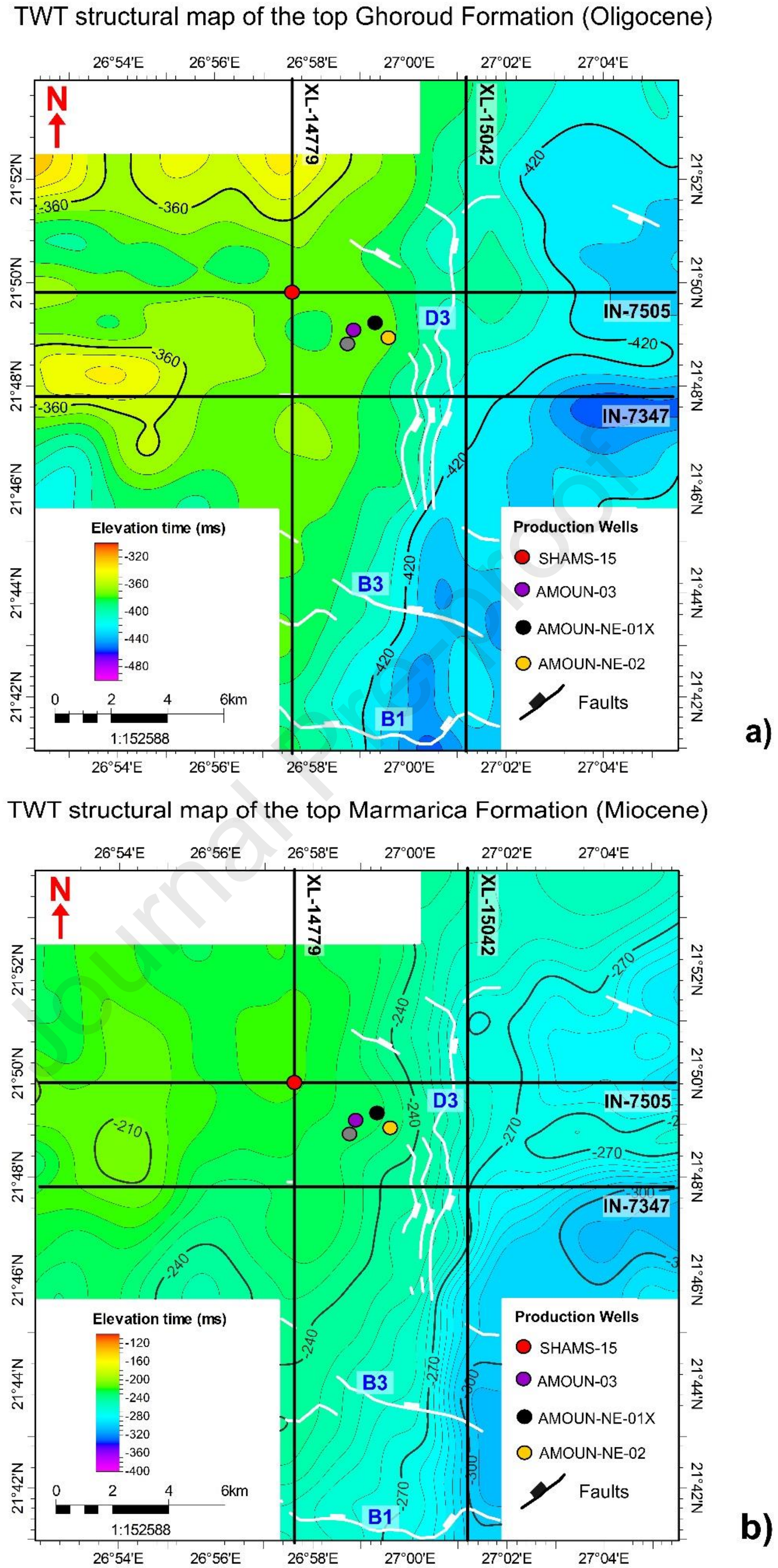
TWT structural map of the top Ghoroud Formation (Oligocene)
XL-14779
XL-15042
IN-7505
IN-7347
D3
B3
B1
Elevation time (ms)
Production Wells
SHAMS-15
AMOUN-03
AMOUN-NE-01X
AMOUN-NE-02
Faults
1:152588
a)
TWT structural map of the top Marmarica Formation (Miocene)
XL-14779
XL-15042
IN-7505
IN-7347
D3
B3
B1
Elevation time (ms)
Production Wells
SHAMS-15
AMOUN-03
AMOUN-NE-01X
AMOUN-NE-02
Faults
1:152588
b)

Fig. 14.

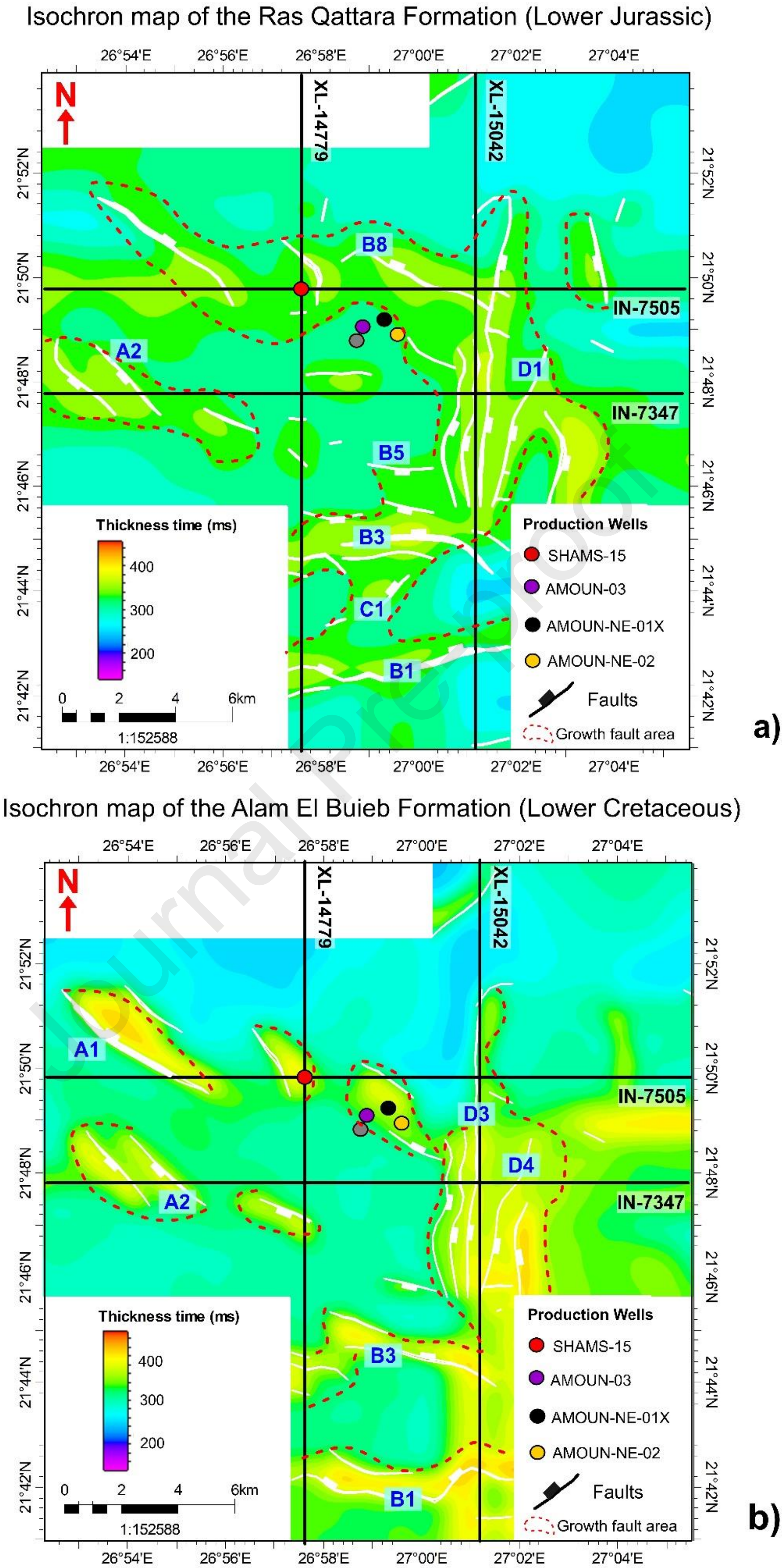
Isochron map of the Ras Qattara Formation (Lower Jurassic)
26°54'E
26°56'E
26°58'E
27°00'E
27°02'E
27°04'E
21°52'N
21°50'N
21°48'N
21°46'N
21°44'N
21°42'N
N
XL-14779
XL-15042
IN-7505
IN-7347
A2
B8
B5
B3
C1
B1
D1
Thickness time (ms)
400
300
200
0
2
4
6km
1:152588
Production Wells
SHAMS-15
AMOUN-03
AMOUN-NE-01X
AMOUN-NE-02
Faults
Growth fault area
a)
Isochron map of the Alam El Buieb Formation (Lower Cretaceous)
A1
A2
B3
B1
D3
D4
b)

Fig. 15.

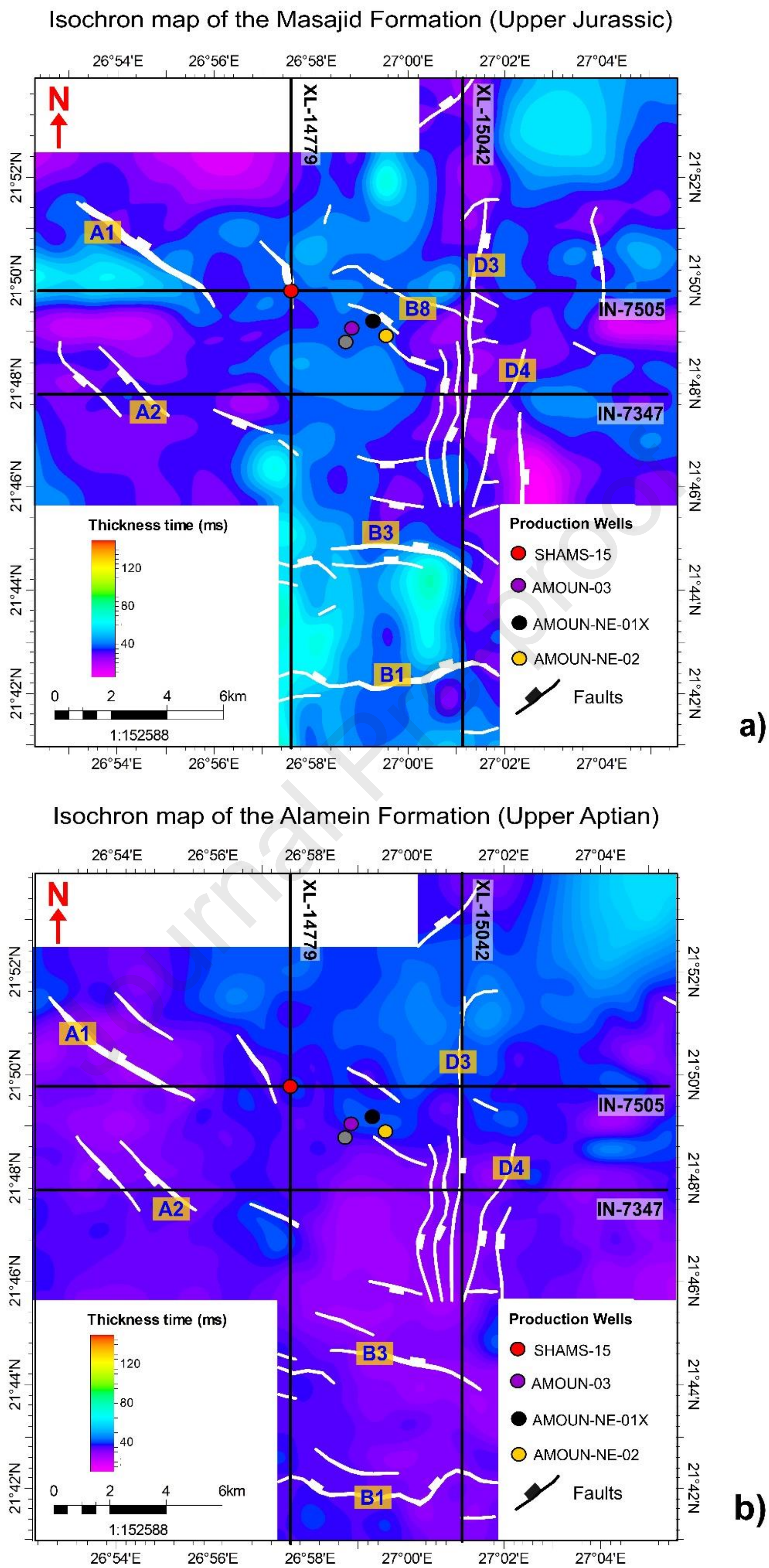
Isochron map of the Masajid Formation (Upper Jurassic)
26°54'E
26°56'E
26°58'E
27°00'E
27°02'E
27°04'E
21°52'N
21°50'N
21°48'N
21°46'N
21°44'N
21°42'N
N
XL-14779
XL-15042
A1
A2
B8
B3
B1
D3
D4
IN-7505
IN-7347
Thickness time (ms)
120
80
40
0
2
4
6km
1:152588
Production Wells
SHAMS-15
AMOUN-03
AMOUN-NE-01X
AMOUN-NE-02
Faults
a)
Isochron map of the Alamein Formation (Upper Aptian)
b)

Fig. 16.

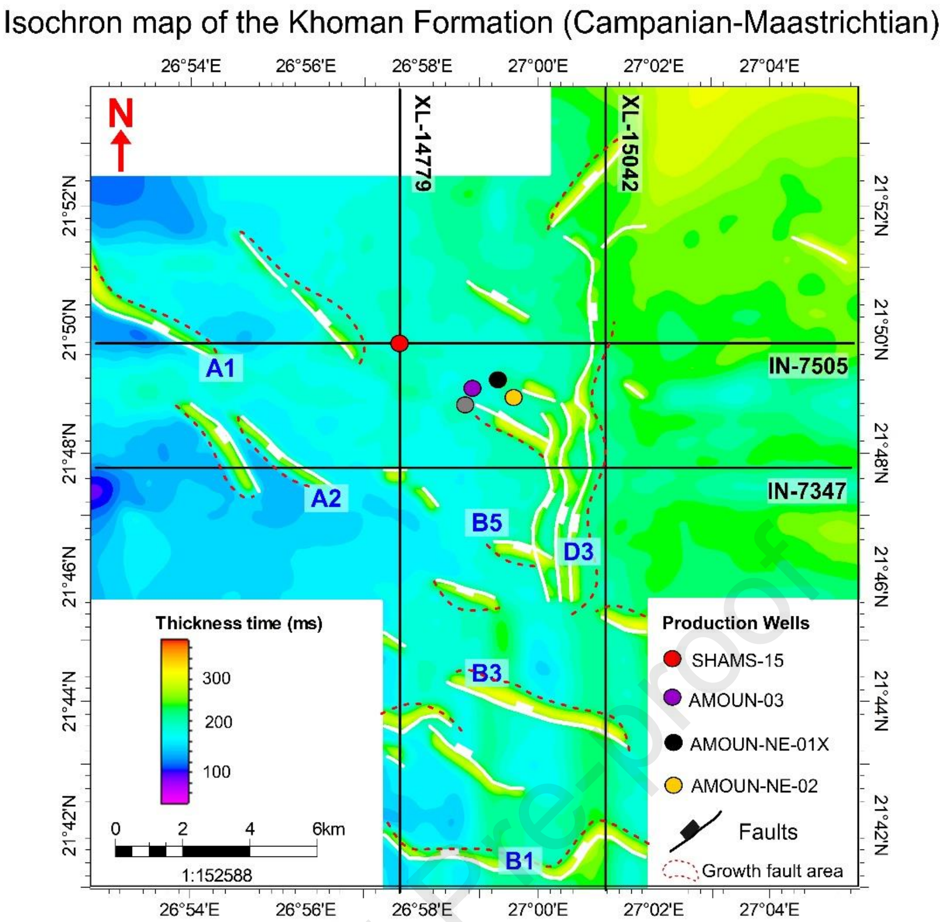
Isochron map of the Khoman Formation (Campanian-Maastrichtian)
26°54'E
26°56'E
26°58'E
27°00'E
27°02'E
27°04'E
21°52'N
21°50'N
21°48'N
21°46'N
21°44'N
21°42'N
N
XL-14779
XL-15042
IN-7505
IN-7347
A1
A2
B5
D3
B3
B1
Thickness time (ms)
300
200
100
0
2
4
6km
1:152588
Production Wells
SHAMS-15
AMOUN-03
AMOUN-NE-01X
AMOUN-NE-02
Faults
Growth fault area

Fig. 17.

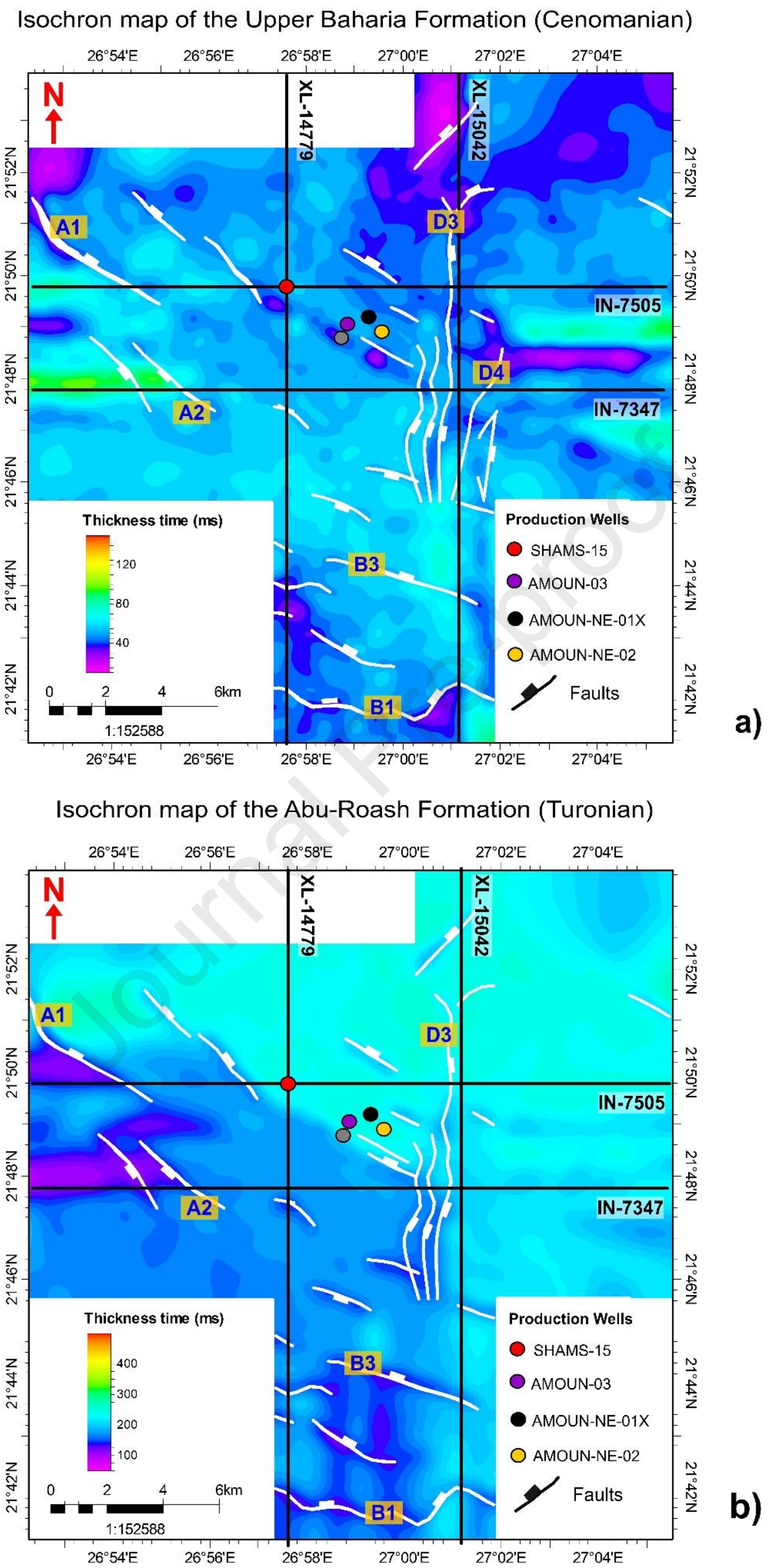
Isochron map of the Upper Baharia Formation (Cenomanian)
26°54'E
26°56'E
26°58'E
27°00'E
27°02'E
27°04'E
21°52'N
21°50'N
21°48'N
21°46'N
21°44'N
21°42'N
N
XL-14779
XL-15042
A1
A2
D3
D4
B3
B1
IN-7505
IN-7347
Thickness time (ms)
120
80
40
0
2
4
6km
1:152588
Production Wells
SHAMS-15
AMOUN-03
AMOUN-NE-01X
AMOUN-NE-02
Faults
a)
Isochron map of the Abu-Roash Formation (Turonian)
Thickness time (ms)
400
300
200
100
b)

Fig. 18.

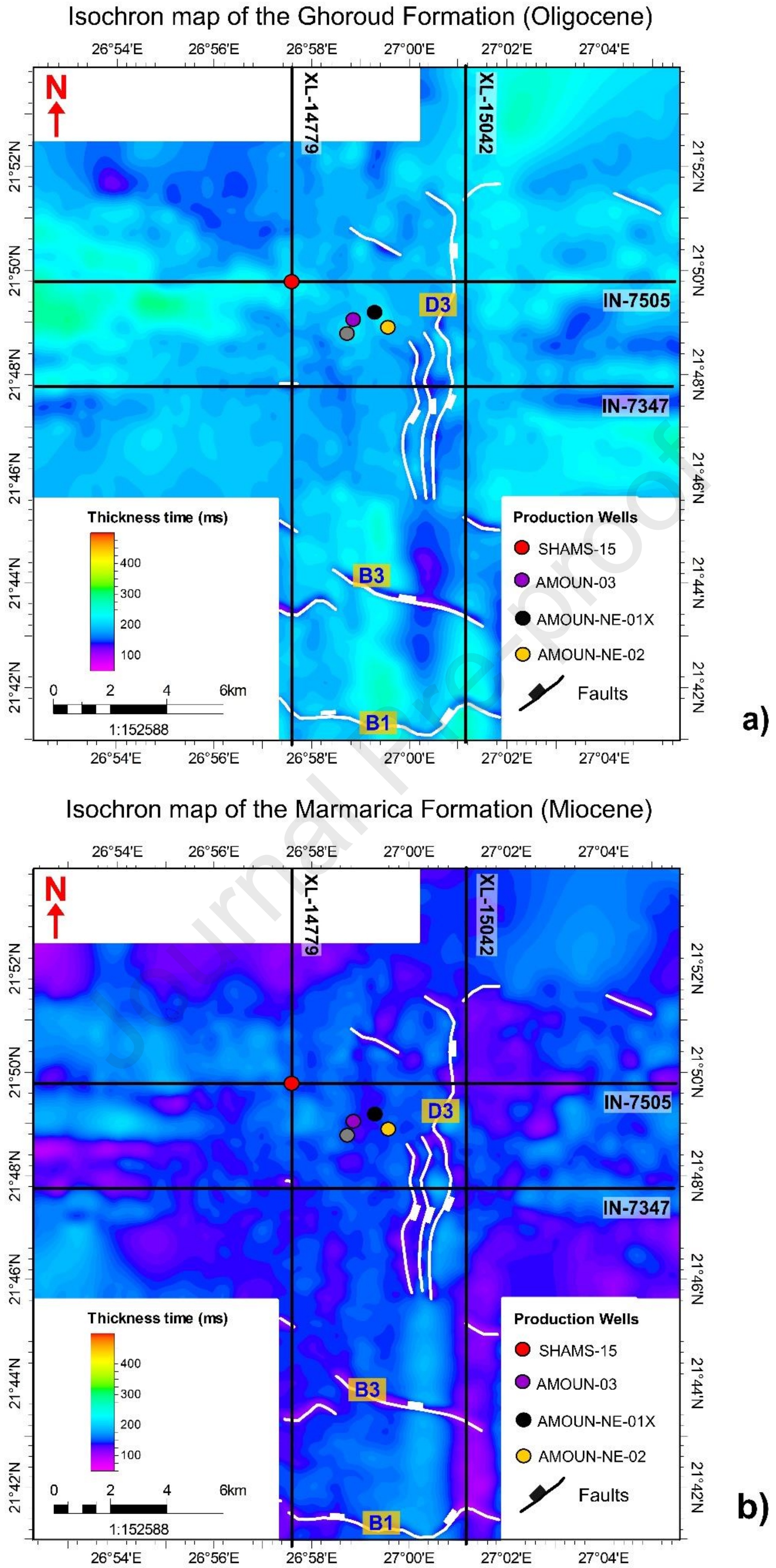
Isochron map of the Ghoroud Formation (Oligocene)
26°54'E
26°56'E
26°58'E
27°00'E
27°02'E
27°04'E
21°52'N
21°50'N
21°48'N
21°46'N
21°44'N
21°42'N
N
XL-14779
XL-15042
IN-7505
IN-7347
D3
B3
B1
Thickness time (ms)
400
300
200
100
0
2
4
6km
1:152588
Production Wells
SHAMS-15
AMOUN-03
AMOUN-NE-01X
AMOUN-NE-02
Faults
a)
Isochron map of the Marmarica Formation (Miocene)
b)

Fig. 19.

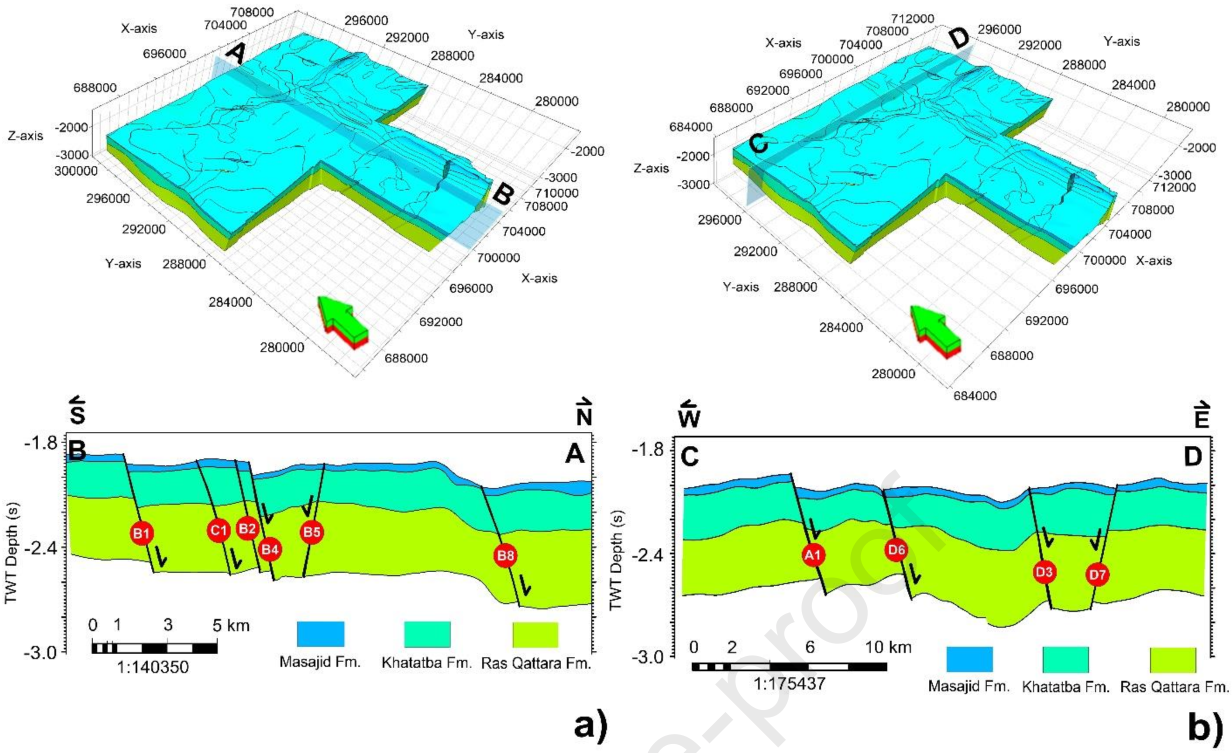
X-axis
Y-axis
Z-axis
A
B
C
D
S
N
W
E
TWT Depth (s)
-1.8
-2.4
-3.0
B1
C1
B2
B4
B5
B8
A1
D6
D3
D7
0 1 3 5 km
1:140350
0 2 6 10 km
1:175437
Masajid Fm.
Khatatba Fm.
Ras Qattara Fm.
a)
b)

Fig. 20.

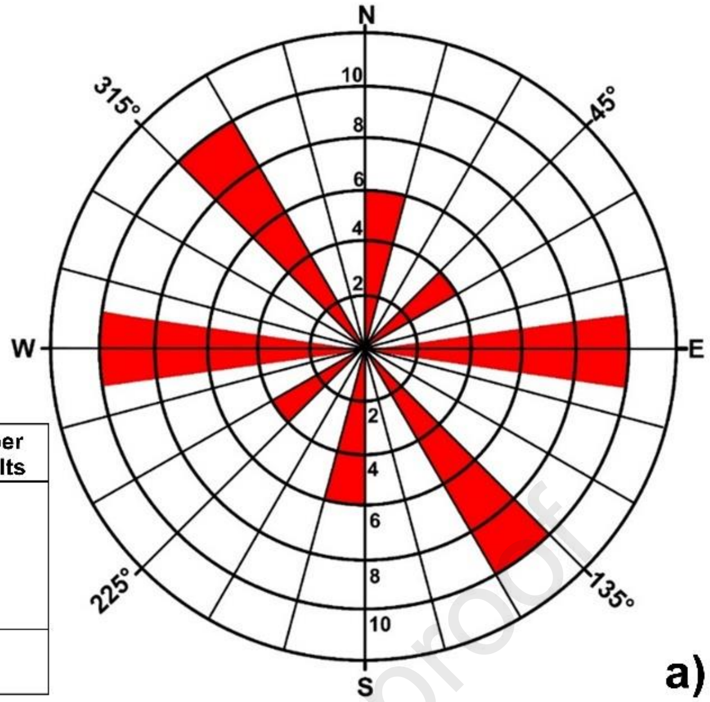

Strike	Number of faults
NW	10
NNE	6
NE	4
E-W	10
Total number of faults	**30**

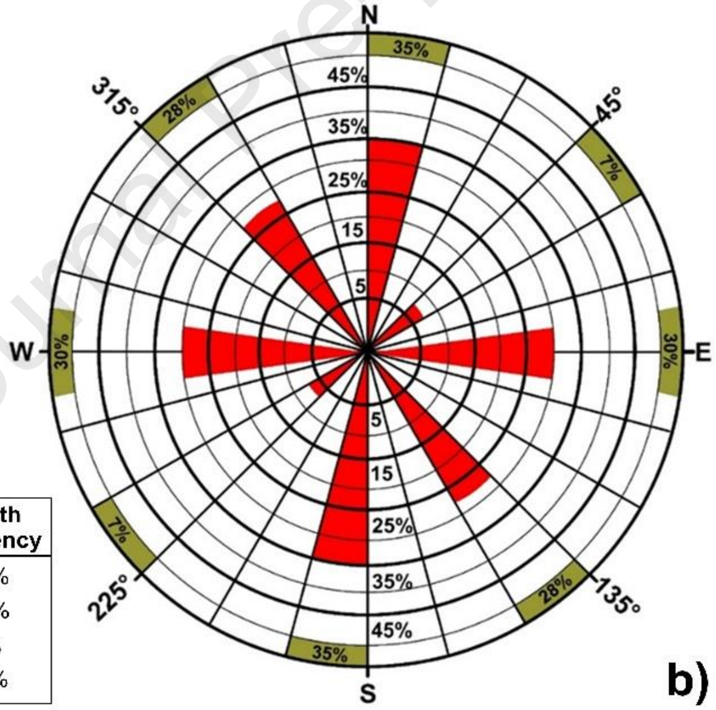

Strike	Length frequency
NW	28%
NNE	35%
NE	7%
E-W	30%

Fig. 21.

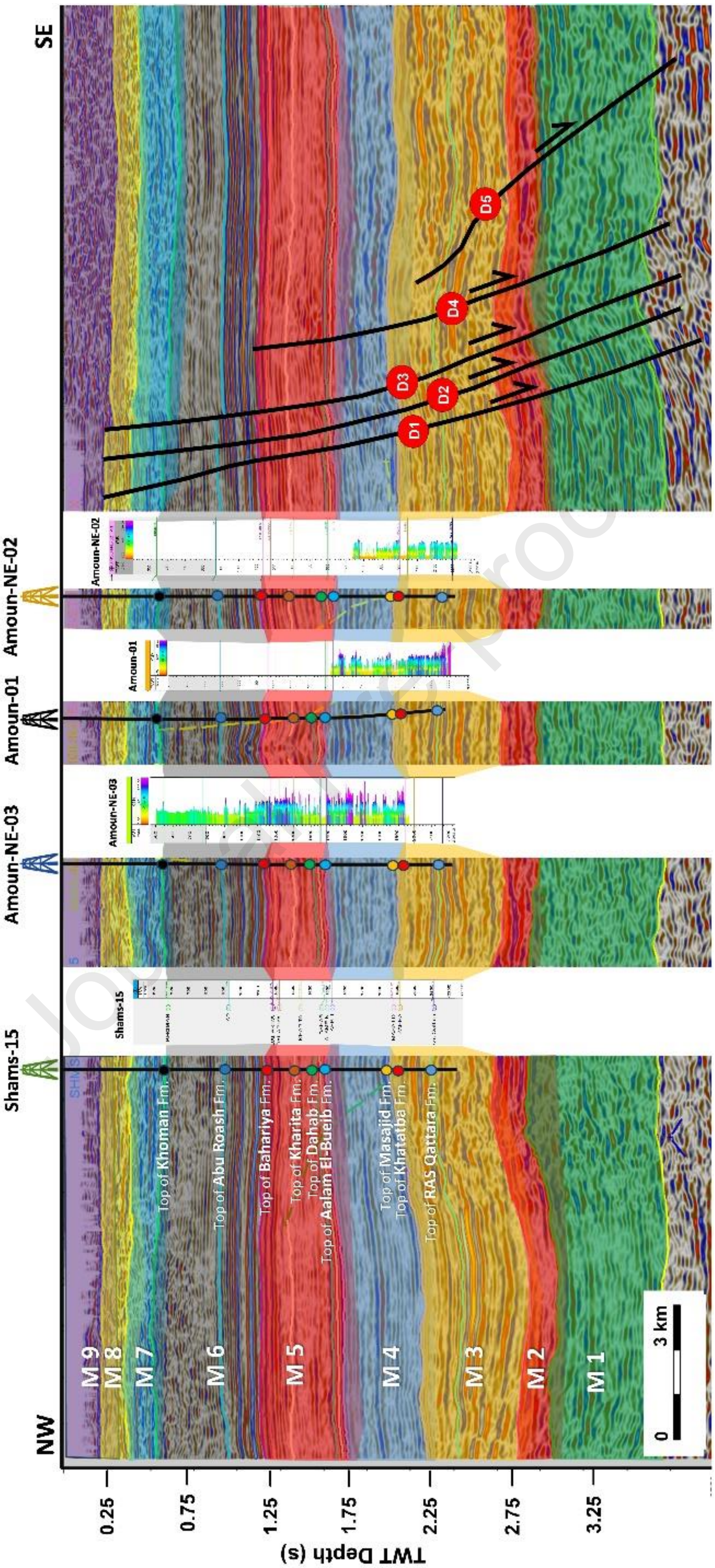
NW
SE
Shams-15
Amoun-NE-03
Amoun-01
Amoun-NE-02
M 9
M 8
M 7
M 6
M 5
M 4
M 3
M 2
M 1
Top of Khoman Fm.
Top of Abu Roash Fm.
Top of Bahariya Fm.
Top of Kharita Fm.
Top of Dahab Fm.
Top of Aalam El-Bueib Fm.
Top of Masajid Fm.
Top of Khatatba Fm.
Top of RAS Qattara Fm.
D1
D2
D3
D4
D5
0
3 km
TWT Depth (s)
0.25
0.75
1.25
1.75
2.25
2.75
3.25

Fig. 22.

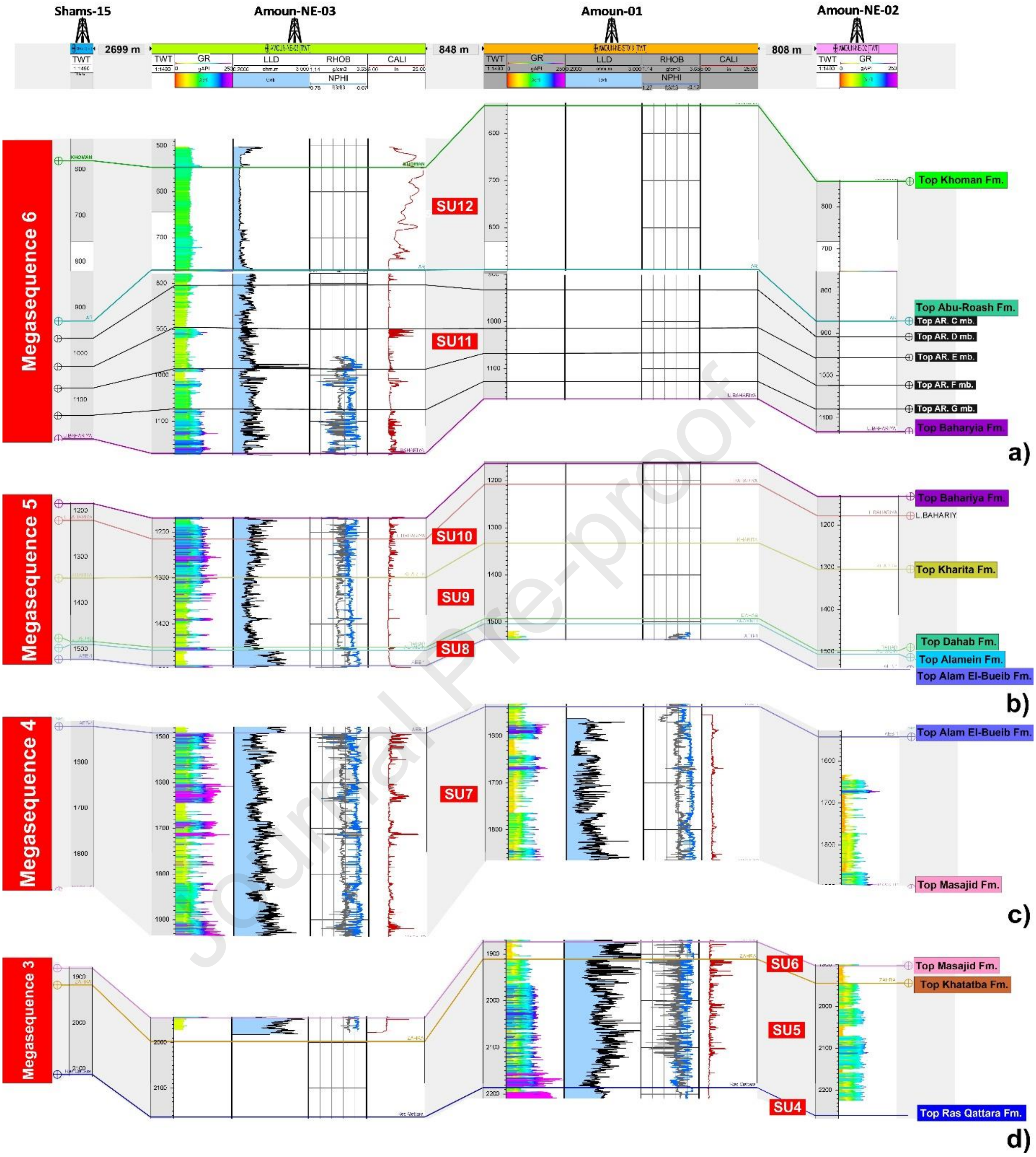

Shams-15
Amoun-NE-03
Amoun-01
Amoun-NE-02
2699 m
848 m
808 m
TWT
GR
LLD
RHOB
CALI
NPHI
Megasequence 6
Megasequence 5
Megasequence 4
Megasequence 3
SU12
SU11
SU10
SU9
SU8
SU7
SU6
SU5
SU4
Top Khoman Fm.
Top Abu-Roash Fm.
Top AR. C mb.
Top AR. D mb.
Top AR. E mb.
Top AR. F mb.
Top AR. G mb.
Top Baharyia Fm.
Top Bahariya Fm.
L.BAHARIY
Top Kharita Fm.
Top Dahab Fm.
Top Alamein Fm.
Top Alam El-Bueib Fm.
Top Masajid Fm.
Top Khatatba Fm.
Top Ras Qattara Fm.
a)
b)
c)
d)

Fig. 23.

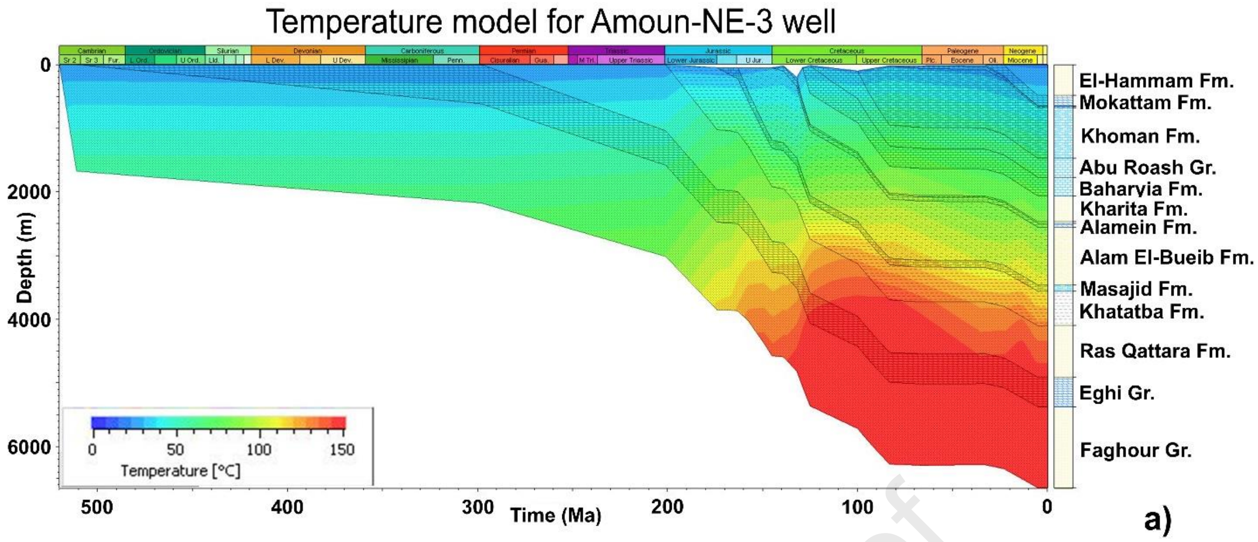
Temperature model for Amoun-NE-3 well
Depth (m)
0
2000
4000
6000
Temperature [°C]
0
50
100
150
500
400
300
Time (Ma)
200
100
0
El-Hammam Fm.
Mokattam Fm.
Khoman Fm.
Abu Roash Gr.
Baharyia Fm.
Kharita Fm.
Alamein Fm.
Alam El-Bueib Fm.
Masajid Fm.
Khatatba Fm.
Ras Qattara Fm.
Eghi Gr.
Faghour Gr.
a)

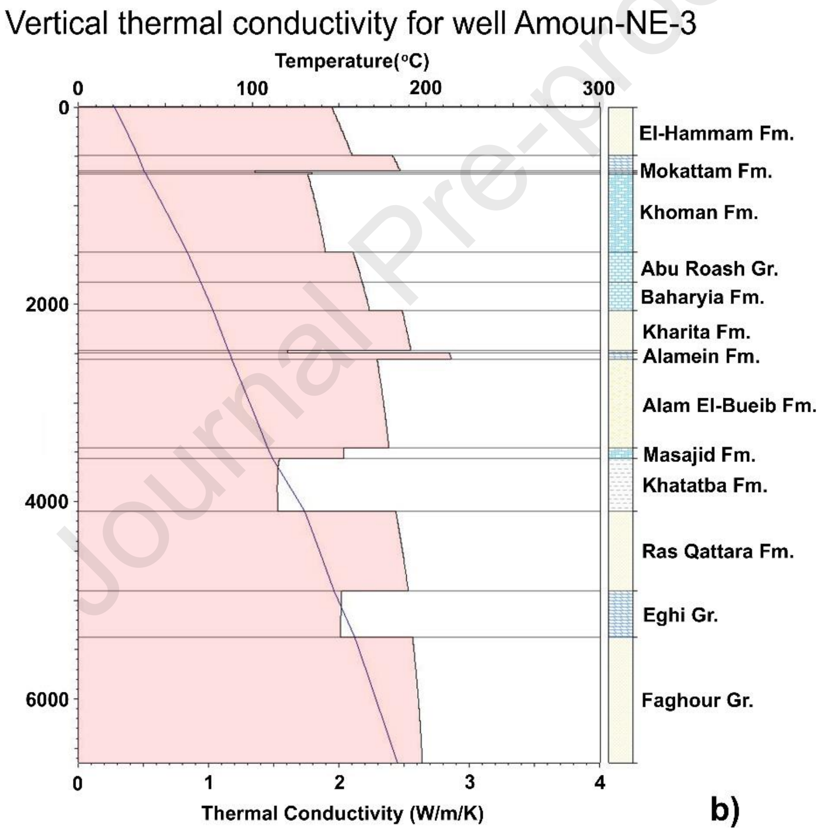
Vertical thermal conductivity for well Amoun-NE-3
Temperature(°C)
0
100
200
300
0
2000
4000
6000
0
1
2
3
4
Thermal Conductivity (W/m/K)
El-Hammam Fm.
Mokattam Fm.
Khoman Fm.
Abu Roash Gr.
Baharyia Fm.
Kharita Fm.
Alamein Fm.
Alam El-Bueib Fm.
Masajid Fm.
Khatatba Fm.
Ras Qattara Fm.
Eghi Gr.
Faghour Gr.
b)

Fig. 24.

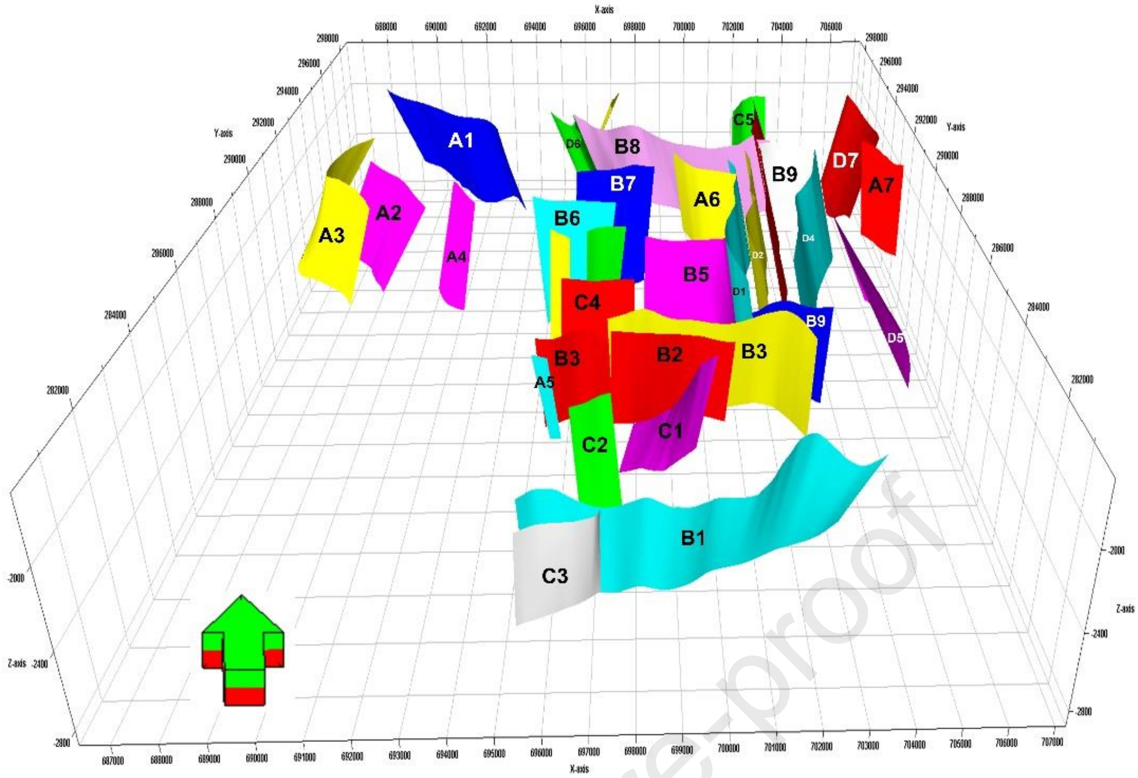
X-axis
Y-axis
Z-axis
A1
A2
A3
A4
A5
A6
A7
B1
B2
B3
B5
B6
B7
B8
B9
C1
C2
C3
C4
C5
D1
D2
D4
D5
D6
D7

Fig. 25.

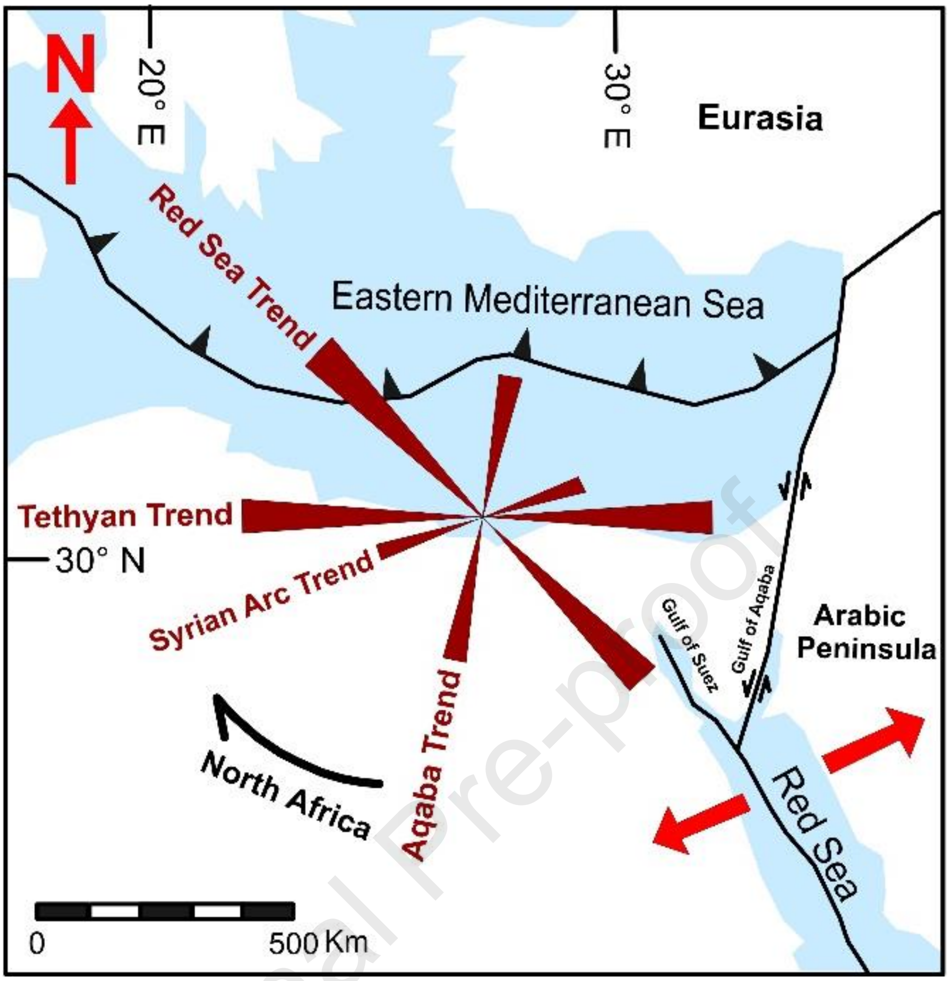
N
20° E
30° E
Eurasia
Red Sea Trend
Eastern Mediterranean Sea
Tethyan Trend
30° N
Syrian Arc Trend
Aqaba Trend
North Africa
Gulf of Suez
Gulf of Aqaba
Arabic Peninsula
Red Sea
0
500 Km

Fig. 26.

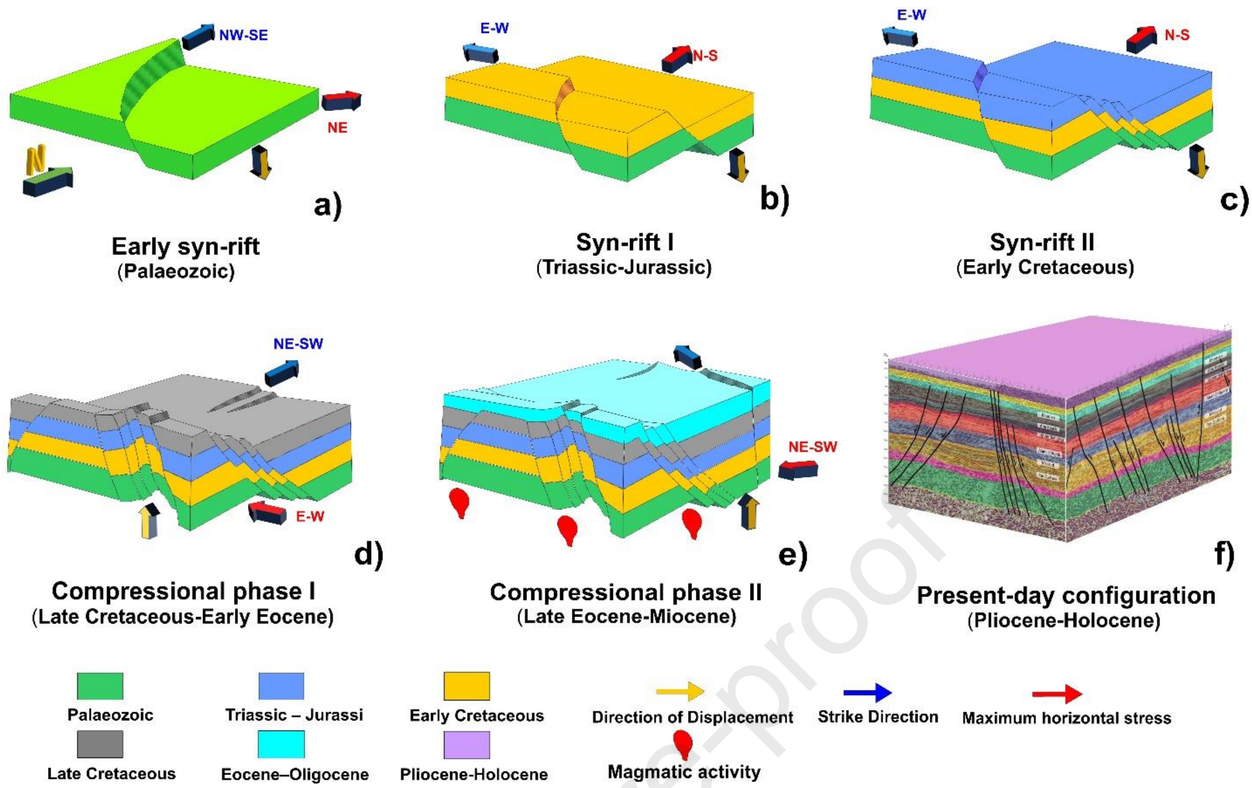
NW-SE
NE
N
a)
Early syn-rift
(Palaeozoic)
E-W
N-S
b)
Syn-rift I
(Triassic-Jurassic)
E-W
N-S
c)
Syn-rift II
(Early Cretaceous)
NE-SW
E-W
d)
Compressional phase I
(Late Cretaceous-Early Eocene)
NE-SW
e)
Compressional phase II
(Late Eocene-Miocene)
f)
Present-day configuration
(Pliocene-Holocene)
Palaeozoic
Triassic – Jurassi
Early Cretaceous
Direction of Displacement
Strike Direction
Maximum horizontal stress
Late Cretaceous
Eocene–Oligocene
Pliocene-Holocene
Magmatic activity

Fig. 27.

Triassic-Jurassic continental rifting between NE Africa, Apulia and the Arabic Plate

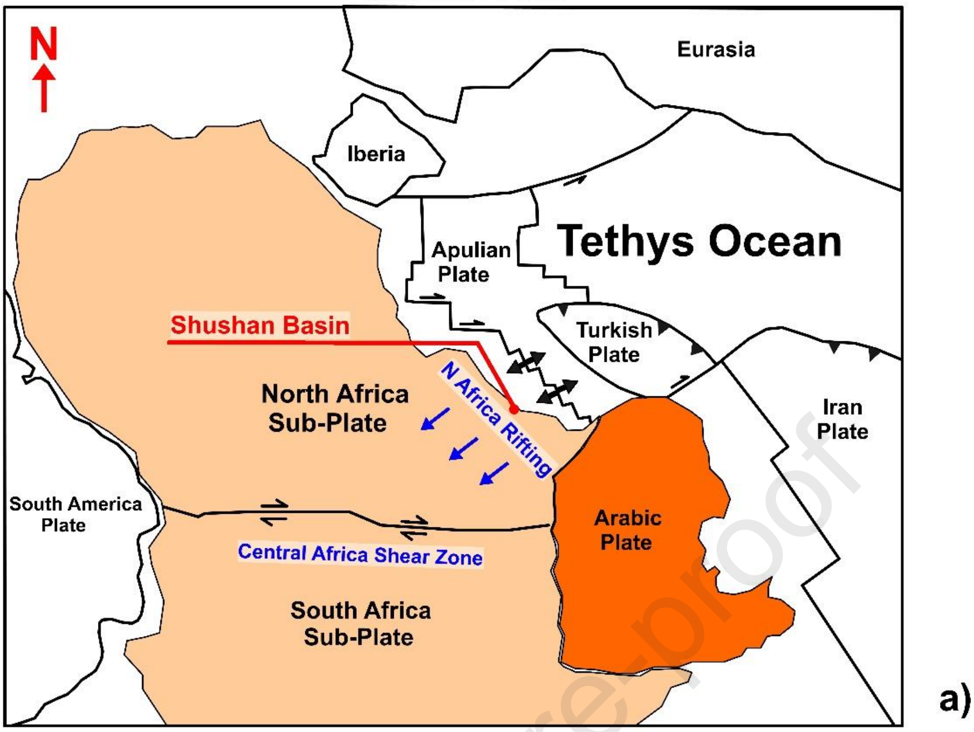

Late Cretaceous of Syrian Arc compression in the Late Cretaceous

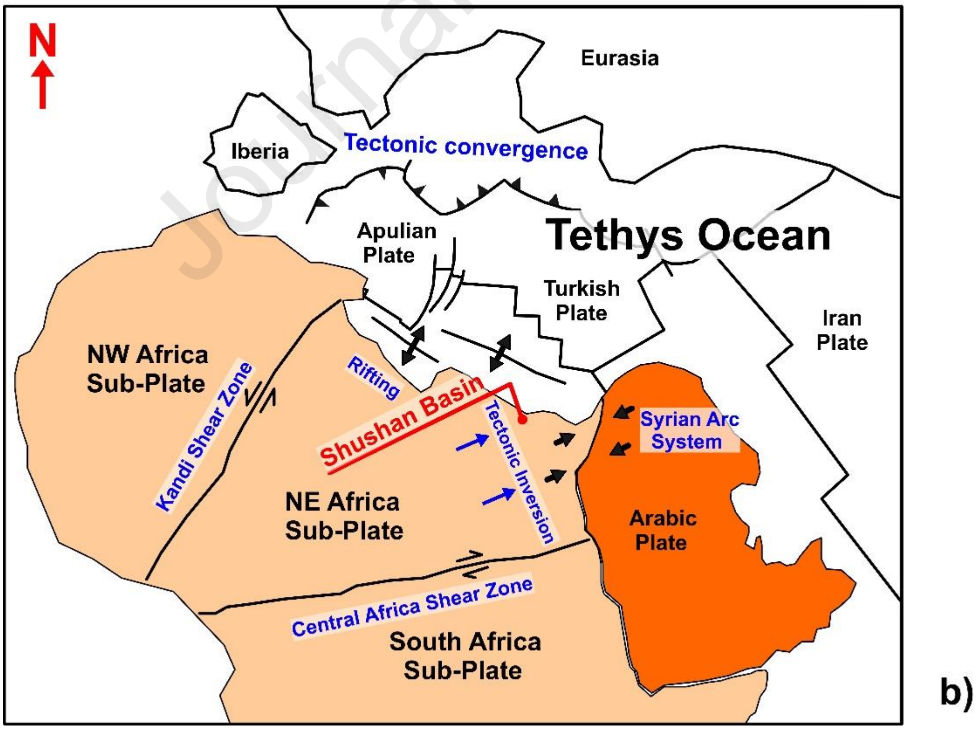

Fig. 28.

Oligocene onset of continental rifting in the Red Sea region

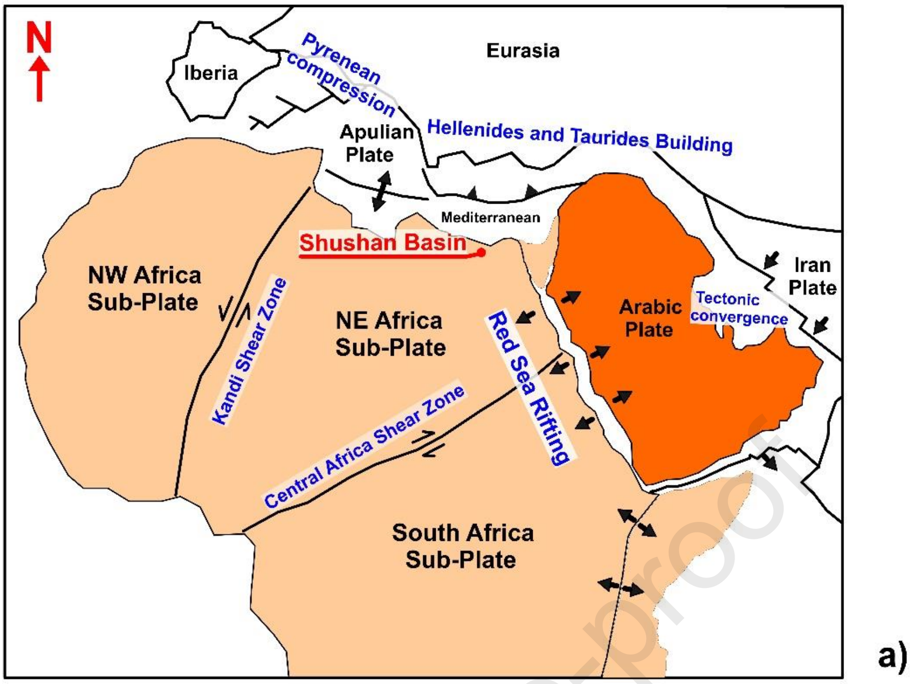

Late Cenozoic continental breakup between NW Africa and the Arabian Plate

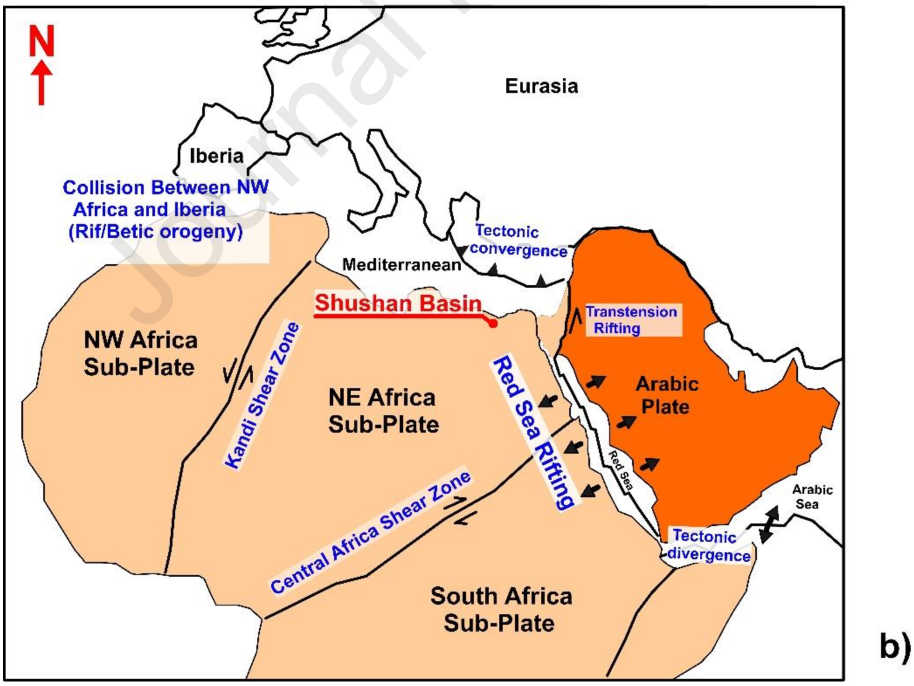

Fig. 29.

The Shushan Basin documents 9 seismic megasequences and 4 major tectonic episodes

Faults are categorized into four families: Red Sea, Tethyan, Syrian Arc and Aqaba

Tectonic inversion was followed by a (post-rift) thermal episode

This thermal episode controlled the generation of hydrocarbons in the Shushan Basin

Declaration of interests

☒ The authors declare that they have no known competing financial interests or personal relationships that could have appeared to influence the work reported in this paper.

☐ The authors declare the following financial interests/personal relationships which may be considered as potential competing interests: